

AD-A071 816

BATTELLE COLUMBUS LABS OHIO  
INVESTIGATING LOCALIZED CORROSION AND SPUTTERING FEASIBILITY OF--ETC(U)  
MAY 79 R B DIEGLE, D M LINEMAN

F/G 11/6

N00014-77-C-0488

NL

UNCLASSIFIED

1 OF 1  
AD  
A071816

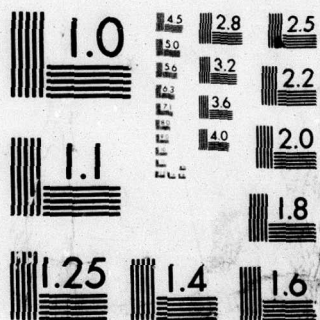


END

DATE  
FILMED

8-79

DDC



MICROCOPY RESOLUTION TEST CHART  
NATIONAL BUREAU OF STANDARDS-1963-A



# OFFICE OF NAVAL RESEARCH


Contract N00014-77-C-0488

## INTERIM TECHNICAL REPORT

For the Period May 1, 1977 to  
April 30, 1979

## INVESTIGATING LOCALIZED CORROSION AND SPUTTERING FEASIBILITY OF AMORPHOUS CHROMIUM-CONTAINING ALLOYS

By  
R. B. Diegle and D. M. Lineman

 **Battelle**  
Columbus Laboratories  
505 King Avenue  
Columbus, Ohio 43201

Accession For	
NTIS GRA&I	<input checked="" type="checkbox"/>
DDC TAB	<input type="checkbox"/>
Unannounced	<input type="checkbox"/>
Justification	
By <u>Ms. Beatty, ONR/Code 47/</u> <u>676-4325</u>	
Distribution/	
Availability Codes	
Dist.	Avail and/or special
A	

DDC  
RECEIVED  
JUL 27 1979  
D

Reproduction of this report in whole or in part is permitted  
for any purpose of the United States Government

### DISTRIBUTION STATEMENT A

Approved for public release;  
Distribution Unlimited

Unclassified

SECURITY CLASSIFICATION OF THIS PAGE (When Data Entered)

REPORT DOCUMENTATION PAGE		READ INSTRUCTIONS BEFORE COMPLETING FORM
1. REPORT NUMBER ONR 00014-77-C-0488	2. GOVT ACCESSION NO.	3. RECIPIENT'S CATALOG NUMBER
4. TITLE (and Subtitle) (6) Investigating Localized Corrosion and Sputtering Feasibility of Amorphous Chromium-Containing Alloys		5. TYPE OF REPORT & PERIOD COVERED Interim Technical May 1977 <del>APR</del> 1979
7. AUTHOR(s) (10) R. B. Diegle and D. M. Lineman		8. CONTRACT OR GRANT NUMBER(s) (15) N 00014-77-C-0488
9. PERFORMING ORGANIZATION NAME AND ADDRESS Battelle's Columbus Laboratories 505 King Avenue Columbus, Ohio 43201		10. PROGRAM ELEMENT, PROJECT, TASK AREA & WORK UNIT NUMBERS (12) 82p.
11. CONTROLLING OFFICE NAME AND ADDRESS Procuring Contracting Officer Office of Naval Research Dept. of the Navy 800 N Quincy St. Arlington, Va. 22217		12. REPORT DATE (11) May 1979
14. MONITORING AGENCY NAME & ADDRESS (if different from Controlling Office) Defense Contract Administration Services c/o Defense Electronics Supply Center Building 5 Dayton, OHio 45444		13. NUMBER OF PAGES
15. SECURITY CLASS. (of this report) Unclassified		15a. DECLASSIFICATION/DOWNGRADING SCHEDULE
16. DISTRIBUTION STATEMENT (of this Report) <div style="border: 1px solid black; padding: 5px; text-align: center;"> <b>DISTRIBUTION STATEMENT A</b>            Approved for public release;            Distribution Unlimited         </div>		
17. DISTRIBUTION STATEMENT (of the abstract entered in Block 20, if different from Report)		
18. SUPPLEMENTARY NOTES		
19. KEY WORDS (Continue on reverse side if necessary and identify by block number) amorphous alloys      pitting sputtering              crevice corrosion corrosion                passivity		
20. ABSTRACT (Continue on reverse side if necessary and identify by block number) For the past two years research has been directed toward understanding and utilizing the corrosion resistant properties of amorphous alloys based on the composition Fe-Ni-Cr-P-B. The research had two objectives: (a) separating initiation from propagation stages of localized corrosion phenomena and characterizing the tendency for each; and (b) developing a sputtering technique as a means for preparing these alloys.		

(Continued)

DD FORM 1 JAN 73 1473

EDITION OF 1 NOV 65 IS OBSOLETE

Unclassified

SECURITY CLASSIFICATION OF THIS PAGE (When Data Entered)

407 080

50



Unclassified

SECURITY CLASSIFICATION OF THIS PAGE(When Data Entered)

→ Propagation of localized corrosion was studied in prepared crevices, which circumvented the need for initiation at structural heterogeneities at alloy surfaces. A series of amorphous alloys with chromium contents ranging from 0 to 16 atomic percent was investigated. Classical anodic polarization experiments in acidified chloride electrolytes indicated that the chromium-containing alloys were extremely passive, pitting occurring only above about 1 V(SCE) in 1 M NaCl at pH 1. The existence of classical active-passive polarization behavior suggested that the susceptibility of these alloys to crevice corrosion would be considerably less than that of crystalline stainless alloys, such as Type 304 and Incoloy 800 steels. Experiments in the crevice cells indicated that the amorphous alloys do crevice corrode, but only at very noble potentials comparable to those required for pitting. The initial crevice corrosion potential varied from about 0.6 V(SCE) to about 1.5 V(SCE) in neutral 1 M NaCl as chromium was increased from 2 to 16 atomic percent; these values are approximate in nature, but they accurately reflect the resistance to crevice corrosion exhibited by this alloy system. The potential of the anode (crevice) specimen did not decrease substantially during crevice attack, indicating the possible presence of a partially protective film during corrosion. Specimens containing deformation-induced surface micro-cracks experience a transient form of crevice corrosion at considerably less noble potentials. However, the crevices rapidly widened into pit-shaped voids and quickly passivated, apparently as a result of ingress of less corrosive electrolyte from the bulk solution.

→ The sputtering research resulted in a procedure for depositing amorphous alloys with corrosion resistance almost as good as that conferred by liquid quenching. The deposits were free of porosity, extremely adherent to the copper substrates, and easily handled. Structural characterization revealed an essentially completely amorphous structure. The sputtered alloys corroded at rates that ranged from about 1 to 10 times faster than those of melt spun alloys under conditions of open circuit exposure and anodic polarization. They retained the excellent resistance to pitting exhibited by their melt spun counterparts. Sputtering has been shown to be an alternate technique to that of liquid quenching for preparing amorphous corrosion resistant Fe-Ni-Cr-P-B alloys.

Unclassified

SECURITY CLASSIFICATION OF THIS PAGE(When Data Entered)

### **ACKNOWLEDGMENTS**

The work performed under this contract was supported and monitored by the Office of Naval Research, Metallurgy Program. This support is appreciated, together with that of Dr. Frank Gardner (ONR, Boston), who provided a personal interest in this program.

In addition, the authors are grateful for the assistance of Dr. Dan Merz, of Battelle's Pacific Northwest Laboratories, in preparing the sputtered samples. The authors are also pleased to acknowledge the contributions of R. E. Maringer and R. L. White, Battelle's Columbus Laboratories, for melt spinning amorphous samples and for skillful assistance in scanning electron microscopy, respectively.



## ABSTRACT

For the past two years research has been directed toward understanding and utilizing the corrosion resistant properties of amorphous alloys based on the composition Fe-Ni-Cr-P-B. The research had two objectives: (a) separating initiation from propagation stages of localized corrosion phenomena and characterizing the tendency for each; and (b) developing a sputtering technique as a means for preparing these alloys.

Propagation of localized corrosion was studied in prepared crevices, which circumvented the need for initiation at structural heterogeneities at alloy surfaces. A series of amorphous alloys with chromium contents ranging from 0 to 16 atomic percent was investigated. Classical anodic polarization experiments in acidified chloride electrolytes indicated that the chromium-containing alloys were extremely passive, pitting occurring only above about 1 V(SCE) in 1 M NaCl at pH 1. The existence of classical active-passive polarization behavior suggested that the susceptibility of these alloys to crevice corrosion would be considerably less than that of crystalline stainless alloys, such as Type 304 and Incoloy 800 steels. Experiments in the crevice cells indicated that the amorphous alloys do crevice corrode, but only at very noble potentials comparable to those required for pitting. The initial crevice corrosion potential varied from about 0.6 V(SCE) to about 1.5 V(SCE) in neutral 1 M NaCl as chromium was increased from 2 to 16 atomic percent; these values are approximate in nature, but they accurately reflect the resistance to crevice corrosion exhibited by this alloy system. The potential of the anode (crevice) specimen did not decrease substantially during crevice attack, indicating the possible presence of a protective film during corrosion. Specimens containing deformation-induced surface microcracks experienced a transient form of crevice corrosion at considerably less noble potentials. However, the crevices rapidly widened into pit-shaped voids and quickly passivated, apparently as a result of ingress of less corrosive electrolyte from the bulk solution.

The sputtering research resulted in a procedure for depositing amorphous alloys with corrosion resistance almost as good as that conferred by liquid quenching. The deposits were free of porosity, extremely adherent to the copper substrates, and easily handled. Structural characterization revealed an essentially completely amorphous structure. The sputtered alloys corroded at rates that ranged from about 1 to 10 times faster than those of melt spun alloys under conditions of open circuit exposure and anodic polarization. They retained the excellent resistance to pitting exhibited by their melt spun counterparts. Sputtering has been shown to be an alternate technique to that of liquid quenching for preparing amorphous corrosion resistant Fe-Ni-Cr-P-B alloys.

## TABLE OF CONTENTS

	Page
INTRODUCTION .....	1
OBJECTIVES .....	3
MATERIALS AND PROCEDURES .....	3
Phase 1—Localized Corrosion .....	3
Phase 2—Sputtering .....	9
RESULTS AND DISCUSSION .....	11
Phase 1—Localized Corrosion .....	11
Structural Characterization of Melt Spun Alloys .....	11
Polarization in Simulated Crevice Solutions .....	11
Crevice Corrosion Experiments .....	24
Summary and Interpretation of Phase I Research .....	44
Phase 2—Sputtering .....	45
Sputtering Selectivity .....	45
Surface Characterization .....	46
Structural Characterization .....	48
Crystallization Behavior .....	48
Corrosion Under Open Circuit Conditions .....	54
Anodic Polarization Behavior .....	56
Summary .....	65
CONCLUSIONS .....	67

### APPENDIX A

CALCULATION OF RATE OF CREVICE CORROSION ON COLD ROLLED FILAMENT SURFACES .....	68
--	----

### APPENDIX B

LISTING OF ALL TECHNICAL REPORTS, PUBLICATIONS, AND PRESENTATIONS RESULTING FROM THIS CONTRACT .....	69
---	----



TABLE 1. COMPOSITIONS OF ALLOYS USED IN RESEARCH PROGRAM .....	4
TABLE 2. DEPENDENCE OF CRITICAL CURRENT DENSITIES FOR PASSIVATION, $i_c$ , ON pH FOR AMORPHOUS ALLOYS POLARIZED IN 1 M NaCl AT 22 C .....	20
TABLE 3. RESULTS OF COMPOSITIONAL ANALYSIS OF CAST TARGETS AND SPUTTERED DEPOSITS OF TWO ALLOYS .....	46
TABLE 4. TEMPERATURES AND HEATS OF CRYSTALLIZATION OF SPUTTERED AND MELT-SPUN AMORPHOUS ALLOYS .....	54

### LIST OF FIGURES

FIGURE 1. SCHEMATIC DIAGRAM OF BATTELLE'S MELT SPINNING APPARATUS USED TO PRODUCE THE ALLOYS STUDIED IN THIS PROGRAM .....	5
FIGURE 2. FILAMENTS PRODUCED BY MELT SPINNING. FILAMENTS WERE TYPICALLY ABOUT 30 $\mu\text{m}$ THICK AND 800 $\mu\text{m}$ WIDE .....	5
FIGURE 3. SCHEMATIC DIAGRAM OF SANDWICH-TYPE CREVICE CELL USED FOR PRELIMINARY (FIRST-YEAR) STUDIES OF CREVICE CORROSION .....	7
FIGURE 4. SCHEMATIC DIAGRAM OF INSTRUMENTED CREVICE CELL USED FOR IN-DEPTH (SECOND-YEAR) STUDIES OF CREVICE CORROSION .....	8
FIGURE 5. WEDGE-SHAPED SECTION OF A SPUTTERED DEPOSIT ON COPPER SUBSTRATE. THE DEPOSIT IS ABOUT 75 $\mu\text{m}$ THICK .....	10
FIGURE 6. DIFFERENTIAL SCANNING CALORIMETRY (DSC) CURVES FOR MELT SPUN ALLOYS WITH INDICATED Cr CONTENTS. SCAN RATE WAS 5 C/MINUTE. PEAKS INDICATE EXOTHERMIC CRYSTALLIZATION .....	12
FIGURE 7. CRITICAL AND PASSIVE CURRENT DENSITIES VERSUS Cr CONTENT FOR AMORPHOUS ALLOYS POLARIZED IN 1 M NaCl, pH 2.4. OPEN SYMBOLS REFER TO ALLOYS PRODUCED AT BATTELLE AND SOLID SYMBOLS REFER TO METGLAS 2826 and 2826A .....	13
FIGURE 8. CRITICAL AND PASSIVE CURRENT DENSITIES VERSUS Cr CONTENT FOR AMORPHOUS ALLOYS POLARIZED IN 6 PERCENT FeCl <sub>3</sub> , pH 1.4 .....	14
FIGURE 9. POTENTIODYNAMIC POLARIZATION CURVES FOR THE 0 ATOMIC PERCENT Cr AMORPHOUS ALLOY (METGLAS 2826) IN 1 M NaCl ADJUSTED TO SEVERAL pH VALUES.....	15

# LIST OF FIGURES (continued)

	Page
FIGURE 10. POTENTIODYNAMIC CURVES FOR THE 2 ATOMIC PERCENT Cr AMORPHOUS ALLOY IN 1 M NaCl ADJUSTED TO SEVERAL pH VALUES ..	16
FIGURE 11. POTENTIODYNAMIC POLARIZATION CURVES FOR THE 7 ATOMIC PERCENT Cr AMORPHOUS ALLOY IN 1 M NaCl ADJUSTED TO SEVERAL pH VALUES .....	17
FIGURE 12. POTENTIODYNAMIC POLARIZATION CURVES FOR THE 16 ATOMIC PERCENT Cr AMORPHOUS ALLOY IN 1 M NaCl ADJUSTED TO SEVERAL pH VALUES .....	18
FIGURE 13. POTENTIODYNAMIC POLARIZATION CURVE FOR THE 16 ATOMIC PERCENT Cr AMORPHOUS ALLOY IN 1 N HCl .....	19
FIGURE 14. POTENTIODYNAMIC POLARIZATION CURVES FOR AMORPHOUS MELT SPUN ALLOYS OF THE INDICATED Cr CONTENTS, AND FOR CRYSTALLINE T304 AND INCOLOY 800 ALLOYS .....	22
FIGURE 15. POTENTIODYNAMIC POTENTIOSTATIC POLARIZATION CURVES FOR THE 2 ATOMIC PERCENT Cr AMORPHOUS ALLOY .....	23
FIGURE 16. SEM PHOTOGRAPHS OF METGLAS 2826A AFTER A 25 PERCENT REDUCTION IN THICKNESS BY COLD ROLLING. (a) As-rolled surface; (b) after polarization for one hour at 0.60 V(SCE) in 1 M NaCl, pH 7 .....	25
FIGURE 17. POTENTIODYNAMIC/POTENTIOSTATIC POLARIZATION CURVES FOR THE 16 ATOMIC PERCENT Cr AMORPHOUS ALLOY IN THE UNDEFORMED AND COLD ROLLED CONDITIONS .....	27
FIGURE 18. POTENTIODYNAMIC POLARIZATION CURVES FOR METGLAS 2826A IN THE NON-COLD ROLLED CONDITION, AND AFTER POTENTIOSTATIC POLARIZATION FOR ONE HOUR AT 0.60 V(SCE) .....	28
FIGURE 19. SEM PHOTOGRAPHS OF SURFACE OF METGLAS 2826A FILAMENTS AFTER A 25 PERCENT REDUCTION IN THICKNESS. (a) Pits formed after polarization for one hour at 0.60 V(SCE) in 1 M NaCl, pH 7; (b) another region on same specimen after potentiodynamic polarization to 1.5 V(SCE) ...	29
FIGURE 20. SEM PHOTOGRAPHS OF SURFACES OF METGLAS 2826A THAT WAS REDUCED IN THICKNESS BY ABOUT 10 PERCENT BY PUNCHING. (a) Surface after punching; (b) another region after punching, then polarization for one hour at 0.60 V(SCE) in 1 M NaCl, pH 7 .....	30
FIGURE 21. CELL CURRENT AND APPLIED POTENTIAL VERSUS TIME FOR T304 STAINLESS STEEL IN THE SANDWICH-TYPE CREVICE TEST CELL .....	31
FIGURE 22. CELL CURRENT AND APPLIED POTENTIAL VERSUS TIME FOR THE 2 ATOMIC PERCENT Cr AMORPHOUS ALLOY IN THE SANDWICH-TYPE CREVICE TEST CELL .....	33



# LIST OF FIGURES (continued)

	Page
FIGURE 23. CELL CURRENT AND APPLIED POTENTIAL VERSUS TIME FOR THE 7 ATOMIC PERCENT Cr AMORPHOUS ALLOY IN THE SANDWICH-TYPE CREVICE TEST CELL .....	34
FIGURE 24. CELL CURRENT AND APPLIED POTENTIAL VERSUS TIME FOR THE 16 ATOMIC PERCENT Cr AMORPHOUS ALLOY IN THE SANDWICH-TYPE CREVICE TEST CELL .....	35
FIGURE 25. CELL CURRENT, ANODE POTENTIAL, AND ANOLYTE pH VERSUS TIME FOR TYPE 304 STAINLESS STEEL EVALUATED IN THE INSTRUMENTED CREVICE CELL IN 1 M NaCl, pH 7, OXYGENATED, AT 22 C .....	37
FIGURE 26. CELL CURRENT, ANODE POTENTIAL, AND ANOLYTE pH VERSUS TIME FOR TYPE 304 STAINLESS STEEL EVALUATED IN THE INSTRUMENTED CREVICE CELL IN 1 M NaCl, pH 7, OXYGENATED, AT 22 C .....	38
FIGURE 27. CELL CURRENT, ANODE POTENTIAL, AND ANOLYTE pH VERSUS TIME FOR THE 2 Cr AMORPHOUS ALLOY EVALUATED IN THE INSTRUMENTED CREVICE CELL IN 1 M NaCl, pH 7, OXYGENATED, AT 22 C .....	39
FIGURE 28. CELL CURRENT, ANODE POTENTIAL, AND ANOLYTE pH VERSUS TIME FOR THE 7 Cr AMORPHOUS ALLOY EVALUATED IN THE INSTRUMENTED CREVICE CELL IN 1 M NaCl, pH 7, OXYGENATED, AT 22 C .....	40
FIGURE 29. CELL CURRENT, ANODE POTENTIAL, AND ANOLYTE pH VERSUS TIME FOR THE 16 Cr AMORPHOUS ALLOY EVALUATED IN THE INSTRUMENTED CREVICE CELL IN 1 M NaCl, pH 7, OXYGENATED, AT 22 C .....	41
FIGURE 30. CELL CURRENT AND ANODE POTENTIAL VERSUS TIME FOR THE 16 Cr AMORPHOUS ALLOY EVALUATED IN THE INSTRUMENTED CREVICE CELL IN 1 N HCl, OXYGENATED, at 22 C .....	42
FIGURE 31. CELL CURRENT, ANODE POTENTIAL, AND ANOLYTE pH VERSUS TIME FOR THE 16 Cr AMORPHOUS ALLOY EVALUATED IN THE INSTRUMENTED CREVICE CELL IN 1 M NaCl, pH 7, OXYGENATED, at 22 C .....	43
FIGURE 32. CELL CURRENT, ANODE POTENTIAL, AND ANOLYTE pH VERSUS TIME FOR METGLAS 2826A EVALUATED IN THE INSTRUMENTED CREVICE CELL IN 1 M NaCl, pH 7, OXYGENATED, AT 22 C .....	44
FIGURE 33. SEM PHOTOGRAPHS OF SURFACE OF SPUTTERED DEPOSITS. (a) 16 Cr (LN <sub>2</sub> substrate); (b) enlarged view of (a); (c) 16 Cr (water-cooled substrate); (d) 2 Cr (LN <sub>2</sub> substrate) .....	47
FIGURE 34. SEM PHOTOGRAPHS OF SURFACES OF 16 Cr FILAMENT PREPARED BY MELT SPINNING. (a) Shiny side (in contact with vacuum during melt spinning); (b) dull side (in contact with copper wheel during melt spinning) .....	49

## LIST OF FIGURES (continued)

FIGURE 35. TEM PHOTOGRAPH OF 16 Cr DEPOSIT SPUTTERED ONTO A LIQUID NITROGEN-COOLED COPPER SUBSTRATE .....	50
FIGURE 36. SAED PATTERN OF 16 Cr DEPOSIT SPUTTERED ONTO LIQUID NITROGEN-COOLED COPPER SUBSTRATE .....	51
FIGURE 37. TEM PHOTOGRAPH OF 16 Cr DEPOSIT SPUTTERED ONTO A WATER-COOLED COPPER SUBSTRATE .....	52
FIGURE 38. DSC CURVES FOR 2 Cr ALLOY PRODUCED EITHER BY MELT SPINNING OR BY SPUTTERING. SCAN RATE WAS 20 C/MIN .....	53
FIGURE 39. CORROSION RATES, OBTAINED BY MEASUREMENT OF WEIGHT LOSS AFTER 167 HOURS OF EXPOSURE IN 10 PERCENT FeCl <sub>3</sub> SOLUTION, FOR SPUTTERED AND MELT SPUN SPECIMENS .....	55
FIGURE 40. ANODIC POTENTIODYNAMIC POLARIZATION CURVES OF SPUTTERED AND MELT SPUN 2 Cr ALLOYS IN 1 M NaCl, pH 7, DEAERATED .....	57
FIGURE 41. ANODIC POTENTIODYNAMIC POLARIZATION CURVES OF SPUTTERED AND MELT SPUN 2 Cr ALLOYS IN 1 M NaCl, pH 3, DEAERATED .....	58
FIGURE 42. ANODIC POTENTIODYNAMIC POLARIZATION CURVES OF SPUTTERED AND MELT SPUN 2 Cr ALLOYS IN 1 M NaCl, pH 1, DEAERATED .....	59
FIGURE 43. SEM PHOTOGRAPHS OF 2 Cr SPUTTERED DEPOSITS POLARIZED FOR ONE HOUR IN 1 M NaCl, pH 3, AT THE FOLLOWING POTENTIALS: (a) 0.60 V(SCE); (b) 1.10 V(SCE) .....	60
FIGURE 44. ANODIC POTENTIODYNAMIC POLARIZATION CURVES OF SPUTTERED AND MELT SPUN 16 Cr ALLOYS IN 1 M NaCl, pH 7, DEAERATED .....	61
FIGURE 45. ANODIC POTENTIODYNAMIC POLARIZATION CURVES OF SPUTTERED AND MELT SPUN 16 Cr ALLOYS IN 1 M NaCl, pH 3, DEAERATED .....	62
FIGURE 46. ANODIC POTENTIODYNAMIC POLARIZATION CURVES OF SPUTTERED AND MELT SPUN 16 Cr ALLOYS IN 1 M NaCl, pH 1, DEAERATED .....	63
FIGURE 47. SEM PHOTOGRAPHS OF PITS ON 16 Cr SPUTTERED DEPOSITS POLARIZED IN 1 M NaCl, pH 3, to 1.8 V(SCE). (a) Sputtered on water-cooled substrate; (b) sputtered onto LN <sub>2</sub> -cooled substrate .....	64
FIGURE 48. ANODIC POTENTIODYNAMIC POLARIZATION CURVES OF 16 Cr DEPOSITS SPUTTERED ONTO EITHER WATER-COOLED OR LIQUID NITROGEN-COOLED COPPER SUBSTRATES. ELECTROLYTE WAS 1 M NaCl, pH 7 AND 3, DEAERATED .....	66



## INTRODUCTION

The advent of amorphous alloys containing Fe, Ni, and Cr has led to intensive research into their properties, especially corrosion behavior. A primary reason for interest in corrosion behavior is the similarity of composition of these amorphous alloys with conventional chromium-bearing stainless steels. Specifically, the simultaneous presence of Fe, Ni, and Cr provided, for the first time, an opportunity for studying corrosion on alloys that are free of crystalline defects.

Early studies showed that this class of amorphous alloys, of compositions Fe-Ni-Cr-P-B and Fe-Ni-Cr-P-C, possesses remarkable resistance to localized corrosion attack, namely, pitting.<sup>(1-4)</sup> Straightforward potentiodynamic polarization techniques in acidified chloride electrolytes showed that the critical pitting potential,  $E_{cp}$ , was several tenths of a volt more positive than that of conventional crystalline stainless steels of similar chromium content. One group of researchers demonstrated that the minimum amount of chromium needed to confer passivity in the amorphous state was only 8 atomic percent,<sup>(1)</sup> in contrast to the 12 atomic percent required in crystalline stainless steels. Thus, preliminary studies of this new class of materials indicated that they constitute a novel alloy system with not only improved corrosion resistance relative to crystalline stainless steels, but also with the potential for conserving chromium, a critical resource.

The favored hypothesis to account for the pitting resistance of amorphous chromium-containing alloys is based on their extremely homogeneous structure. Because the alloys are amorphous, they are free of grain boundaries, stacking faults, dislocations, and other defects found in crystalline structures. Because they are quenched at rates in excess of  $10^5$  °K/sec, they also exhibit less macrosegregation and microsegregation, and they are free of second phases formed by solid state precipitation. At worst, they are somewhat heterogeneous on an atomic scale because of some short range ordering and clustering phenomena. The alloys, therefore, are presumed to resist pitting because of the difficulty of initiation. That is, it is well known that pitting occurs preferentially at heterogeneous surface sites such as grain boundaries and second phase particles; the fact that these sites are absent in amorphous alloys is used to rationalize the fact that  $E_{cp}$  is several tenths of a volt more noble than in less-perfect alloys. This hypothesis is supported by evidence that passive films formed on Fe-Ni-Cr-P-C alloys are similar in structure to those observed on crystalline stainless steels.<sup>(5)</sup>

Therefore, the key to the resistance of certain amorphous alloys to corrosion appears to result from the difficulty of initiating attack. It stands to reason that if localized corrosion could be *initiated*, it might propagate readily. Indeed, Devine<sup>(6)</sup> demonstrated this fact by

- (1) Naka, M., Hashimoto, K., and Masumoto, T., "High Corrosion Resistance of Chromium-Bearing Amorphous Iron Alloys in Neutral and Acidic Solutions Containing Chloride", *Corr.*, 32 (4), 146 (1976).
- (2) Diegle, R., and Slater, J., "Influence of Crystallinity on Corrosion Behavior of Ferrous Alloys", 32 (4), 155 (1976).
- (3) Hashimoto, K., and Masumoto, T., "Extremely High Corrosion Resistance of Chromium-Containing Amorphous Iron Alloys", *Rapidly Quenched Metals*, Procs., Second Int. Conf. on Rapidly Quenched Metals (1975), Edited by N. J. Grant and B. C. Giessen, p. 285.
- (4) Hashimoto, K., Asami, K., Masumoto, T., and Shimodaira, S., "Characteristics of Passivity of Extremely Corrosion-Resistant Amorphous Iron Alloys", *Corr. Sci.*, 16, 71 (1976).
- (5) Asami, K., Hashimoto, K., Masumoto, T., and Shimodaira, S., "ESCA Study of the Passive Film on an Extremely Corrosion-Resistant Amorphous Iron Alloy", *Corr. Sci.*, 16 (12), 909 (1976).
- (6) Devine, T. M., "Anodic Polarization and Localized Corrosion Behavior of Amorphous  $Ni_{35}Fe_{30}Cr_{15}P_{14}B_6$  in Near-Neutral and Acidic Chloride Solutions", *J. Electrochem. Soc.*, 124 (17), 38 (1977).

promoting crevice attack in Metglas 2826A\* which had been cold rolled to induce surface microcracks. Localized corrosion readily initiated in the cracked specimen at a potential that was well below that required for the intact alloy.

It was also demonstrated<sup>(7)</sup> that the open circuit corrosion rate of Metglas 2826A in acidified chloride solutions sealed from atmospheric oxygen is nearly 1000 times greater than that for specimens in chloride solutions open to the atmosphere. It appears that oxygen is necessary to promote passivity of the amorphous alloys, just as it is for conventional chromium-bearing stainless steels.

The above observations were interpreted as indicating a possible Achilles heel in the otherwise remarkable corrosion resistance of these alloys, namely, that they might be susceptible to *crevice corrosion*. Crevice corrosion does not require heterogeneities in the alloy for initiation, and oxygen depletion can readily occur within crevices; therefore, it was wondered whether the alloys might readily corrode in a crevice geometry, unlike their performance when evaluated in a freely exposed geometry. This is the first major question that the present program at Battelle sought to answer.

The second question addressed in this program related to the utilization of amorphous alloys. Most amorphous alloys of the Fe-Ni-Cr-P-B and Fe-Ni-Cr-P-C varieties are produced by rapid solidification techniques. These techniques include splat quenching, melt extraction, and melt spinning. Of necessity, material produced by these procedures is very thin, typically less than 60  $\mu\text{m}$  because of the high heat transfer required to attain the amorphous state. Thus, these techniques are suitable for providing samples for properties studies, but the splats and filaments that result cannot be used for practical applications, e.g., protective coatings. It is desirable to be able to coat conventional base metal substrates with these alloys to confer their corrosion resistance to less inert materials. Sputtering is one technique which promises such a capability. Sputtering has been used to deposit amorphous alloy structures, including some with improved corrosion resistance.<sup>(8)</sup> It is also used routinely to coat substrates of substantial surface area and often with complex geometries. Therefore, Battelle investigated sputtering as a candidate technique for coating materials with amorphous, highly corrosion resistant alloys.

This report summarizes the preceding two years of research for this program. An interim report<sup>(9)</sup> was issued after the first year of research describing the progress of work and the results obtained by that time. This second interim report includes the highlights of the first year of work and a detailed account of the second year of research.

(7) Diegle, R. B., unpublished research.

(8) Nowak, W. B., "Microcrystalline Amorphous Iron Alloy Films for Corrosion-Resistant Coatings", *Mat. Sci. and Eng.*, 23, 301 (1976).

(9) Diegle, R. B., Lineman, D. M., and Boyd, W. K., "Investigating Localized Corrosion and Sputtering Feasibility of Amorphous Chromium-Containing Alloys", Interim Technical Report No. ONR-00014-77-C-0488 to Office of Naval Research, April, 1978.

\*Tradename for Allied Chemical's amorphous  $\text{Fe}_{32}\text{Ni}_{36}\text{Cr}_{14}\text{P}_{14}\text{B}_6$  alloy.



## OBJECTIVES

The objectives of this research program were twofold, namely:

- (1) to investigate the propagation of localized corrosion on amorphous chromium-containing alloys as a phenomenon separate from initiation, and to characterize the susceptibility of these alloys to both stages of corrosion; and
- (2) to develop a sputtering procedure for applying these alloys to base metals, thereby providing a means for utilizing their superior corrosion-resistant properties.

## MATERIALS AND PROCEDURES

The materials and procedures described below are separated into two parts relating to localized corrosion studies and sputtering, respectively.

### Phase 1 — Localized Corrosion

Five alloy compositions were prepared at Battelle for this research program. The chromium concentration was varied from 2 to 14 atomic percent to determine the effect of chromium on conferring corrosion resistance under the exposure conditions used in the research. The compositions of the alloys are presented in Table 1. The alloy from Allied Chemical Corporation was included as representative of an amorphous alloy of composition similar to the 16 atomic percent Cr Battelle alloy, but produced at another laboratory. T304 stainless was included as an example of a commercial stainless steel. Incoloy 800 was evaluated because the Fe, Ni, and Cr levels approximated those in the 16 atomic percent Battelle alloy, but they were present in a crystalline rather than an amorphous structure. Thus, the combined effect of these three elements in the concentrations and ratios present in Incoloy 800 could be studied in both crystalline and amorphous alloys.

The compositions of the alloys produced at Battelle were verified by chemical and X-ray analysis early in the second year of research. Compositions of alloys prepared by Allied and of those purchased from mills were taken from product literature and mill heat analyses, respectively.

It should be noted that compositions of the five Battelle alloys are somewhat different from those reported in the first Interim Technical Report.<sup>(9)</sup> Specifically, the Cr levels are 2 atomic percent greater than were originally reported, about 2 percent V is present, and the concentration of P is 15 rather than 14 percent. The extra 2 percent each of Cr and V originated from the ferrophosphorus alloy that was used to introduce phosphorus into the melts. The purity of the ferrophosphorus was less than originally thought, and therefore, its use introduced small amounts of Cr and V. Thus, it is necessary to amend statements made in the first Interim Technical Report that refer to a "zero Cr alloy", "three Cr alloy", etc., to take into account the presence of the extra 2 atomic percent of Cr in each melt. The effect of 2 atomic percent V on corrosion behavior is not known, but is thought at this time to be small.

TABLE 1. COMPOSITIONS OF ALLOYS USED IN RESEARCH PROGRAM

Preparation Technique	Source	Amorphous	Composition, atomic percent									
			Fe	Ni	Cr	V	P	B	Si	C	Mn	Ti
Melt spinning	Battelle	Yes	45	30	2	2	15	6				
		Yes	42	30	5	2	15	6				
		Yes	40	30	7	2	15	6				
		Yes	37	30	10	2	15	6				
		Yes	31	30	16	2	15	6				
Melt spinning	Allied	Yes	40	40	0		14	6				
		Yes	32	36	14		12	6				
Sputtering	Battelle	Yes	45	30	2	2	15	6				
		Yes	31	30	16	2	15	6				
Conventional (casting and rolling)	Mill	No	69	8	20				1.2	0.00	1.7	(T304 stainless steel)
		No	46	31	22					0.00		0.008 (Incoloy 800)

The Battelle alloys were first cast into pancake-shaped ingots by conventional casting techniques involving induction melting of pure components in a controlled atmosphere. Next, 30-gram portions from each of five crystalline ingots were removed and melt spun into amorphous filaments. The melt spinning was performed as shown schematically in Figure 1. The liquid impinged on a water-cooled copper wheel rotating at 25.4 m/sec in argon. The resulting filaments were about 30  $\mu$ m thick and 800  $\mu$ m wide. The results of a typical experimental run are shown in Figure 2.

The amorphous structure of melt spun filaments was characterized by differential scanning calorimetry (DSC), since this technique previously has been used successfully to study the nature of the amorphous state in certain alloys.<sup>(10)</sup> The corrosion behavior of the filaments and all other alloys was studied primarily by anodic polarization, which was performed either potentiodynamically or potentiostatically. Electrodes were prepared by soldering short (about 2 cm) lengths of filament or other specimen onto copper wires that passed through glass tubes about 20 cm long. The copper wire, which served as an electrical lead, and the solder were masked with an acid-resistant lacquer, thereby providing specimen holders that were specially adapted to the filaments produced by the melt spinning process. Experiments were performed in a glass cell equipped with an external heating mantle, internal thermoregulator, Luggin capillary, counterelectrodes separated by glass-frits, and a fritted bubbler for deaeration with tank nitrogen. Polarization was performed with an electronic potentiostat with potentials measured relative to a saturated calomel electrode (SCE) that was external to the cell. Potentiodynamic sweeps were performed with a solid state electronic sweep generator from the open circuit potential to various anodic values. Specimen surfaces

(10) Yeh, H., and Maddin, R., "Phase Transformations in Amorphous Fe-P-C Alloys", *Rapidly Quenched Metals*, Ed. by N. J. Grant and B. C. Giessen, Massachusetts Institute of Technology, Boston (1976), p. 281.



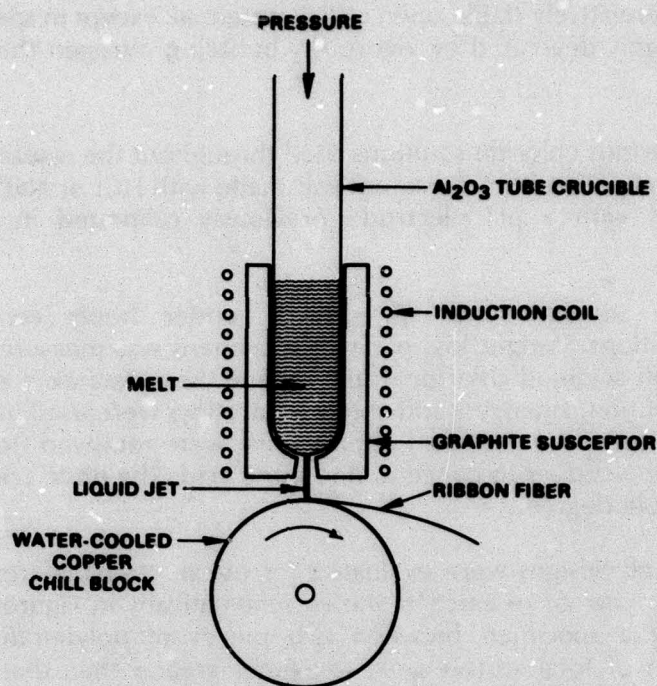


**FIGURE 1. SCHEMATIC DIAGRAM OF BATTELLE'S MELT SPINNING APPARATUS USED TO PRODUCE MOST ALLOYS STUDIED IN THIS PROGRAM**



**FIGURE 2. FILAMENTS PRODUCED BY MELT SPINNING. FILAMENTS WERE TYPICALLY ABOUT 30  $\mu\text{m}$  THICK AND 800  $\mu\text{m}$  WIDE**

were prepared by first cathodically polarizing the alloy to  $-1.5V(SCE)$  for up to 2 minutes to achieve an active and relatively stable open circuit potential. Except in special cases, the electrolytes were thoroughly deaerated by vigorously bubbling nitrogen through them prior to each experiment.

The pH of the various chloride solutions used throughout the research was carefully adjusted prior to each experiment. Adjustment was made with HCl or NaOH, and the pH was periodically checked with a pH electrode previously calibrated in appropriate buffer solutions.

Some corrosion measurements were made under freely corroding (i.e., non-potentiostated) conditions. Weight loss of small specimens was measured after exposure in glass vessels filled with acidified chloride solutions, and these data were converted to a time-average rate of dissolution. Filaments and commercial alloys were used in the forms in which they were received. However, sputtered deposits first were removed from the copper substrates by dissolving the copper in concentrated nitric acid. The nitric acid did not attack the deposits to a detectable degree.

Several crevice cell designs were evaluated for use in studying crevice corrosion. The cell used for the first year of research is shown schematically in Figure 3. The crevice was formed by clamping a specimen between two pieces of polytetrafluorethylene (PTFE, Teflon<sup>®</sup>). A specimen of total surface area ten times greater than that within the crevice served as the external (cathode) specimen. In practice, the two electrodes were electrically connected externally to the electrochemical cell through a zero-resistance ammeter (ZRA). The external electrode was polarized potentiostatically to a specific anodic potential, and the resulting current flowing between crevice and external specimens ("cell current") was recorded over a period of time. This procedure enabled determination of: (a) whether crevice corrosion occurred; (b) critical potential for initiation,  $E_{cc}$ ; (c) time required for its initiation; and (d) severity of attack, as measured by the steady state cell current. The cell thus enabled measurement of crevice corrosion in real time for the nonideal geometry of melt-spun filaments.

The cell described above was useful for preliminary studies of crevice corrosion, particularly for screening alloy compositions to obtain a ranking of their susceptibility to crevice attack. However, it did not provide any information concerning the electrochemical conditions occurring within the crevice that gave rise to crevice corrosion. For this purpose, a cell was needed in which the crevice region was instrumented with appropriate electrodes. Therefore, a cell design that has been used for studies of crevice corrosion in another alloy system was adopted.<sup>(11)</sup> The cell is shown schematically in Figure 4. It was comprised of a small crevice chamber of about one cc volume in contact with one liter of bulk electrolyte through a fine fritted disc. Inside the crevice chamber was coiled about three cm<sup>2</sup> of filament, which served as the anode during the crevice experiments. A silver-silver chloride (Ag/AgCl) micro reference electrode and a semi-micro combination pH electrode also penetrated into the crevice region, thereby enabling measurements of electrode potential and pH of crevice electrolyte to be made continuously during each experiment. An electrical lead that was soldered to the filament and masked with an acid-resistant lacquer exited the crevice and was connected to a bundle of similar filaments in the bulk electrolyte through a ZRA. Thus, crevice corrosion current, or "cell current" flowing between the crevice

(11) Efrid, K. D., and Verink, E. D., Jr., "The Crevice Protection Potential for 90-10 Copper Nickel", *Corrosion*, 33 (9), 328 (1977).



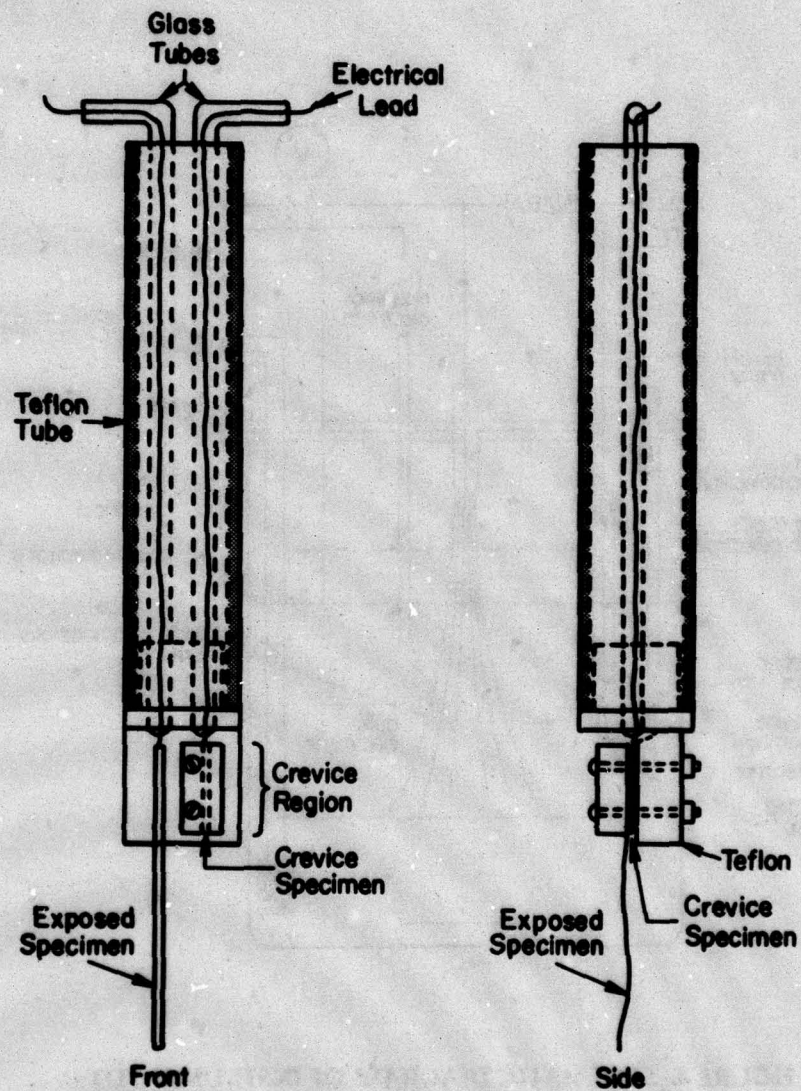


**FIGURE 3. SCHEMATIC DIAGRAM OF SANDWICH-TYPE CREVICE CELL USED FOR PRELIMINARY (FIRST-YEAR) STUDIES OF CREVICE CORROSION**

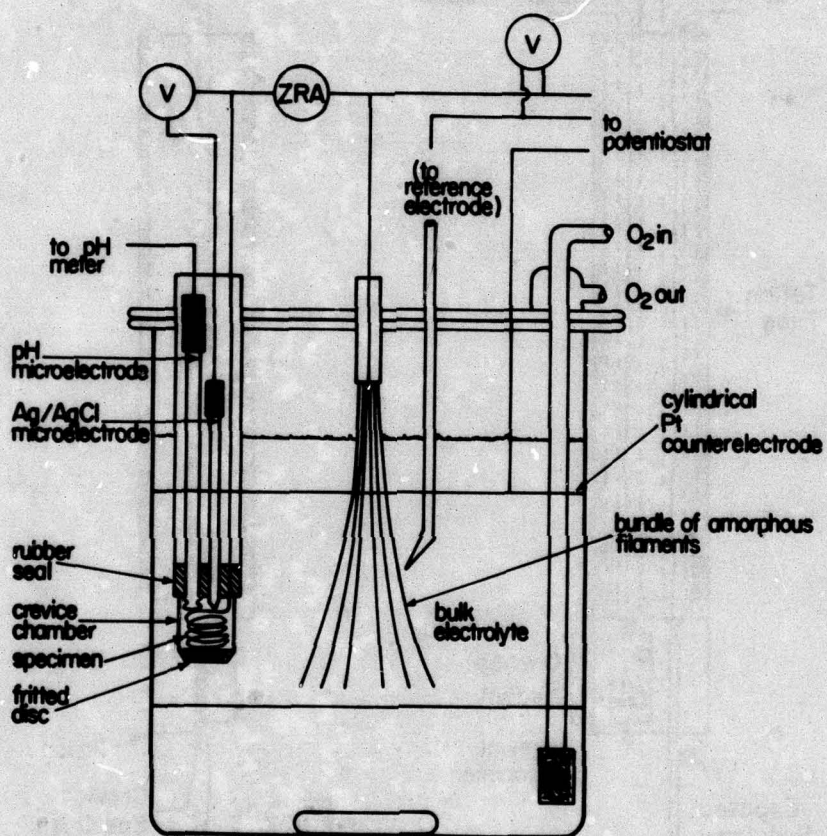


**FIGURE 4. SCHEMATIC DIAGRAM OF INSTRUMENTED CREVICE USED FOR IN-DEPTH (SECOND-YEAR) STUDIES OF CREVICE CORROSION**



specimen (anode) and external specimen (cathode) could be measured as a function of experimental parameters. The anode-to-cathode area ratio was maintained at about 1:10 throughout the experimentation.

The electrolyte used during most of the research with this cell was 1 M NaCl. It was maintained at a pH of 7 throughout each experiment by periodic titration with appropriate amounts of dilute NaOH or HCl solution. Thus, the pH of the anolyte was allowed to vary but that of the catholyte was held constant. The catholyte also was oxygenated during each experiment to ensure an adequate supply of cathodic reactant. Most experiments were performed at ambient temperature, although some were performed at temperatures up to 85 C.

In practice the cell was assembled and steady state conditions of electrode potential and anolyte pH were allowed to develop. Next, the crevice and external electrodes were electrically connected through the ZRA and the resulting current flow, if any, was monitored by means of the proportional signal output from the ZRA. Relatively few experiments were conducted under freely corroding conditions because crevice corrosion did not occur at detectable rates in reasonable time intervals (about 24 hours). Therefore, the external electrode bundle usually was polarized anodically by means of an electronic potentiostat. Often a series of potentials was applied stepwise during a single experiment, which was terminated when the crevice specimen was dissolved.

Localized corrosion also was studied in crevices formed directly on the freely exposed surfaces of amorphous filaments. These in situ crevices were produced by cold rolling the filaments by a reduction of up to 30 percent. Although the crevices could not be detected by SEM examination of surfaces of the cold rolled filaments, all experimental evidence indicates that they indeed were created during the deformation process. Corrosion also was studied on filament surfaces deformed in compression with a tool steel punch. Thinning the filaments in compression with a punch produced intense deformation but without the simultaneous formation of tensile microcracks.

### Phase 2—Sputtering

All sputtering research reported in this document was performed at BNW. The sputtering was under the direct supervision of Dr. Dan Merz, with technical input from Dr. Shelly Dahlgren. Target material was supplied by Battelle's Columbus Laboratories.

Two targets were used for sputtering. Their compositions were essentially identical to those of the first and fifth alloys listed in Table 1, namely, 45Fe-30Ni-2Cr-2V-15P-6B and 31Fe-30Ni-16Cr-2V-15P-6B. The melts were homogenized by periodic agitation and holding at temperature for about one hour, then they were poured in vacuum into suitable molds. The resulting ingots were ground into cylindrical configurations suitable for use as sputtering targets and shipped to BNW for sputtering. Sputtering was performed in a krypton atmosphere onto copper substrates. The rate of sputtering was about 25 to 40  $\mu\text{m/hr}$ . The 16 Cr alloy was sputtered, in separate experiments, onto copper that either was water cooled or cooled by liquid nitrogen. The 2 Cr alloy was sputtered only onto a liquid nitrogen chilled substrate. A photograph of part of a sputtered deposit is shown in Figure 5.

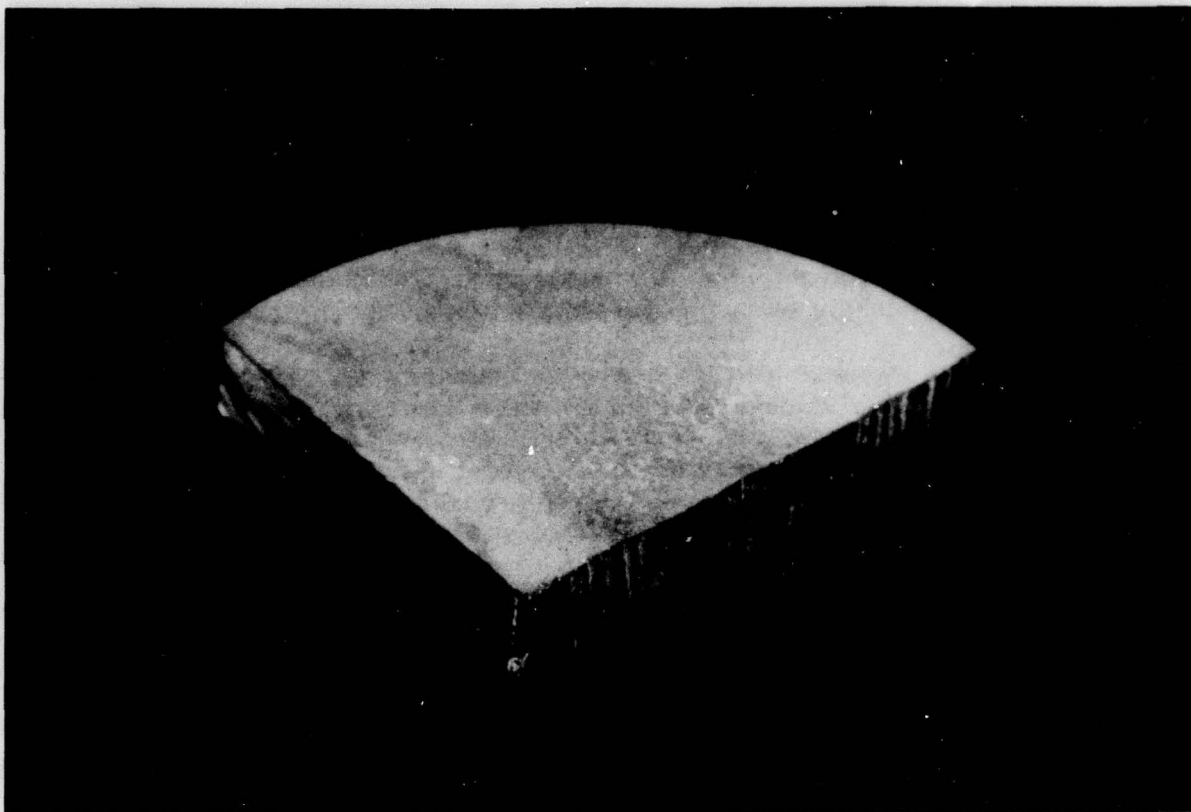


**FIGURE 5. WEDGE-SHAPED SECTION OF A SPUTTERED DEPOSIT ON COPPER SUBSTRATE. THE DEPOSIT IS ABOUT 75  $\mu\text{m}$  THICK**

Because of the novel method of fabrication of the sputtered deposits, their structure was studied in some detail. Their physical properties were characterized by SEM (surface topography), X-ray fluorescence (composition), X-ray diffraction, TEM and selected area electron diffraction (state of crystallinity), and differential scanning calorimetry (temperature and heat of crystallization). The deposits also were evaluated by potentiodynamic and potentiostatic polarization in acidified chloride solutions. Open circuit corrosion rates were measured by exposure of pre-weighed specimens in glass vessels containing a corrodent, and then re-weighing to determine the weight lost by corrosion. For most of the research the deposits were left intact on the copper substrates, which were masked with an inert lacquer in preparation for anodic polarization experiments. However, for DSC and weight loss measurements the deposits first were removed from their substrates by dissolving the copper in concentrated nitric acid. The acid did not noticeably affect the deposits during the brief exposure periods involved.



## RESULTS AND DISCUSSION

### Phase 1—Localized Corrosion

#### Structural Characterization of Melt Spun Alloys

Several melt spun alloys were evaluated by DSC to determine whether they exhibited the sharp, narrow peaks characteristic of crystallization of metallic glasses. These peaks were readily apparent, as shown in Figure 6. The crystallization temperatures were: 2 Cr, 427 C; 7 Cr, 437 C; and 16 Cr, 476 C. These temperatures are within the 400-500 C temperature range in which amorphous Fe-Ni-Cr-P-B alloys are known to crystallize. It is therefore concluded that the alloys produced at Battelle by melt spinning were amorphous in the current sense of the term.<sup>(a)</sup>

#### Polarization in Simulated Crevice Solutions

Behavior of the amorphous and crystalline alloys in simulated crevice solutions was characterized extensively by potentiodynamic and potentiostatic polarization. These experiments were performed to predict: (a) whether crevice corrosion should logically be expected to occur; (b) whether it should be severe or slight relative to crevice corrosion of crystalline alloys; and (c) the degree to which increasing the chromium content could be expected to ameliorate the severity of attack encountered in crevices.

Data from a series of polarization curves are condensed and presented in Figures 7 and 8. These figures show the dependences of the critical current density required to initiate passivity,  $i_c$ , and the minimum passive current density,  $i_p$ , on chromium content for two chloride solutions. In Figure 7 it is evident that  $i_c$  decreased by a factor of 30 and  $i_p$  by a factor of 5 when chromium was increased from 2 to 16 atomic percent. In Figure 8,  $i_c$  and  $i_p$  were decreased by factors of 92 and 3, respectively, over the same chromium range. Several features of this polarization behavior are noteworthy:

- (1) The degree of passivity achieved by the 2 Cr alloy was remarkably good ( $5 \cdot 10^{-6}$  and  $9.7 \cdot 10^{-6}$  A/cm<sup>2</sup>) considering the extremely corrosive nature of these two electrolytes.
- (2) The effect of increasing the chromium content was much stronger on facilitating passivation than on enhancing the degree of passivity ultimately reached.
- (3) Although it is not evident in these figures, these alloys did not exhibit localized corrosion attack<sup>(b)</sup> at potentials below that required for oxygen evolution, which was about 1 V(SCE) and above.

(a) The term "amorphous" as used in this report refers to materials that do not possess crystallinity which is detectable by straightforward techniques, such as DSC, selected area electron diffraction, and X-ray diffraction.

(b) Intense scrutiny by SEM revealed an occasional pit that grew to less than 10  $\mu$ m in depth, and then apparently stopped growing and passivated.

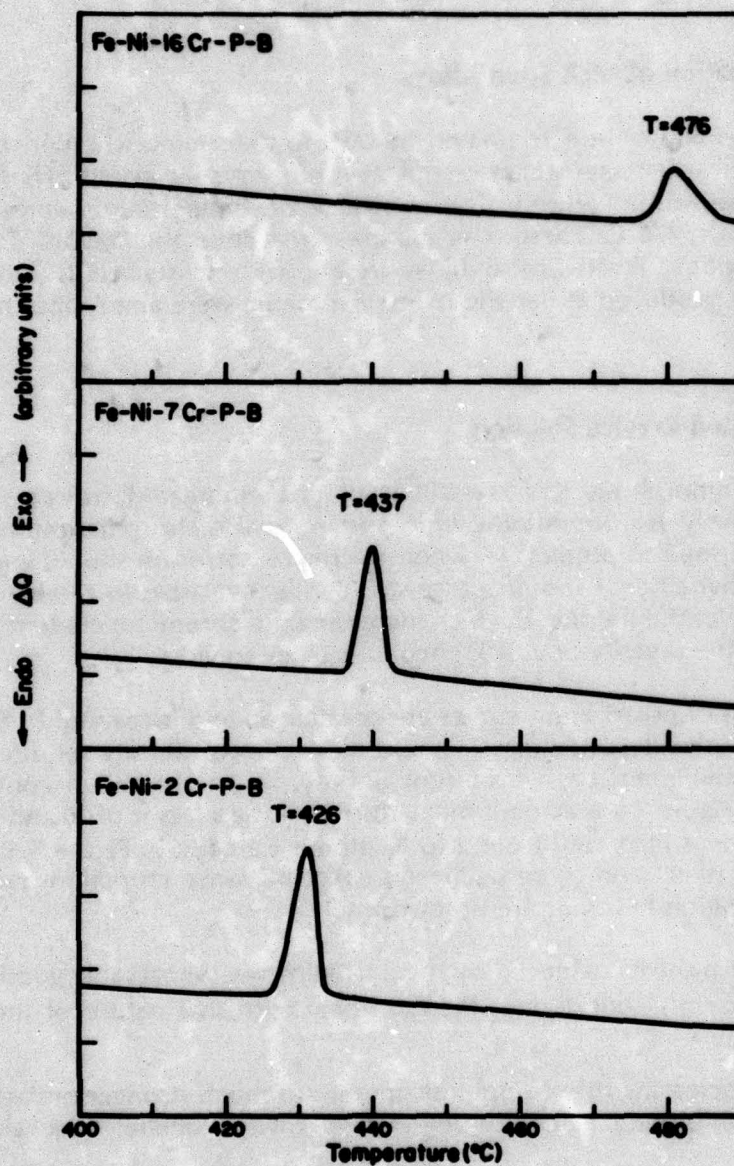


**FIGURE 6. DIFFERENTIAL SCANNING CALORIMETRY (DSC) CURVES FOR MELT SPUN ALLOYS WITH INDICATED Cr CONTENTS. SCAN RATE WAS 5 C/MINUTE. PEAKS INDICATE EXOTHERMIC CRYSTALLIZATION**



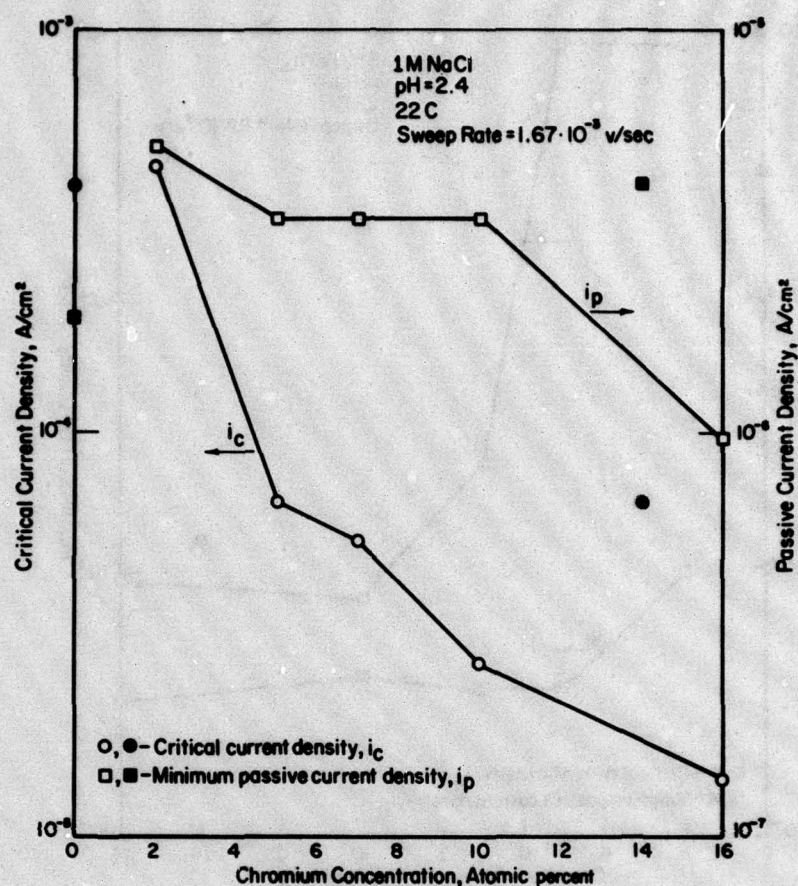


**FIGURE 7. CRITICAL AND PASSIVE CURRENT DENSITIES VERSUS Cr CONTENT FOR AMORPHOUS ALLOYS POLARIZED IN 1 M NaCl, pH 2.4. OPEN SYMBOLS REFER TO ALLOYS PRODUCED AT BATTELLE AND SOLID SYMBOLS REFER TO METGLAS 2826 AND 2826A**

- (4) The Metglas 2826A alloy exhibited deviations in  $i_c$  and  $i_p$  generally by factors of 10 or less relative to data obtained from the BCL alloys. Metglas 2826A displayed higher corrosion rates even though it contained more Ni and less Fe than the in-house alloys.

Paralleling the second observation above, the effect of chromium in crystalline alloys also has been observed to decrease  $i_c$  by a greater degree than  $i_p$ <sup>(12)</sup>. Apparently, chromium is needed to enhance protection of films formed at potentials corresponding to active dissolution of the Fe-Ni-P-B alloy, because at these potentials the oxidation products of iron are more soluble than those of Cr<sup>(13)</sup>. At more noble potentials corresponding to passivity of Fe-

(12) Beauchamp, R. L., "Polarization Characteristics of High-Purity Iron-Rich Iron-Chromium-Nickel Alloys in Sulfuric Acid Solutions", Ph.D. dissertation, The Ohio State University, 1966.

(13) Okamoto, G., "Passive Film on 18-8 Stainless Steel-Structure and Its Function", Corr. Sci., 13, 471 (1973).

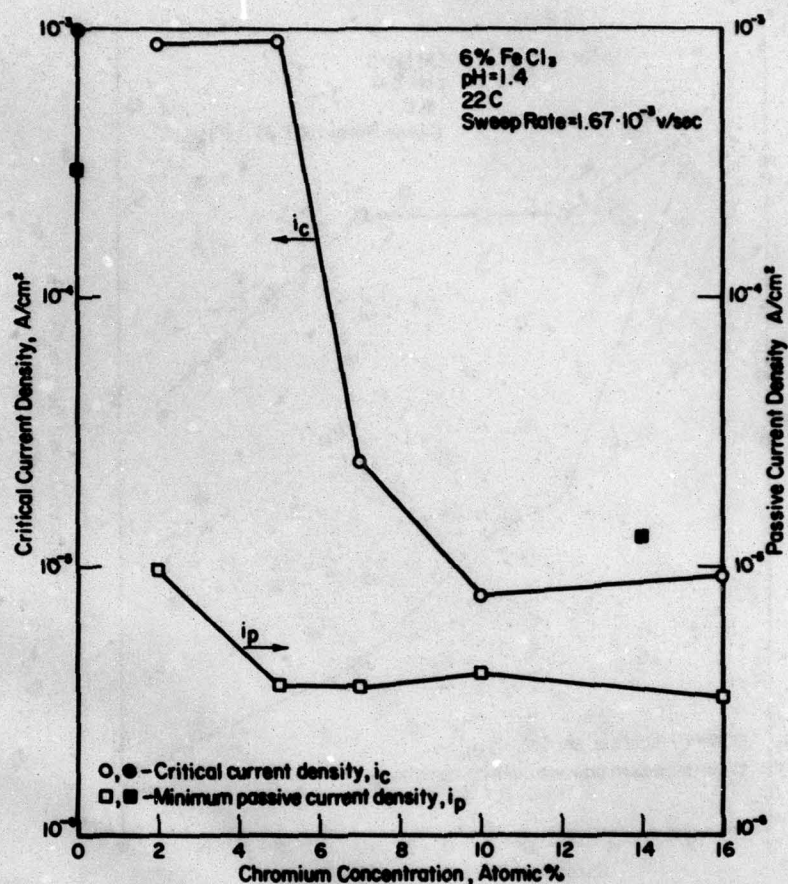


**FIGURE 8. CRITICAL AND PASSIVE CURRENT DENSITIES VERSUS Cr CONTENT FOR AMORPHOUS ALLOYS POLARIZED IN 6 PERCENT FeCl<sub>3</sub>, pH 1.4. SEE FIGURE 7 FOR EXPLANATION OF SYMBOLS**

Ni-P-B, the role of Cr is less significant because iron is able to develop a fairly protective passive film by itself. Here, the effect of Cr is to enhance the protection provided by the passivating iron-rich layer.

The above data can be used to predict several features concerning crevice and other forms of localized corrosion of these amorphous alloys. For localized corrosion or occluded cell corrosion (O.C.C.) to occur, an alloy must exhibit two features regarding polarization behavior. First, it must be able to passivate in the electrolyte of interest. Second, increasing the chloride level and/or decreasing the pH should accelerate the rate of attack. This type of behavior ensures stability of active-passive cells on the alloy surface, and hence the possibility of O.C.C. The first of these requirements, i.e., existence of passive behavior, is satisfied for the amorphous alloys as shown in Figures 7 and 8. The pH dependence is discussed below.

The effect of pH on polarization behavior is documented in Figures 9 through 13. Figures 9 through 12 show potentiodynamic polarization curves for BCL alloys with chromium contents of 0, 2, 7, and 16 atomic percent. The effect of decreasing the pH from 7



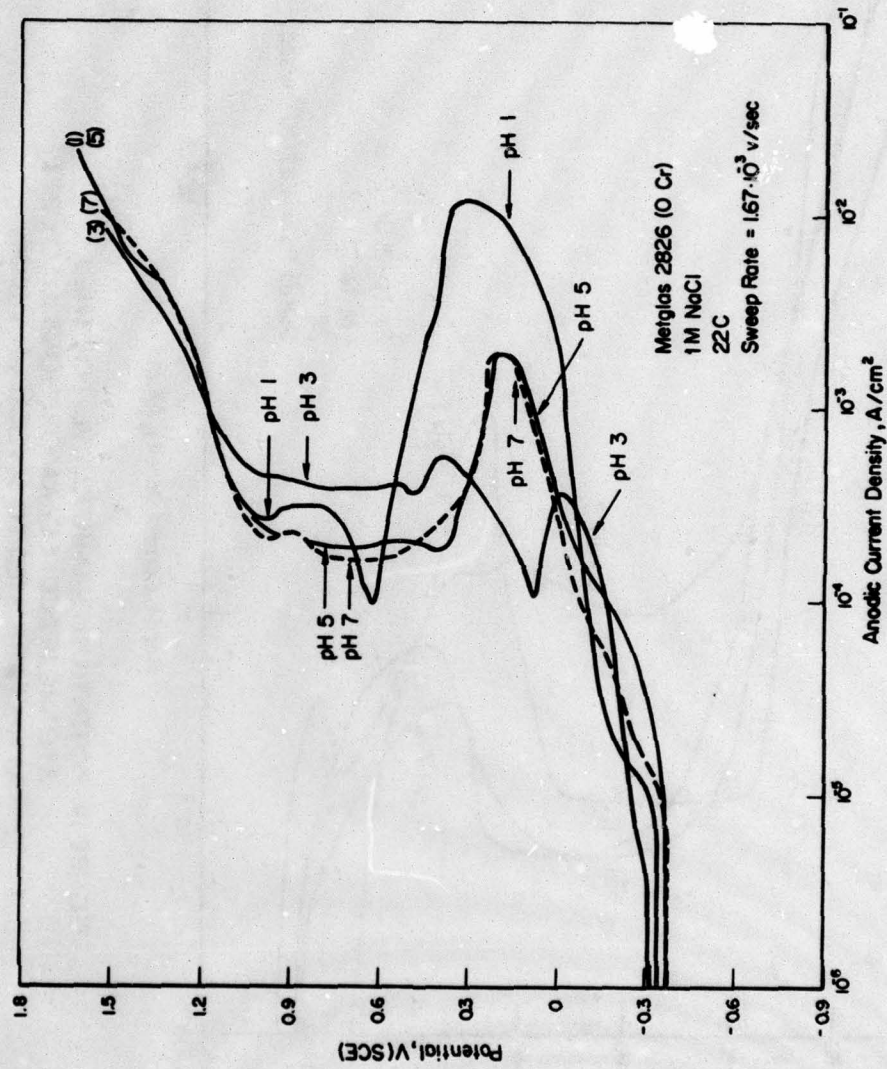


FIGURE 9. POTENTIODYNAMIC POLARIZATION CURVES  
FOR THE 0 ATOMIC PERCENT Cr AMORPHOUS  
ALLOY (METGLAS 2826) IN 1 M NaCl ADJUSTED  
TO SEVERAL pH VALUES

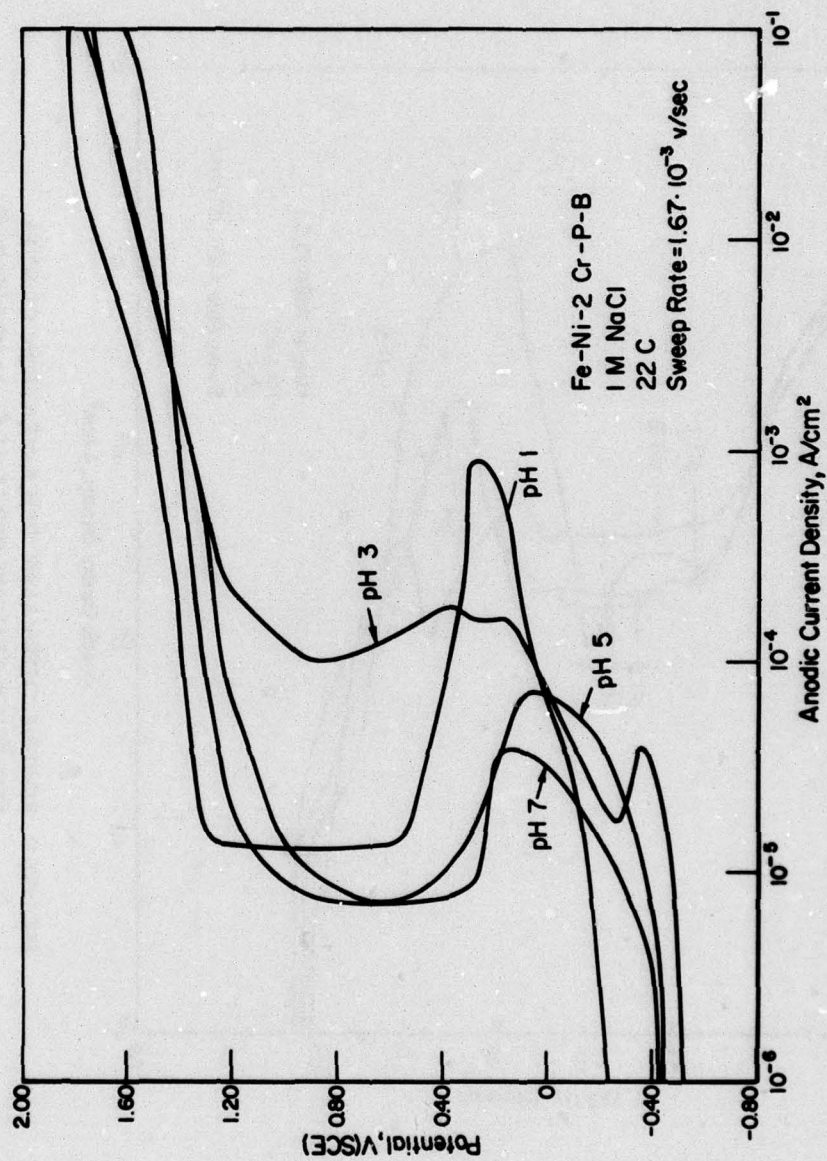


FIGURE 10. POTENTIODYNAMIC CURVES FOR THE 2 ATOMIC PERCENT Cr AMORPHOUS ALLOY IN 1 M NaCl ADJUSTED TO SEVERAL pH VALUES



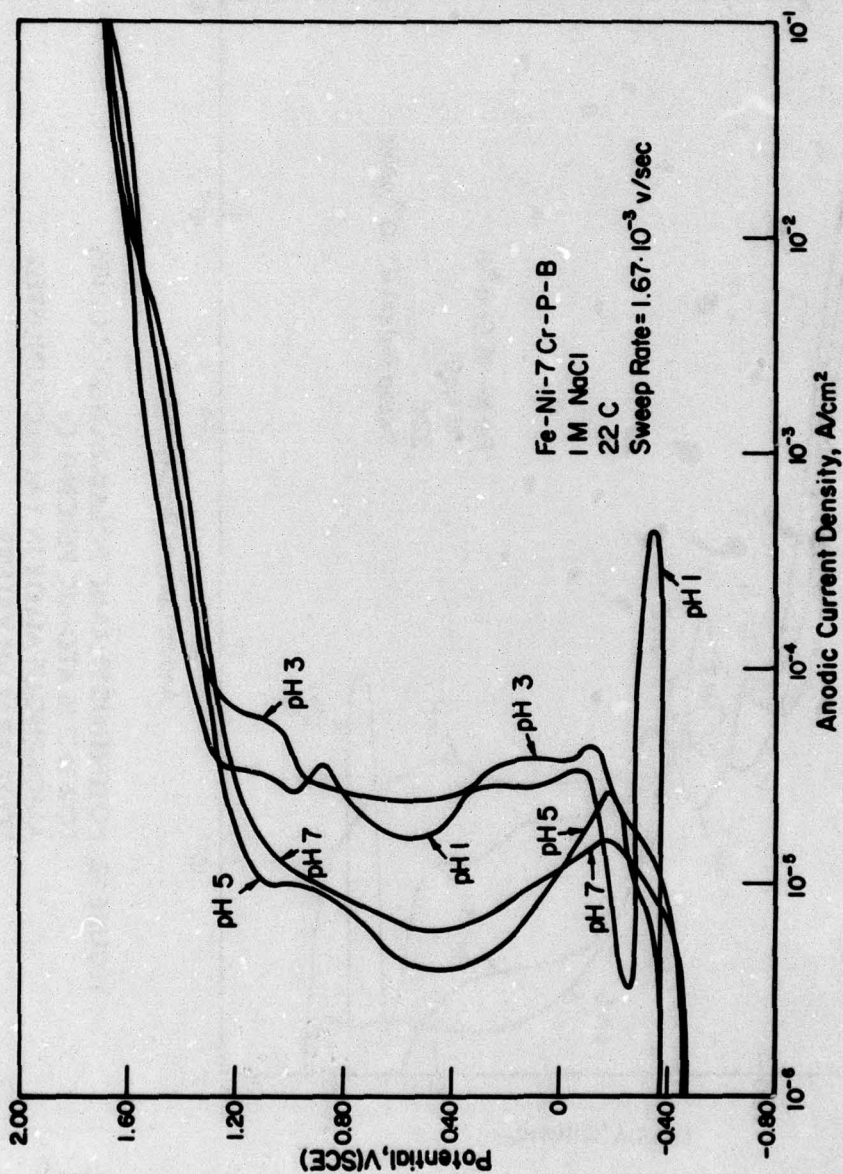


FIGURE 11. POTENTIODYNAMIC POLARIZATION CURVES  
FOR THE 7 ATOMIC PERCENT Cr AMORPHOUS  
ALLOY IN 1 M NaCl ADJUSTED TO SEVERAL pH  
VALUES

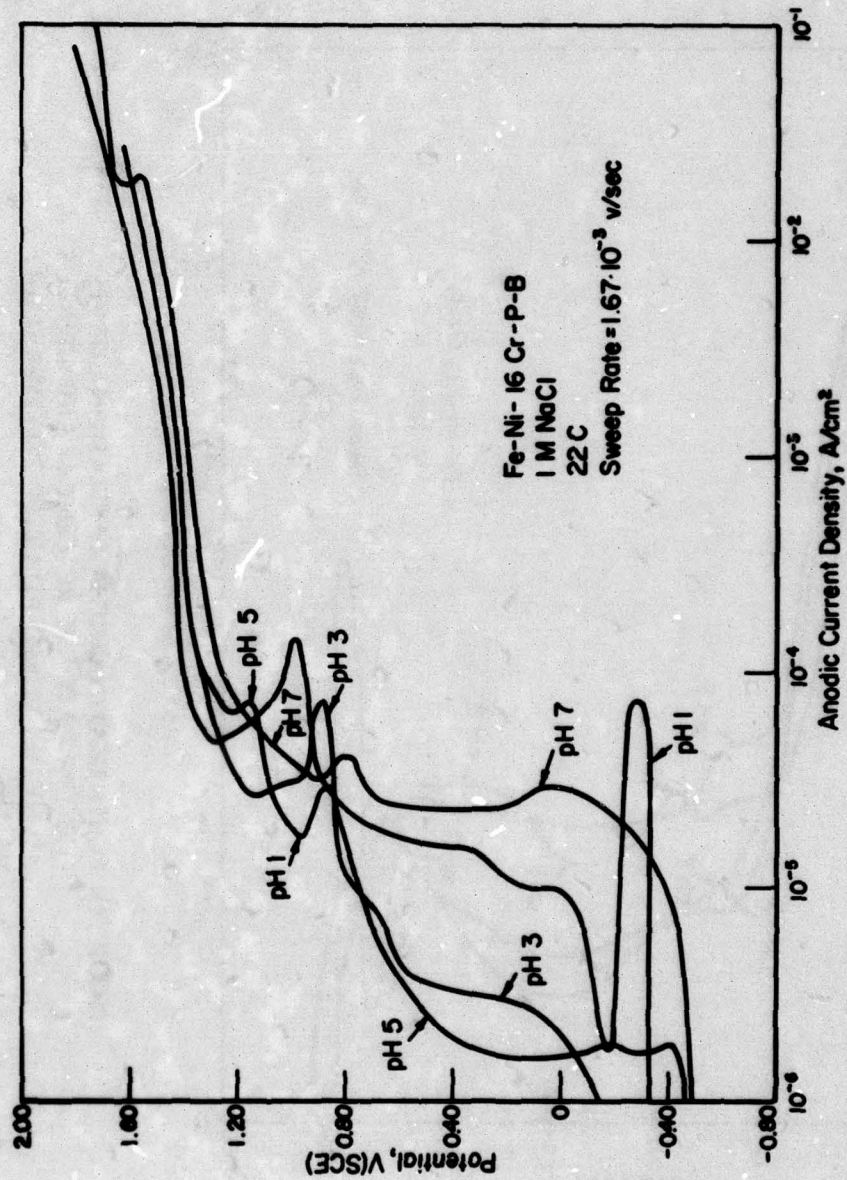


FIGURE 12. POTENTIODYNAMIC POLARIZATION CURVES  
FOR THE 16 ATOMIC PERCENT Cr  
AMORPHOUS ALLOY IN 1 M NaCl ADJUSTED  
TO SEVERAL pH VALUES



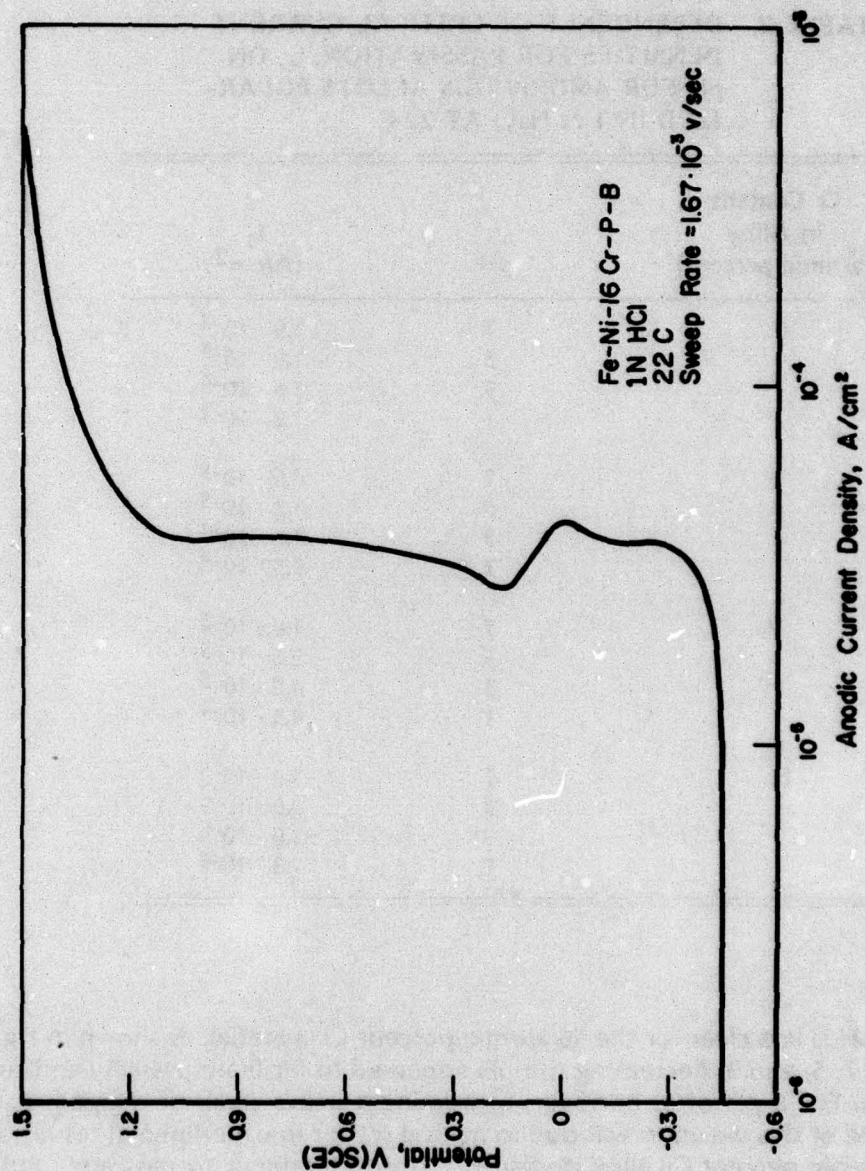


FIGURE 13. POTENTIODYNAMIC POLARIZATION CURVE  
FOR THE 16 ATOMIC PERCENT Cr AMORPHOUS  
ALLOY IN 1 N HCl

to 1 is straightforward for the 2 and 7 atomic percent chromium alloys, Figures 10 and 11. Specifically, as pH decreased  $i_c$  increased uniformly, although  $i_p$  exhibited no obvious dependence. Acidification of the electrolyte, therefore, intensified active dissolution, as required for the occurrence of O.C.C. The dependence of  $i_c$  on pH is shown in Table 2.

**TABLE 2. DEPENDENCE OF CRITICAL CURRENT DENSITIES FOR PASSIVATION,  $i_c$ , ON pH FOR AMORPHOUS ALLOYS POLARIZED IN 1 M NaCl AT 22 C**

Cr Content in Alloy (atomic percent)	pH	$i_c$ (A/cm <sup>2</sup> )
0	7	$1.9 \cdot 10^{-3}$
	5	$1.9 \cdot 10^{-3}$
	3	$5.6 \cdot 10^{-4}$
	1	$1.2 \cdot 10^{-2}$
2	7	$4.0 \cdot 10^{-5}$
	5	$7.3 \cdot 10^{-5}$
	3	$1.8 \cdot 10^{-4}$
	1	$9.5 \cdot 10^{-4}$
7	7	$1.6 \cdot 10^{-5}$
	5	$2.6 \cdot 10^{-5}$
	3	$4.2 \cdot 10^{-5}$
	1	$4.3 \cdot 10^{-4}$
16	7	$2.9 \cdot 10^{-5}$
	5	$2.0 \cdot 10^{-6}$
	3	$3.0 \cdot 10^{-6}$
	1	$7.3 \cdot 10^{-4}$

The role of pH is less clear for the 16 atomic percent Cr material, as shown in Figure 12. For pH values of 7, 5, and 3, decreasing the pH appeared to facilitate passivity and suppress active dissolution. For a pH of 1, however, a prominent active peak developed. It is conceivable that some of this variation was due to natural scatter in experimental results. For example, the 16 atomic percent Cr alloy displayed a strong tendency to passivate, and it was difficult to activate the alloy (by cathodic polarization) and to measure reproducible active peaks. Another possibility is that differences in corrosion behavior between the two surfaces of the filaments contributed to the scatter. Perhaps abrasion prior to polarization would have been a better surface pretreatment than cathodic polarization.



Figure 13 shows polarization behavior of the 16 Cr alloy in 1 N HCl. This curve was generated to depict dissolution behavior in one of the most corrosive solutions that is believed to exist in a pit, i.e., a solution of pH near zero and of molar concentration in chloride ion. A slight active loop is evident with  $i_c$  about  $4.2 \cdot 10^{-5}$  A/cm<sup>2</sup>. The passive current density was in the range of about  $3.0$  to  $3.8 \cdot 10^{-5}$  A/cm<sup>2</sup>, and secondary passivity was not observed.

A comparison of polarization behavior of amorphous alloys with that of crystalline stainless steels is made in Figure 14. Results from Incoloy 800 are particularly significant because the Fe, Ni, and Cr contents of this alloy are somewhat similar to those of the amorphous 16 Cr alloy, but Incoloy 800 is crystalline. Thus, the effects of the three metallic alloy additions can be separated according to state of crystallinity and difference in alloy homogeneity. However, a more strict comparison would necessitate similar P and B levels in the Incoloy 800 alloy as are in the amorphous alloy, but such a composition was not attainable without copious intermetallic phases being present. In essence, both crystalline alloys suffered O.C.C. (in this case, pitting), which initiated at about 0.15 V(SCE). The occurrence of pitting in this electrolyte was expected, and it serves to emphasize the relatively greater resistance to O.C.C. of the amorphous alloys. It is apparent that the corrosion resistance of the amorphous alloys does not derive from the particular levels or ratios of Fe, Ni, and Cr present, as evidenced by the severe pitting of the Incoloy 800. Rather, the effect is far more subtle and presumably results from the homogeneity and unique compositions of the amorphous materials.

To summarize the data presented thus far, it has been shown that the amorphous melt spun alloys exhibit active-passive transitions in chloride solutions, and that acidification of the solutions increases the active dissolution kinetics markedly<sup>(a)</sup>. These facts, and the known dependency of chromium-containing alloys on dissolved oxygen for maintaining passivity, can be used to predict that some degree of susceptibility to crevice corrosion, and O.C.C. in general, exists for the amorphous alloys. That is, depletion of oxygen within a crevice and subsequent pH decrease due to corrosion is expected to establish an active-passive cell capable of maintaining accelerated corrosion. A comparison of corrosion kinetics with crystalline stainless steels suggests, however, that the amorphous alloys should display greater resistance to O.C.C. than the crystalline steels.

Several experiments were performed potentiostatically at various anodic potentials to assess the importance of time on the kinetics of corrosion. That is, because crevice corrosion often takes hours (or longer) to initiate, it was considered advisable to measure dissolution kinetics in simulated crevice solutions over extended time intervals. An interval of one hour generally provided sufficient indication of whether the alloy was passivating or beginning to lose its passive nature. Results of potentiostatic polarization of the 2 atomic percent chromium alloy in pH 2.4, 1 M NaCl are shown in Figure 15. It is apparent that polarization at 0.60 V(SCE) resulted in protective film growth as evidenced by the decrease in current with increasing polarization time. No localized corrosion occurred during the 60-minute polarization period, as verified by subsequent scanning electron microscope (SEM) analysis of the specimen. Note that the potential of 0.60 V(SCE) is well anodic to that which causes pitting of the crystalline stainless alloys represented in Figure 14, yet this low-chromium alloy did not

(a) The effect of chloride concentration has not been included in this characterization of amorphous alloys. It has been demonstrated that the effect of varying the chloride ion concentration over the range 0.02 to 2.0 M exerts a relatively small effect on the polarization behavior of an amorphous chromium-containing alloy, namely, Metglas 2826A<sup>(6)</sup>.

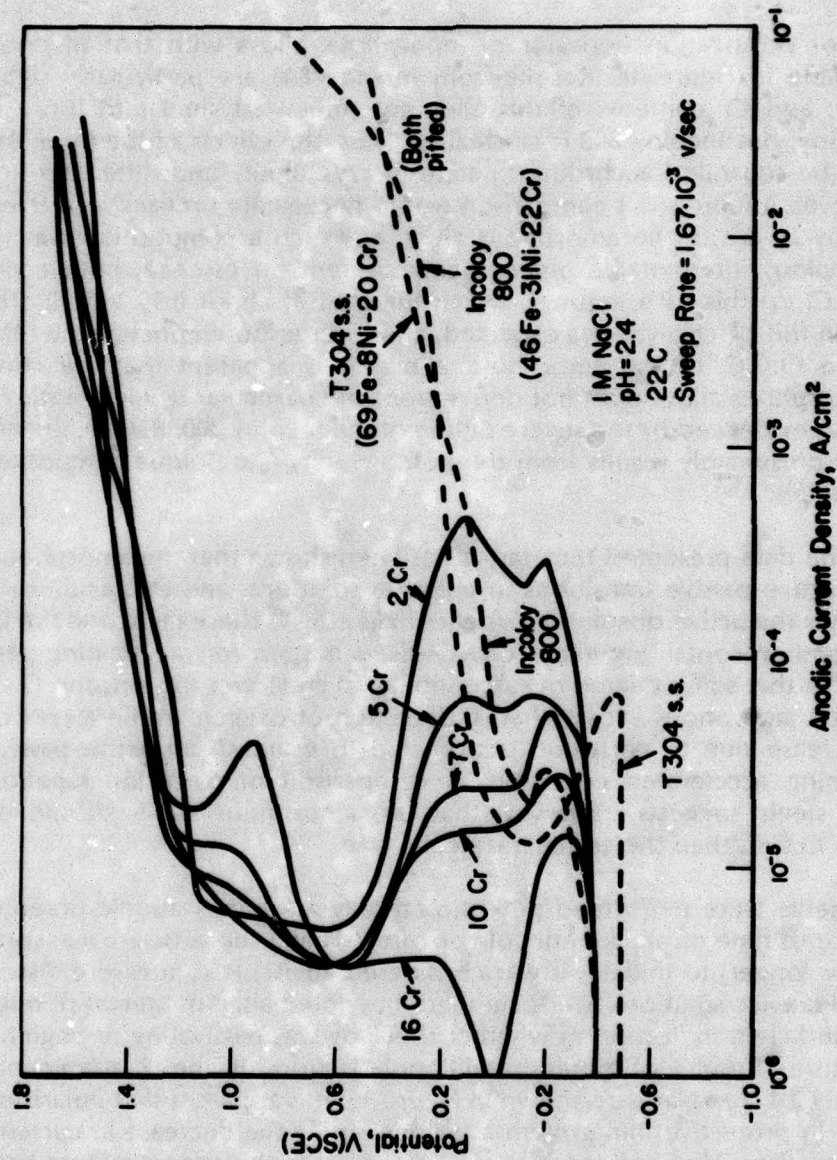


FIGURE 14. POTENTIODYNAMIC POLARIZATION CURVES FOR AMORPHOUS MELT SPUN ALLOYS OF THE INDICATED Cr CONTENTS, AND FOR CRYSTALLINE T304 AND INCOLOY 800 ALLOYS



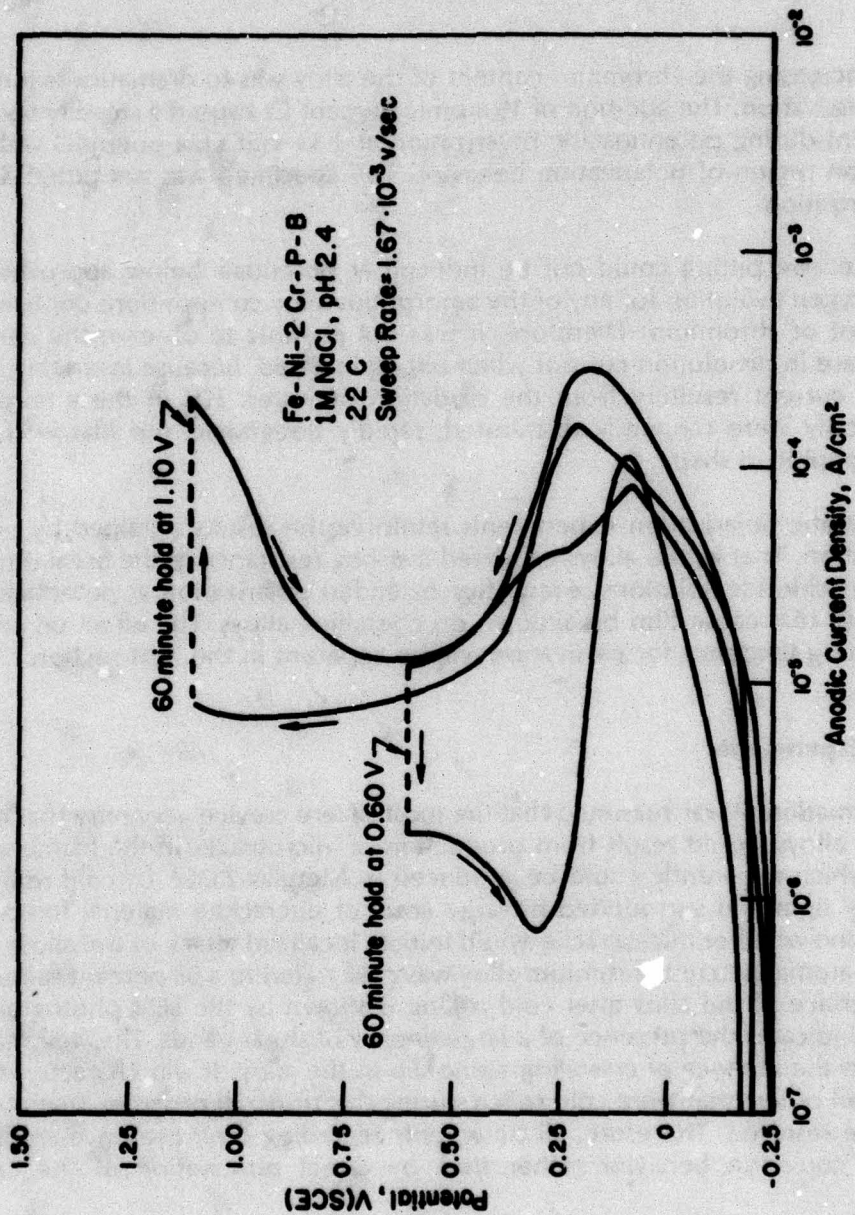


FIGURE 15. POTENTIODYNAMIC/POTENTIOSTATIC  
POLARIZATION CURVES FOR THE 2 ATOMIC  
PERCENT Cr AMORPHOUS ALLOY

undergo pitting. The potential of 1.10 V(SCE) is at the anodic end of the passive potential region (refer to Figure 14). The current density increased from  $8 \cdot 10^{-6}$  to  $2.1 \cdot 10^{-4}$  A/cm<sup>2</sup> over the 60-minute period, suggesting that pitting may have occurred. Although some positive hysteresis occurred during the return sweep, this hysteresis disappeared at 0.3 V(SCE). Examination of the specimen surface by SEM revealed no localized attack whatsoever, even though scratches on the surface had been made with 600 grit silicon carbide paper prior to polarization to penetrate any existing oxide film, and thereby to provide sites for easy initiation of O.C.C.

The effect of increasing the chromium content of the alloy was to dramatically increase the tendency for passivation. The addition of 16 atomic percent Cr caused a steadily decreasing corrosion current during potentiostatic polarization at 1.33 V(SCE), a potential well into the oxygen evolution region of polarization behavior. This specimen was not pitted during the 60 minute polarization.

In general, extensive pitting could not be induced at potentials below approximately that required for oxygen evolution for any of the amorphous alloy compositions containing 2 to 16 atomic percent of chromium. Therefore, it was not possible to observe the conventional sudden increase in dissolution current when pitting initiated, because invariably it was masked by a large current resulting from the oxidation of water. Pits in the amorphous Battelle alloys typically were randomly distributed, rapidly penetrated the filaments, and were non-crystallographic in shape.

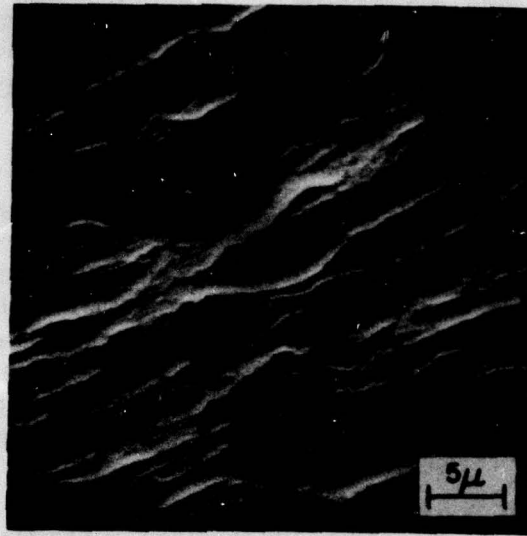
These potentiostatic polarization experiments reinforce the results obtained by potentiodynamic polarization. That is, the alloys exhibited a strong resistance to the breakdown of passivity in acidified chloride solutions, even after extended polarization at potentials that were anodic to those that cause film breakdown on crystalline alloys. The effect on crevice corrosion of this strong tendency for passivation will be apparent in the next section.

### Crevice Corrosion Experiments

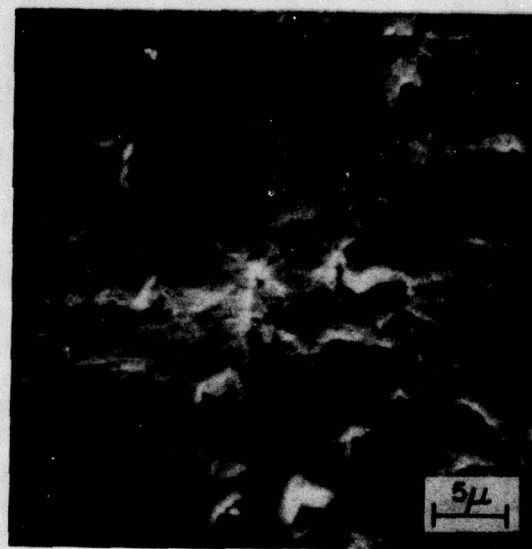
**Effects of Deformation.** It was reasoned that the most severe crevice geometry that could be formed in these alloys would result from production of microcracks in the filament surface. Such cracks, which apparently could be produced in Metglas 2826A by cold rolling<sup>(6)</sup>, would be extremely tight and surrounded by large areas of uncracked material to act as a cathode. To determine whether microcracks would initiate localized attack of the alloys used in this study, the 16 atomic percent chromium alloy was cold rolled to a 38 percent reduction in thickness. The surface of the alloy after cold rolling is shown by the SEM photograph in Figure 16(a), which indicates the presence of a large density of shear bands. The wavy nature of the bands reflects the absence of crystallographic slip in the alloy. It was characteristic of this specimen, and all others that were cold rolled during this research program, that no surface cracks could be resolved. Therefore, all statements regarding their presence are made by inference from corrosion behavior rather than by direct observation of the cracks themselves.

Following cold rolling, the specimens were ultrasonically cleaned in trichloroethylene and acetone, and then potentiostatically polarized in 1 M NaCl at pH 7. Polarization was performed at 0.60 V(SCE), a potential that was expected to be sufficiently anodic to promote crevice corrosion if it would indeed occur. Examination of the cold rolled specimen by SEM, Figure 16(b), revealed many small pits ranging up to about 5  $\mu$ m in diameter. The pits were





(a)



(b)

**FIGURE 16. SEM PHOTOGRAPHS OF METGLAS 2826A AFTER A 25 PERCENT REDUCTION IN THICKNESS BY COLD ROLLING. (a) AS-ROLLED SURFACE; (b) AFTER POLARIZATION FOR ONE HOUR AT 0.60 V(SCE) IN 1 M NaCl, pH 7**

never observed to penetrate the specimen. Examination of a polarized companion specimen that had not been cold rolled showed only three pits, and these were also less than about 5  $\mu\text{m}$  in diameter. The pit density was several orders of magnitude greater on the cold rolled specimen.

Typical results of polarizing a heavily cold rolled (i.e., greater than about 25 percent) specimen and an as-melt spun companion specimen are summarized in Figure 17. Cold rolling caused a large active dissolution peak, and it increased the passive current density significantly over that of the as-spun specimen. However, during the 60-minute arrest at 0.60 V(SCE) the current density decreased rather than increased, the latter being expected if crevice corrosion were increasing in severity. At the end of the 60-minute arrest a negative hysteresis was observed, which again was unexpected based on the assumed occurrence of crevice corrosion during the forward potential sweep. As in the experiment just described, the cold rolled filament was heavily pitted after polarization and the non-cold rolled specimen was not.

The difference in corrosion behavior of the two materials can be rationalized as follows. Upon anodic polarization the microcracks in the cold rolled alloy initiated crevice corrosion, and the measured anodic current density was greater than that for the undeformed alloy. However, after the crevices had grown during the anodic potential scan, during which they widened and became pit-shaped, the electrolyte within each one became diluted with bulk electrolyte. By this point, about the time the 60-minute potentiostatic arrest was complete, all microcracks had corroded, widened, and then passivated as bulk electrolyte mixed with that previously present in them. Previous data show that the bulk electrolyte composition of 1 M NaCl at pH 7 is not sufficiently aggressive to destroy passivity at 0.60 V(SCE); hence, ingress of the electrolyte would indeed be expected to have resulted in passivation at this potential.

The hypothesis that surface microcracks cause a transient type of crevice corrosion that ceases once the cracks widen was tested in two ways. One was to polarize a cold rolled specimen in such a way as to exhaust all sites for crevice attack, and then determine if its subsequent polarization behavior returned to that of a non-deformed specimen. In other words, once all microcracks are widened by corrosion and passivated, they should not influence anodic polarization behavior during subsequent experiments. To test the validity of this hypothesis, a strip of Metglas 2826A was cold rolled to about 30 percent reduction in thickness and polarized for one hour at 0.60 V(SCE) in 1 M NaCl, pH 7. During this time the specimen exhibited enhanced anodic dissolution relative to a non-deformed counterpart; furthermore, after polarization the surface was heavily pitted. After observation by SEM the same specimen was reinserted into the electrolyte and a potentiodynamic anodic polarization curve was obtained. This curve, together with a curve of a non-deformed filament, are displayed in Figure 18. The nearly coincident nature of the two curves supports the hypothesis that microcracks are the cause of the transient localized attack of cold rolled filaments. Additional evidence is presented in Figure 19, which shows the surface of cold rolled Metglas 2826A after the first (potentiostatic) polarization 0.60 V(SCE), and another region after potentiodynamic polarization to 1.50 V(SCE) and back to the free corrosion potential. The morphology of attack, especially pit depth and number of pits per unit area, is similar for the regions shown in Figure 19(a) and 19(b), again indicating that the second polarization did not create significant new localized attack.

The foregoing represents one test of the hypothesis that surface microcracks were the cause of localized attack. However, an alternate explanation is that the intense cold work at certain shear bands caused localized crystallization, and that these crystalline regions ex-



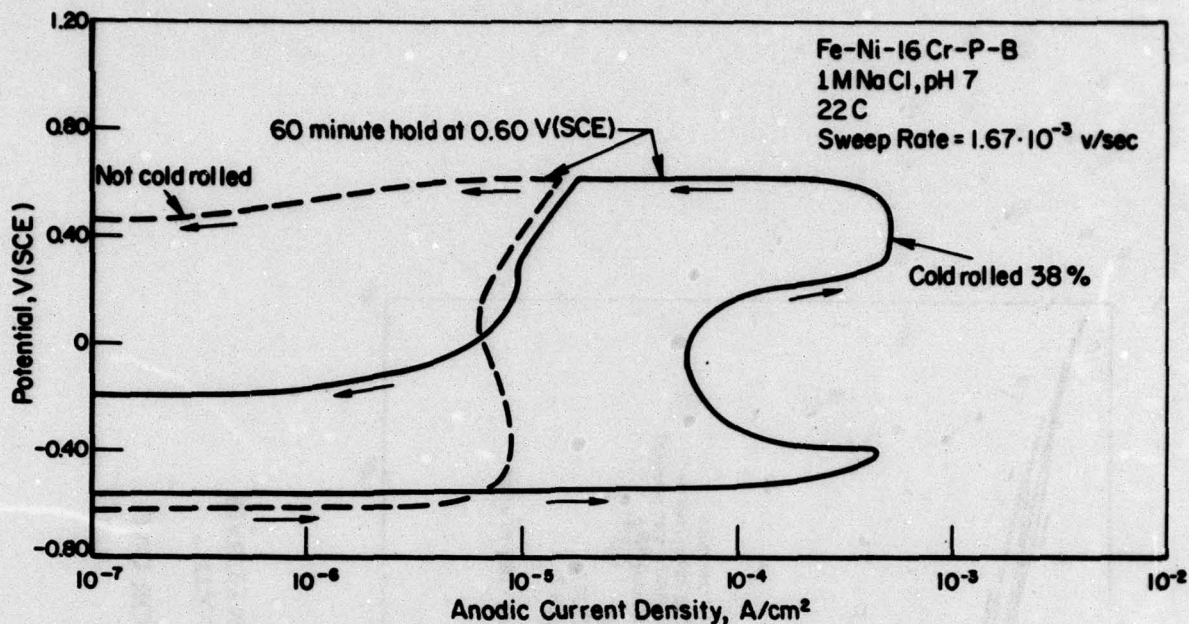


**FIGURE 17. POTENTIODYNAMIC/POTENTIOSTATIC POLARIZATION CURVES FOR THE 16 ATOMIC PERCENT Cr AMORPHOUS ALLOY IN THE UNDEFORMED AND COLD ROLLED CONDITIONS**

perienced accelerated attack. (Metglas 2826A is known to corrode at very rapid rates after thermal crystallization.<sup>(2)</sup>). It was reasoned that intense deformation of filaments with the absence of microcrack formation, should result in polarization behavior that is similar to that of non-deformed filaments, if microcracks and not localized crystallization were the necessary criterion. Deformation in the absence of microcrack formation was achieved by reducing the filament thickness by compression. Specifically, filaments were cold reduced up to about 20 percent in thickness by impact with a tool steel punch. Punching maintained a state of local compression during deformation, unlike cold rolling which created a state of tension on the specimen surface. Because the surface undergoing the most intense deformation was in a state of compression during punching, microcracks were not expected to develop. Results of one such experiment are presented in Figure 20, which shows deformed regions before and after polarization in 1 M NaCl at pH 7. Figure 20(a) documents the fact that the punching process produced intense localized deformation, as evident by the shear bands. Figure 20(b), which is another region of the same specimen after cleaning and polarizing at 0.60 V(SCE) for one hour, shows a complete absence of pits. Thus, deformation in the absence of microcrack formation apparently is not sufficient to produce localized attack during anodic polarization. This statement was verified by examining the surfaces of several specimens that had been thinned by punching and then anodically polarized; in no case was copious pitting observed of the type shown in Figure 19.

It is concluded that deformation of amorphous alloy filaments resulted in a crevice corrosion type of attack at potentials at and below 0.60 V(SCE) in neutral 1 M NaCl solution. It appears to be the cracks themselves, and not the deformation that accompanies crack formation, that promoted this attack. The crevices propagated by corrosion into the alloy to depths of only a few microns, at which time they widened and apparently passivated.

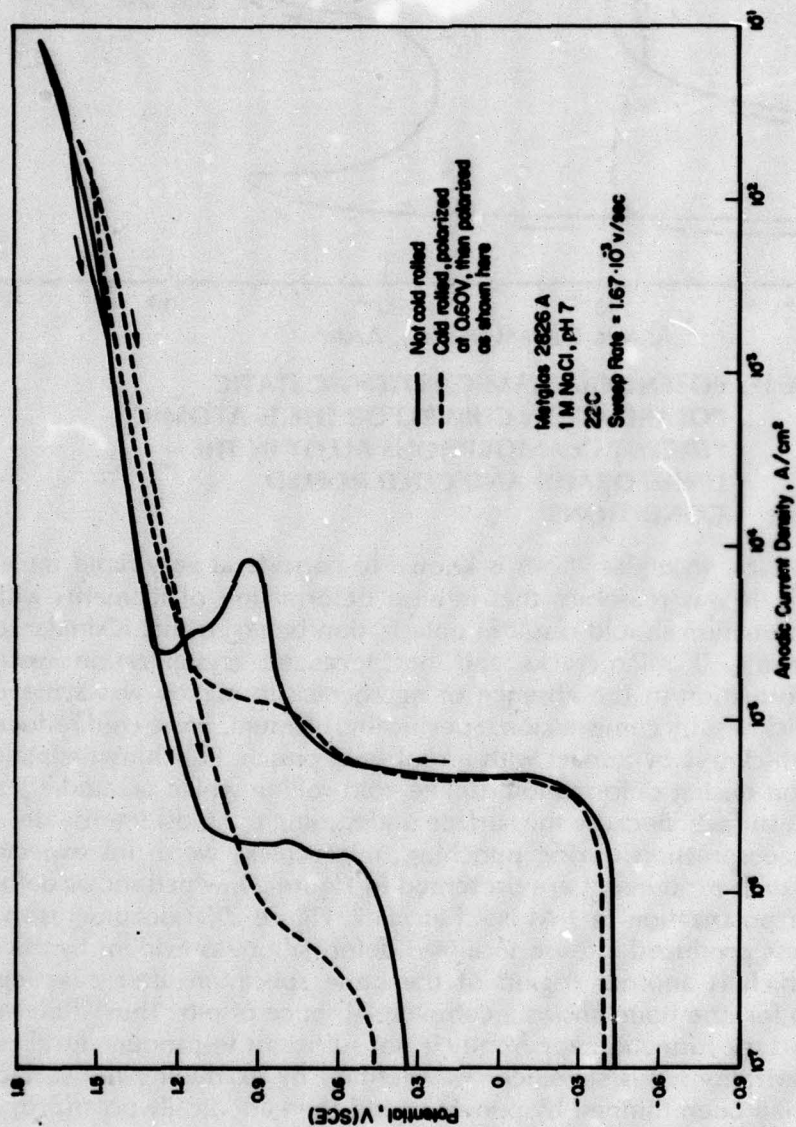
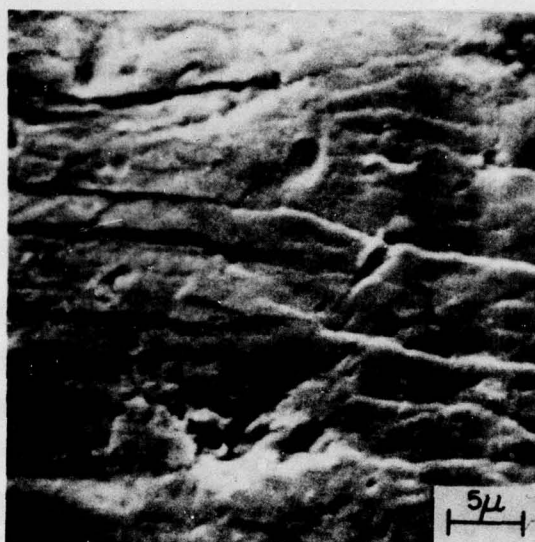
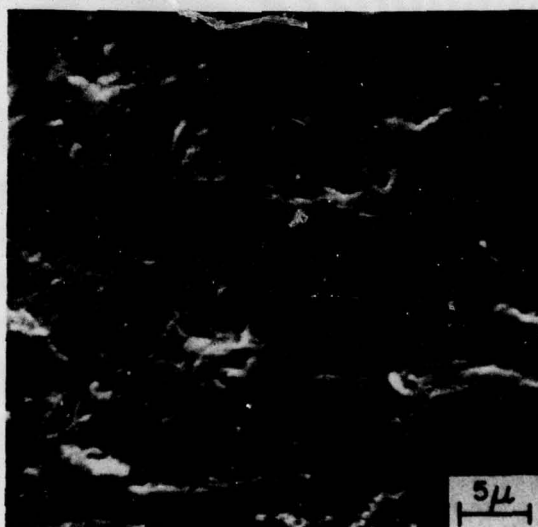


FIGURE 18. POTENTIODYNAMIC POLARIZATION CURVES  
 FOR METGLAS 2826A IN THE NON-COLD  
 ROLLED CONDITION, AND AFTER  
 POTENTIOSTATIC POLARIZATION FOR ONE  
 HOUR AT 0.60 V(SCE)



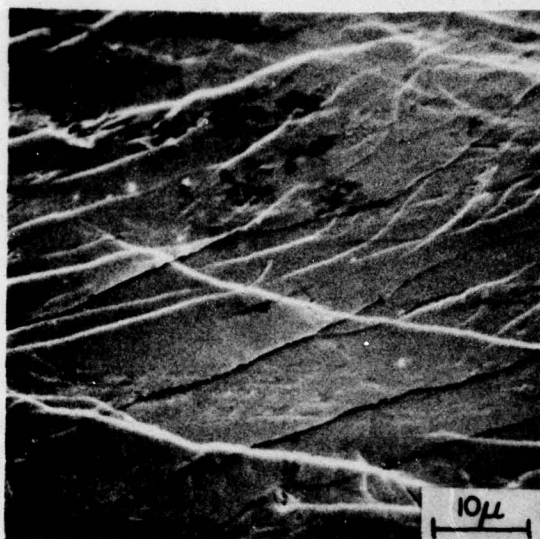


(a)

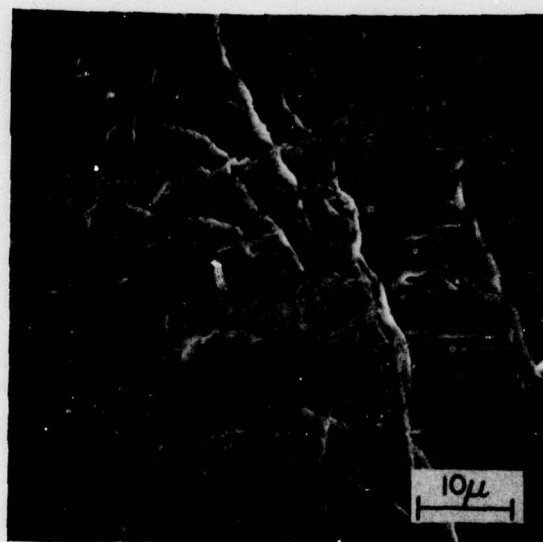


(b)

**FIGURE 19. SEM PHOTOGRAPHS OF SURFACE OF METGLAS 2826A FILAMENTS AFTER A 25 PERCENT REDUCTION IN THICKNESS. (a) PITS FOUND AFTER POLARIZATION FOR ONE HOUR AT 0.60 V(SCE) IN 1 M NaCl, pH 7. (b) ANOTHER REGION ON SAME SPECIMEN AFTER POTENTIODYNAMIC POLARIZATION TO 1.5 V(SCE) IN 1 M NaCl, pH 7**



(a)



(b)

**FIGURE 20. SEM PHOTOGRAPHS OF SURFACES OF METGLAS 2826A THAT WAS REDUCED IN THICKNESS BY ABOUT 10 PERCENT BY PUNCHING. (a) SURFACE AFTER PUNCHING; (b) ANOTHER REGION AFTER PUNCHING, THEN POLARIZATION FOR ONE HOUR AT 0.60 V(SCE) IN 1 M NaCl, pH 7**



**Sandwich-Type Crevice Cell.** It was desired to study crevice corrosion of amorphous alloys in more detail, especially under more reproducible conditions than were possible with cold rolled filaments. Accordingly, the sandwich-type of crevice cell shown in Figure 3 was fabricated, in which a short section of filament specimen was clamped ("sandwiched") between two surfaces to form a prepared crevice. In this way the area of specimen within the crevice, the tightness of the crevice, and the anode-to-cathode area ratio could be carefully controlled to yield more reproducible data. This crevice cell, which was used only during the first year of research, was designed to provide a broad indication of relative crevice corrosion susceptibility quickly and for a variety of alloys. However, it did not yield any information about the electrochemical conditions within the crevice. Research with a cell that provided information of the latter type will be discussed in a subsequent section.

Typical data obtained with the sandwich-type crevice cell are shown in Figure 21, which depicts classical crevice corrosion of T304 stainless steel. This material was used initially to ensure satisfactory operation of the crevice cell, because it readily undergoes crevice corrosion in chloride solutions. Crevice corrosion did not initiate at measurable rates under freely corroding conditions within 24 hours, therefore, subsequent experiments were performed at anodic potentials applied potentiostatically. (Potentials quoted are those external to the crevice.) Figure 21 indicates that about 800 minutes after a potential of 0.100 V(SCE) was applied in 0.1M NaCl at 50 C, crevice corrosion initiated. After the experiment was terminated the crevice specimen was found to be severely corroded and the anolyte possessed a green color, presumably from  $\text{Ni}^{++}$  and  $\text{Fe}^{++}$  ions.

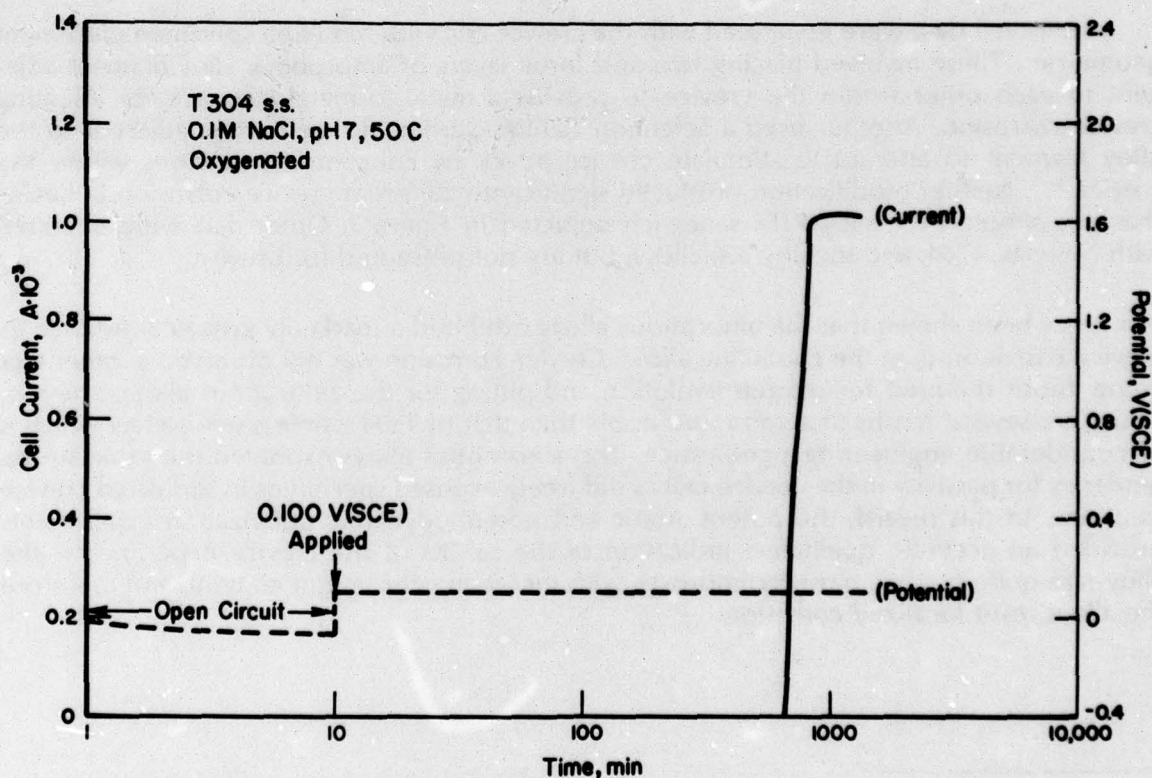


**FIGURE 21. CELL CURRENT AND APPLIED POTENTIAL VERSUS TIME FOR T304 STAINLESS STEEL IN THE SANDWICH-TYPE CREVICE TEST CELL**

Figure 22 shows comparable data for the amorphous alloy containing 2 atomic percent Cr. Crevice corrosion occurred at an applied potential of 1.00 V(SCE), and the critical potential for crevice corrosion,  $E_{cc}$ , presumably was between 0.6 and 1.00 V(SCE). Up to about 24 hours or 1440 minutes were allowed for initiation of crevice corrosion for these experiments. This was an arbitrary choice made to expedite screening of alloys during these trials. Longer waiting periods might have resulted in less noble  $E_{cc}$  potentials because initiation is a time dependent process. Note that the current attained a steady state value. The relatively short time period over which the corrosion current was measured reflects the small dimensions of the filament specimen, which rapidly dissolved after crevice corrosion initiated.

Figure 23 illustrates behavior for the alloy with 7 atomic percent Cr. It was considerably more difficult to initiate crevice corrosion with this alloy, as evident from the series of current decays following the stepwise increases in applied potential. Not until 1.50 V(SCE) was applied did the cell current persist for more than a few minutes. Even at this noble potential the specimen exhibited a tendency to passivate, as indicated by the gradually decreasing current.

The effect of increasing the chromium level to 16 atomic percent is shown in Figure 24. No significant corrosion current was measured until 1.40 V(SCE) was applied. At this value, however, the alloy within the crevice passivated and the current decayed to less than  $10^{-6}$  A. Increasing the applied potential to 1.56 V(SCE) again produced a large current transient, but the alloy was able to passivate and the current rapidly decreased.

Additional data were generated with the crevice cell with modified specimen placement geometries. These involved placing two and three layers of amorphous alloy filament adjacent to each other within the crevice to provide a metal-to-metal interface for initiating crevice corrosion. Another used a Selemion<sup>(a)</sup> anion-permeable membrane adjacent to the alloy filament to attempt to stimulate crevice attack by concentrating cations within the crevice <sup>(14)</sup>. Neither modification produced significantly different crevice corrosion behavior than the simple PTFE-alloy-PTFE sandwich depicted in Figure 3. Other data were obtained with Metglas, T304, and Incoloy 800 alloys, but are not presented for brevity.

It has been shown that the amorphous alloys exhibited a markedly greater resistance to crevice corrosion than the crystalline alloys. Crevice corrosion was not observed at potentials below those required for oxygen evolution and pitting for the amorphous alloys. Their  $E_{cc}$  values are several tenths of a volt more noble than that of T304 stainless steel, a fact which is of considerable engineering significance. The amorphous alloys exhibited the same strong tendency for passivity in the crevice cell as did freely exposed specimens in simulated crevice solutions. In this regard, the potentiostatic and potentiodynamic polarization experiments provided an accurate qualitative indication of the results of the crevice experiments: the alloys are quite passive, passivity improves with increasing chromium content, and therefore the alloys resist localized corrosion.

(14) Suzuki, T., and Kitamura, Y., "Laboratory Evaluation of Crevice Corrosion Resistance of Stainless Steels", *Corr.*, 16 (10), 16 (1977).

(a) Trademark, Asahi Glass Company, Ltd., Japan.



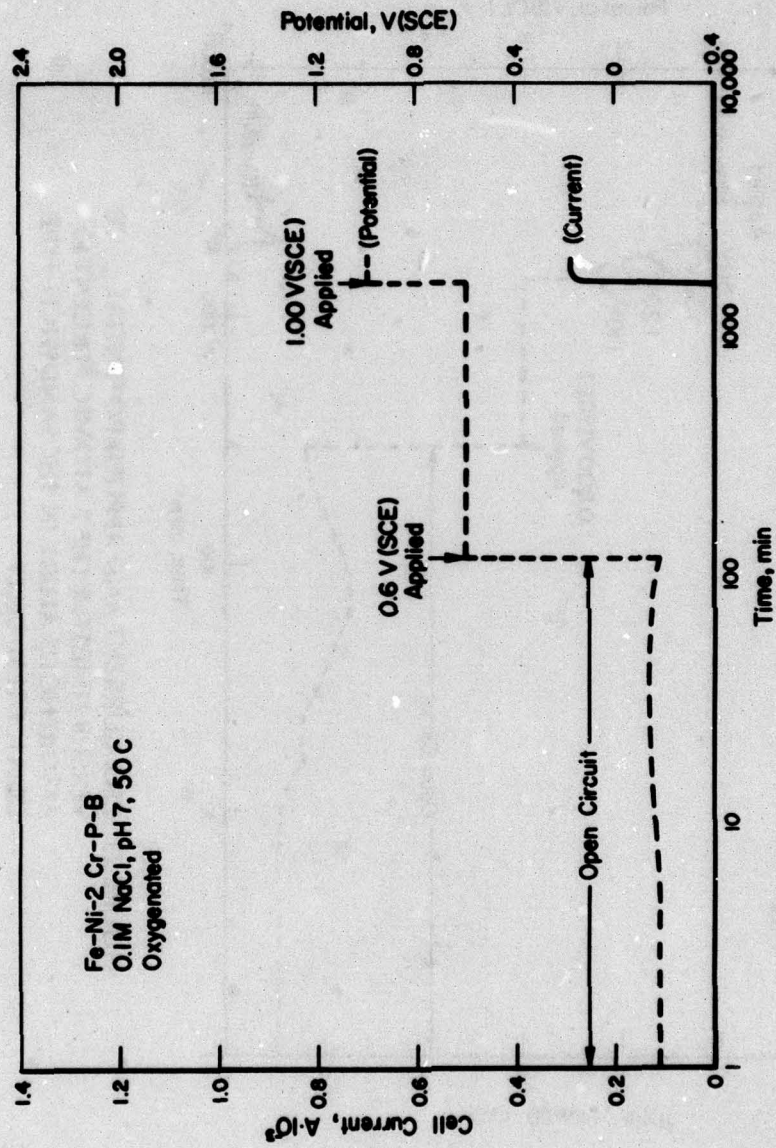


FIGURE 22. CELL CURRENT AND APPLIED POTENTIAL VERSUS TIME FOR THE 2 ATOMIC PERCENT Cr AMORPHOUS ALLOY IN THE SANDWICH-TYPE CREVICE TEST CELL

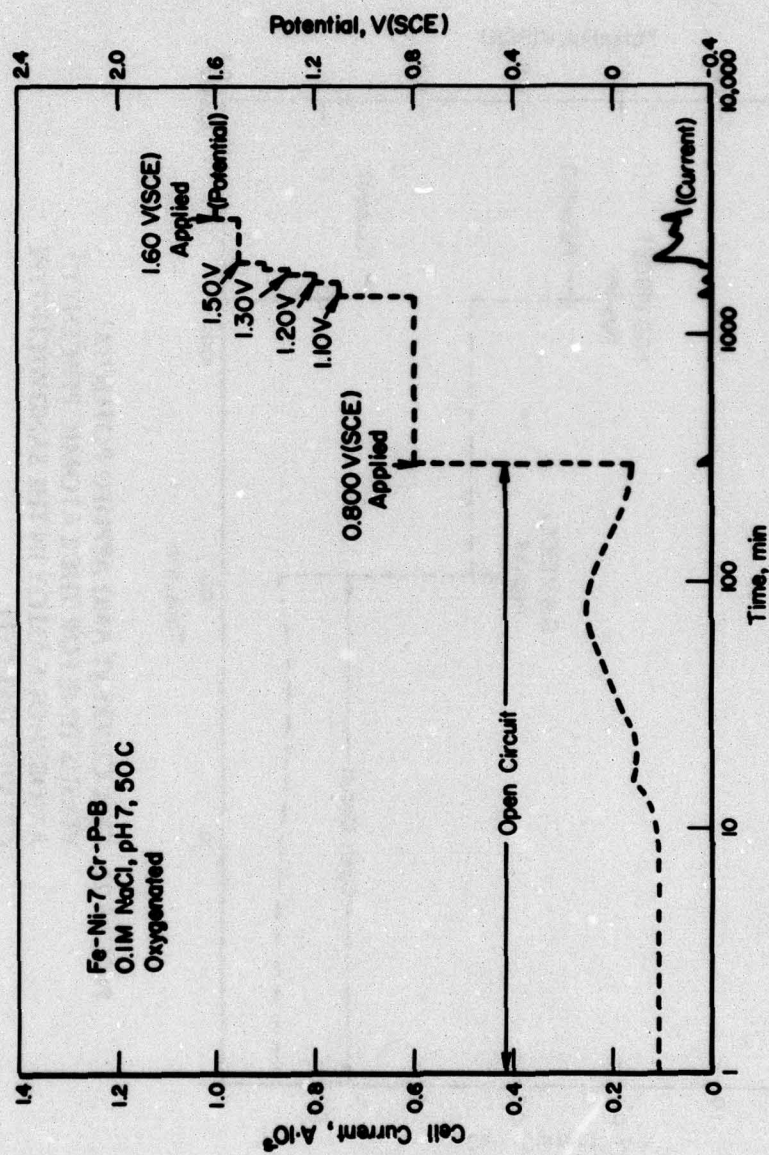


FIGURE 23. CELL CURRENT AND APPLIED POTENTIAL  
VERSUS TIME FOR THE 7 ATOMIC PERCENT Cr  
AMORPHOUS ALLOY IN THE SANDWICH-TYPE  
CREVICE TEST CELL



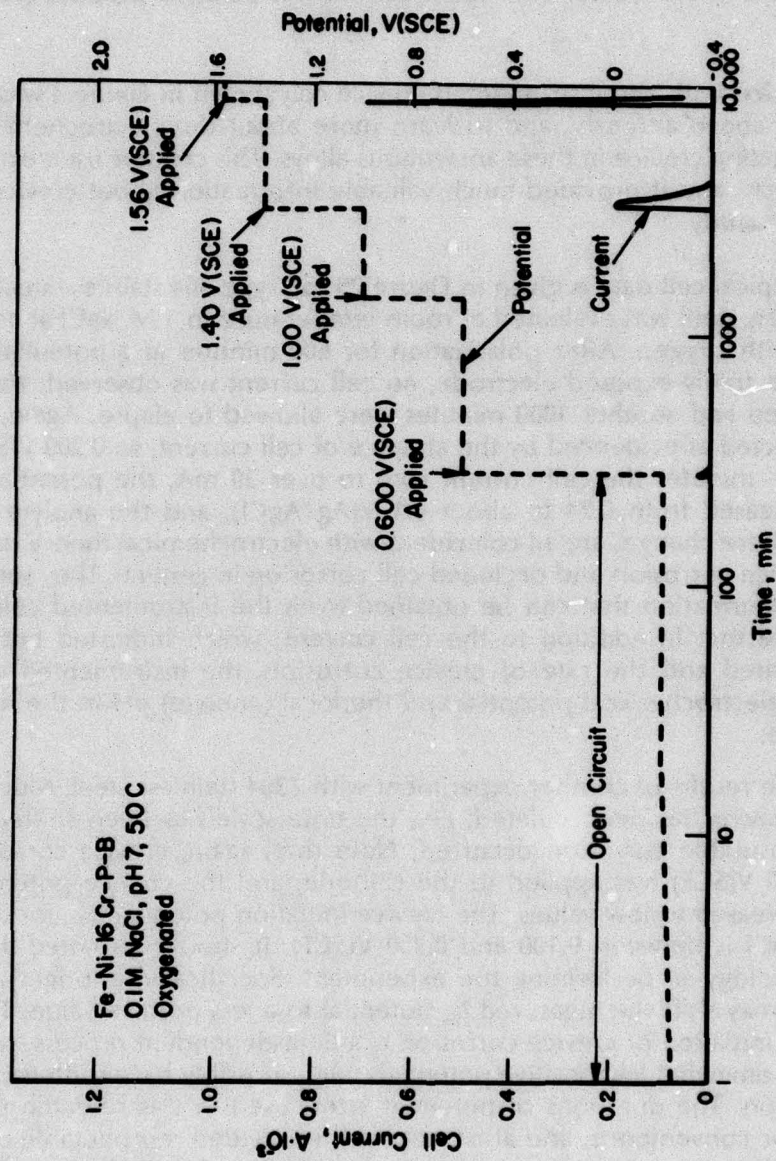


FIGURE 24. CELL CURRENT AND APPLIED POTENTIAL VERSUS TIME FOR THE 16 ATOMIC PERCENT Cr AMORPHOUS ALLOY IN THE SANDWICH-TYPE CREVICE TEST CELL

However, the attack on the cold rolled alloy documented in Figures 17 and 19 is an apparent anomaly in the above reasoning. That is, it is not clear why crevice corrosion occurred in the cold rolled alloy, yet high cell currents were not measured with the crevice cell for this same alloy at equivalent potentials near 0.60 V(SCE). One could attempt to rationalize the different results between the experiments involving cold rolled filaments and those employing the crevice cell by simply assuming that the crevice cell did not form as tight a crevice as did the microcracks. This situation could conceivably have created a more noble  $E_{cc}$  and a smaller corrosion current in the crevice cell. This question was pursued with the crevice cell described below.

**Instrumented Crevice Cell.** The instrumented crevice cell shown in Figure 4 was used to investigate further the above anomaly, and to learn more about the electrochemical conditions within a propagating crevice in these amorphous alloys. This cell was used extensively for second-year research, and it provided much valuable information about crevice corrosion of the alloys under study.

An indication of typical cell data is given in Figure 25 for Type 304 stainless steel. In this experiment T304 stainless steel was evaluated at room temperature in 1 M NaCl at a bulk pH of 7.0 and saturated with oxygen. After polarization for 600 minutes at a potential of 0.00 V(SCE)<sup>(a)</sup> applied to the freely exposed electrode, no cell current was observed; therefore, 0.100 V(SCE) was applied and another 1000 minutes were allowed to elapse. Again, crevice corrosion was not detected as evidenced by the absence of cell current, so 0.200 V(SCE) was applied. In a matter of minutes the cell current rose to over 30 mA, the potential of the crevice specimen decreased from 0.24 to about 0.1 V(Ag/AgCl), and the anolyte pH decreased to about 1.0. These changes are all coincident with electrochemical theory regarding the mechanism of crevice corrosion and occluded cell corrosion in general. They serve to illustrate the types of information that can be obtained from the instrumented cell during crevice corrosion. Note that in addition to the cell current, which indicated both when crevice corrosion initiated and the rate of crevice corrosion, the instrumented cell also provided data on the electrochemical potential and the local (anolyte) pH in the region of the propagating crevice.

Figure 26 shows the results of another experiment with T304 stainless steel. Much of the early current-time behavior has been deleted, i.e., the time scale has been shifted to the right, because no measurable corrosion occurred. Note that, again, crevice corrosion initiated soon after 0.200 V(SCE) was applied to the cathode, and the crevice potential and anolyte pH rapidly decreased to low values. The crevice initiation potential,  $E_{cc}$ , for this alloy in oxygenated 1 M NaCl is between 0.100 and 0.200 V(SCE). It should be noted that  $E_{cc}$  is related to the methodology of performing the experiment. Specifically, a longer arrest at each anodic potential may shift the measured  $E_{cc}$  potential to a less positive value. This shift can occur because the initiation of crevice corrosion is a time-dependent process, such that larger polarizations at somewhat less positive potentials might possibly have shifted  $E_{cc}$  values in the negative direction. The durations of potential arrest used in this research program were selected partly for convenience, and also because they yielded reproducible data that adequately reflected the various crevice corrosion susceptibilities of the different alloys under study.

(a) Potentials of the freely exposed (cathode) specimen are quoted relative to a saturated calomel electrode, SCE, whereas those of the crevice (anode) specimen are quoted relative to a silver-silver chloride electrode, Ag/AgCl. The Ag/AgCl electrode was about 40 mV more positive than the SCE, i.e., 1.00 V(SCE) = 1.04 V(Ag/AgCl).



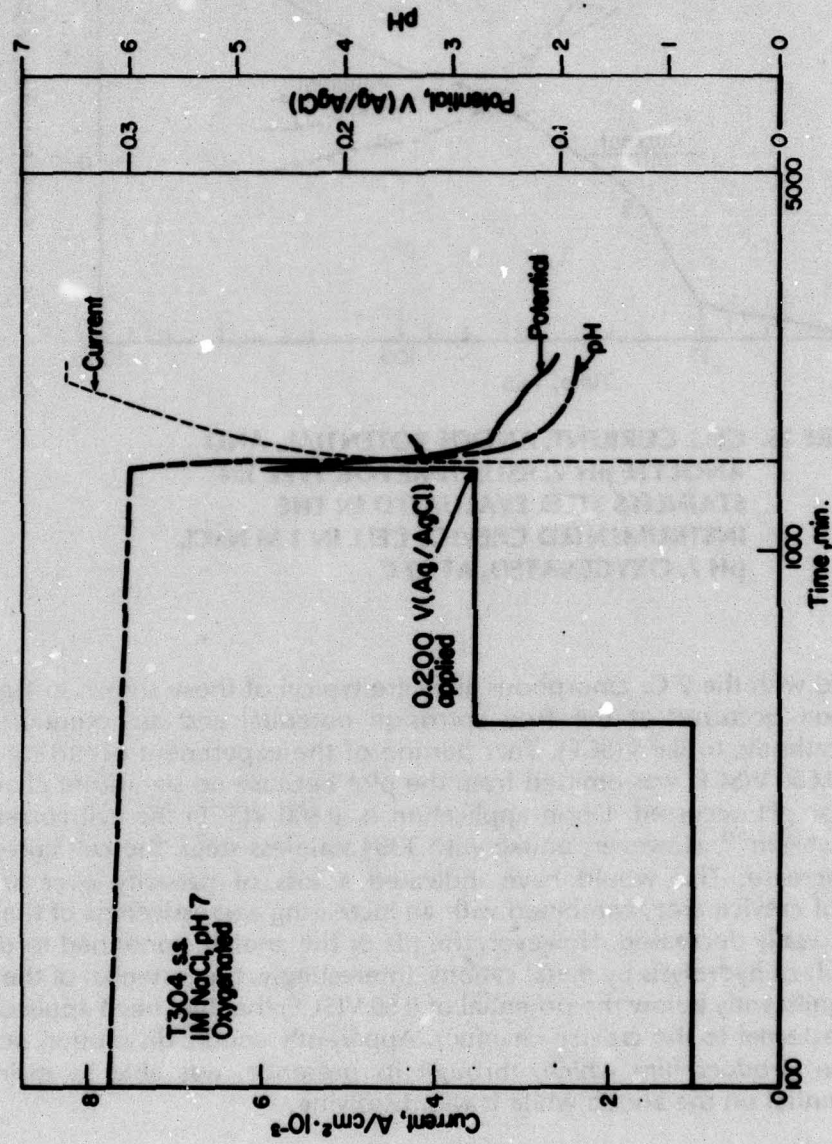
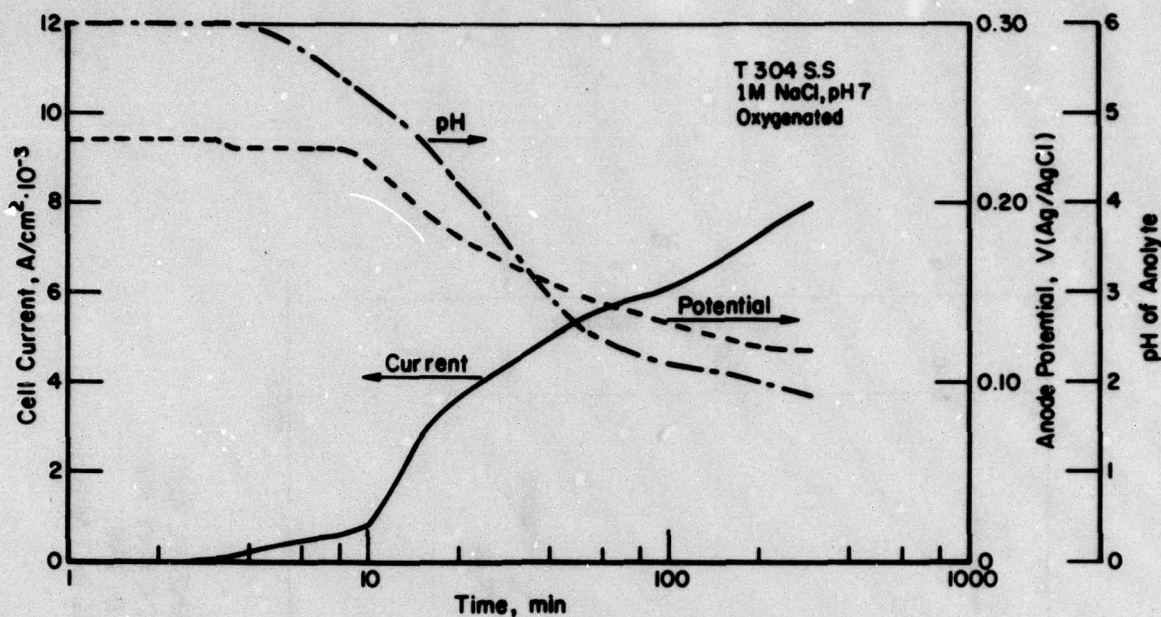


FIGURE 25. CELL CURRENT, ANODE POTENTIAL, AND ANOLYTE pH VERSUS TIME FOR TYPE 304 STAINLESS STEEL EVALUATED IN THE INSTRUMENTED CREVICE CELL IN 1 M NaCl, pH 7, OXYGENATED, AT 22 C

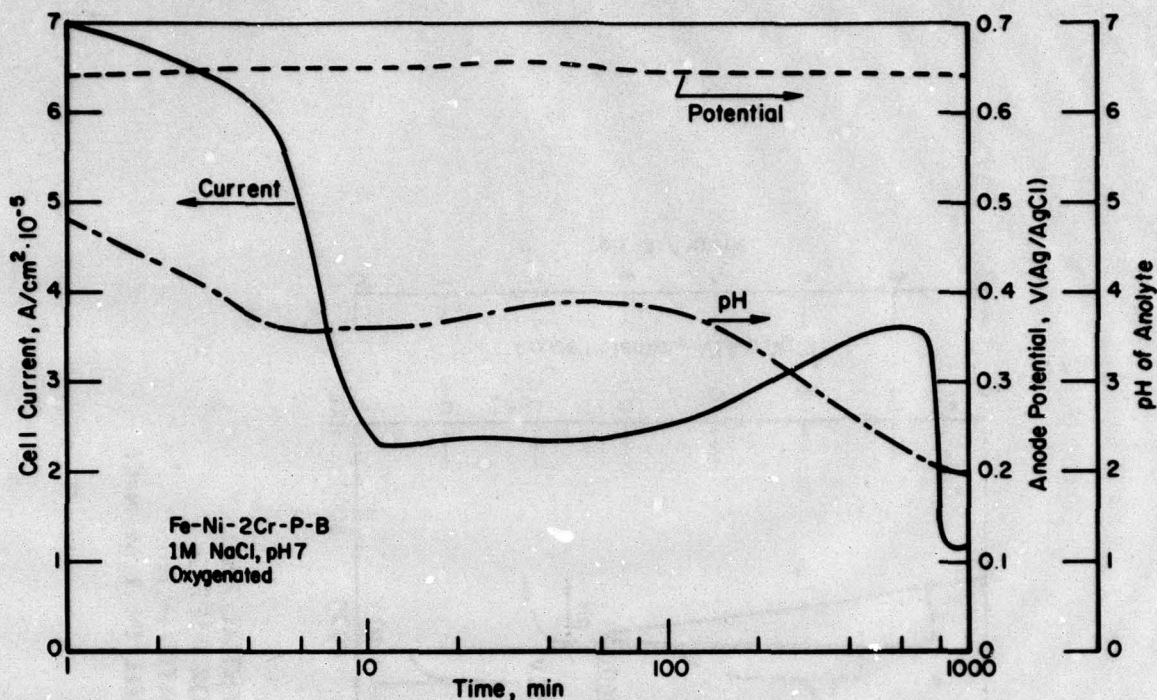


**FIGURE 26. CELL CURRENT, ANODE POTENTIAL, AND ANOLYTE pH VERSUS TIME FOR TYPE 304 STAINLESS STEEL EVALUATED IN THE INSTRUMENTED CREVICE CELL IN 1 M NaCl, pH 7, OXYGENATED, AT 22 C**

Results obtained with the 2 Cr amorphous alloy are typical of those shown in Figure 27. No crevice corrosion occurred at the free corrosion potential and at potentiostatically applied potentials cathodic to 0.6 V(SCE). That portion of the experiment occurring before the application of 0.600 V(SCE) was omitted from the plot because no significant changes in current, potential, or pH occurred. Upon application of 0.600 V(SCE) the cell current rose rapidly to over  $70 \mu\text{A}/\text{cm}^2$ <sup>(a)</sup>. However, unlike with T304 stainless steel, the cell current did not continue to increase. This would have indicated a loss of passivity over an ever-increasing fraction of crevice area, combined with an increasing aggressiveness of the corrodent. Instead, it gradually decreased. However, the pH of the anolyte continued to decline, presumably the result of hydrolysis by metal cations. Interestingly, the potential of the anode did not decrease significantly below the potential of 0.60 V(SCE) that had been applied to the cathode specimen external to the crevice chamber. Apparently anodic dissolution occurred through a corrosion product film which, through its presence, was able to maintain a relatively noble potential on the anode while it was dissolving.

(a) During early research involving the sandwich cell, total cell current was quoted. Subsequently, it was decided to present cell current per unit of anode area in the instrumented cell even though all of the anode area did not become active immediately upon initiation of crevice corrosion.

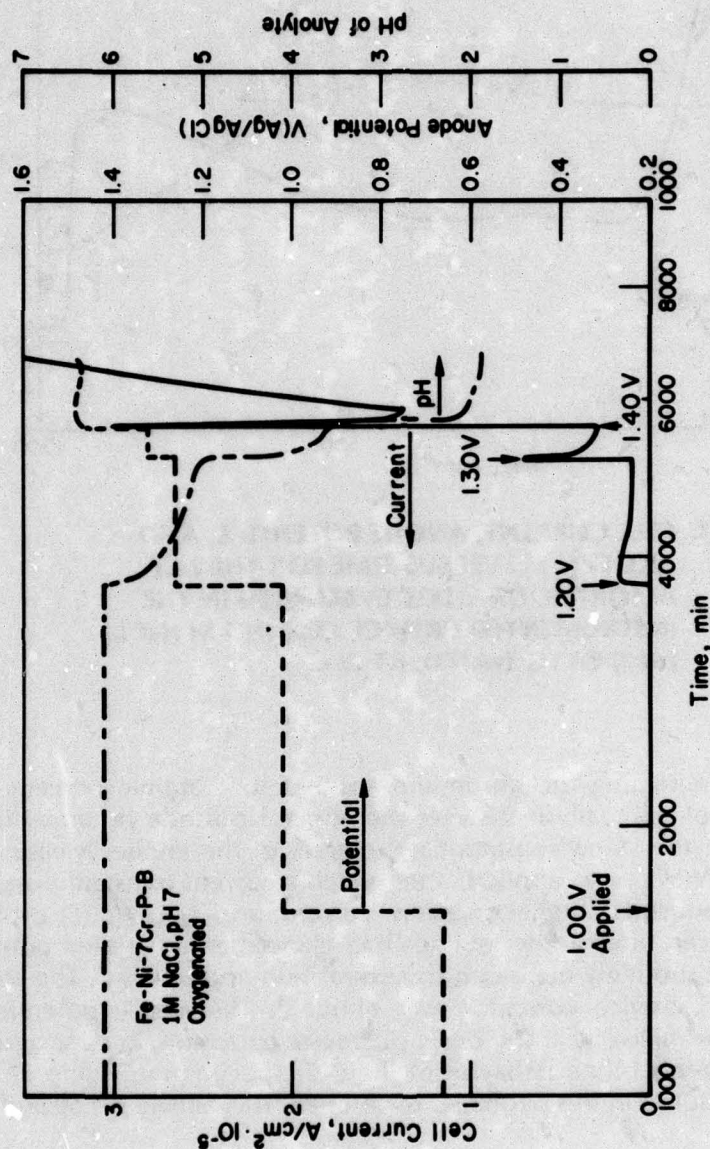




**FIGURE 27. CELL CURRENT, ANODE POTENTIAL, AND ANOLYTE pH VERSUS TIME FOR THE 2 Cr AMORPHOUS ALLOY EVALUATED IN THE INSTRUMENTED CREVICE CELL IN 1 M NaCl, pH 7, OXYGENATED, AT 22 C**

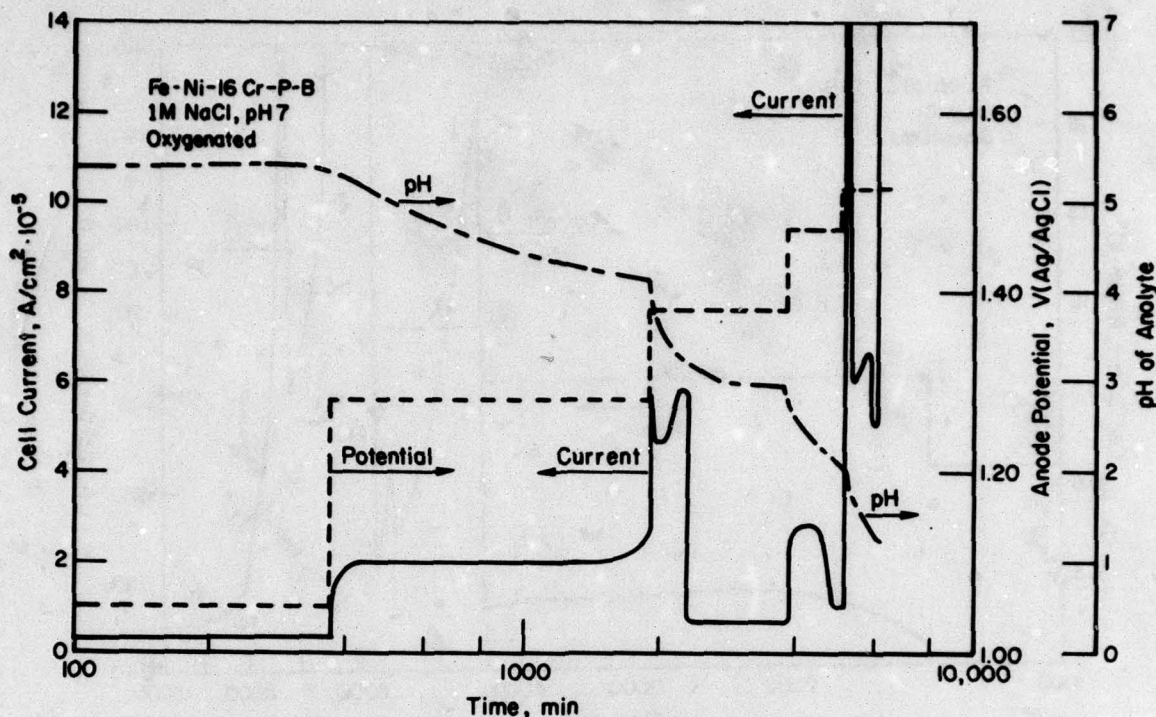
The influence of increasing the chromium content to 7 atomic percent is shown in Figure 28. The effects of manually increasing the applied cathode potential in a stepwise fashion are reflected in the stepwise potential increases of the anode. Measurable current did not flow until 1.20 V(SCE) was applied, after which a current transient ensued. Application of 1.30 V(SCE) produced a higher transient current, and 1.40 V(SCE) produced a still higher transient. However, after a few minutes had elapsed at an applied potential of 1.40 V(SCE), the cell current suddenly increased to several hundred  $\mu\text{A}/\text{cm}^2$ . The solution pH at the beginning of rapid crevice corrosion was about 2. The anode potential fluctuated downward by only a few millivolts at the onset of crevice corrosion, in close agreement with the relatively steady potential-time behavior of the 2 Cr specimen in Figure 27. The crevice corrosion potential measured in this particular experiment was between 1.30 and 1.40 V(SCE).

Figure 29 shows typical behavior for the alloy containing 16 atomic percent of chromium. Application of 1.20 V(SCE) to the cathode produced a cell current of about  $20 \mu\text{A}/\text{cm}^2$ , but this current did not increase over the next 26 hours; rather, it remained constant and the pH of the anolyte continuously decreased through hydrolysis. Increasing the applied potential to 1.30 V(SCE) produced a temporary increase in cell current to a maximum of about  $60 \mu\text{A}/\text{cm}^2$ , after which the current decreased to less than  $10 \mu\text{A}/\text{cm}^2$ . It is suspected that the very sudden decrease in current to this low level may have resulted from breakage of one of the several parallel strands of alloy filament in the crevice chamber. These strands



**FIGURE 28. CELL CURRENT, ANODE POTENTIAL, AND ANOLYTE pH VERSUS TIME FOR THE 7 Cr AMORPHOUS ALLOY EVALUATED IN THE INSTRUMENTED CREVICE CELL IN 1 M NaCl pH 7, OXYGENATED, AT 22 C**





**FIGURE 29. CELL CURRENT, ANODE POTENTIAL, AND ANOLYTE pH VERSUS TIME FOR THE 16 Cr AMORPHOUS ALLOY EVALUATED IN THE INSTRUMENTED CREVICE CELL IN 1 M NaCl, pH 7, OXYGENATED, AT 22 C**

were connected in parallel and coiled inside the chamber to comprise the anode; occasionally a strand was observed to break during an experiment as a result of corrosion and the stress that accompanied coiling of the strands. Breakage of a strand had the effect of instantaneously decreasing the total area of corroding anode, and thus of causing the cell current suddenly to fall to a lower value. In Figure 29, the fact that the cell current remained at the low value of several  $\mu\text{A}/\text{cm}^2$  indicates that the crevice corrosion potential had not been attained. Indeed, it was not until 1.50 V(SCE) was applied that the cell current increased, after a preliminary increase and decline, to relatively large values indicating the onset of rapid crevice corrosion. It is interesting to note that 1.40 V(SCE), even in the presence of anolyte acidified to a pH slightly less than 3, was insufficient to produce continuing crevice attack. Thus, the influence of increasing the chromium content was to confer a very marked ability of the amorphous alloys to maintain a passive state, even in acidified chloride electrolytes at very oxidizing potentials.

An experiment was performed to determine whether the use of a more corrosive electrolyte would substantially alter the observed crevice corrosion susceptibility of these alloys. Figure 30 illustrates the effect of using 1 N HCl instead of neutral 1 M NaCl as the corrodent at the start of the experiment. This electrolyte is quite aggressive toward passive alloys, being 1 molar in chloride ion as well as possessing a pH near zero. (pH-time behavior is not presented in this figure because the anolyte pH was not expected to change significantly during the experiment, and because the pH electrode was not highly accurate in such a low range of pH). Application of potentials less than 1.00 V(SCE) for hundreds of minutes did not

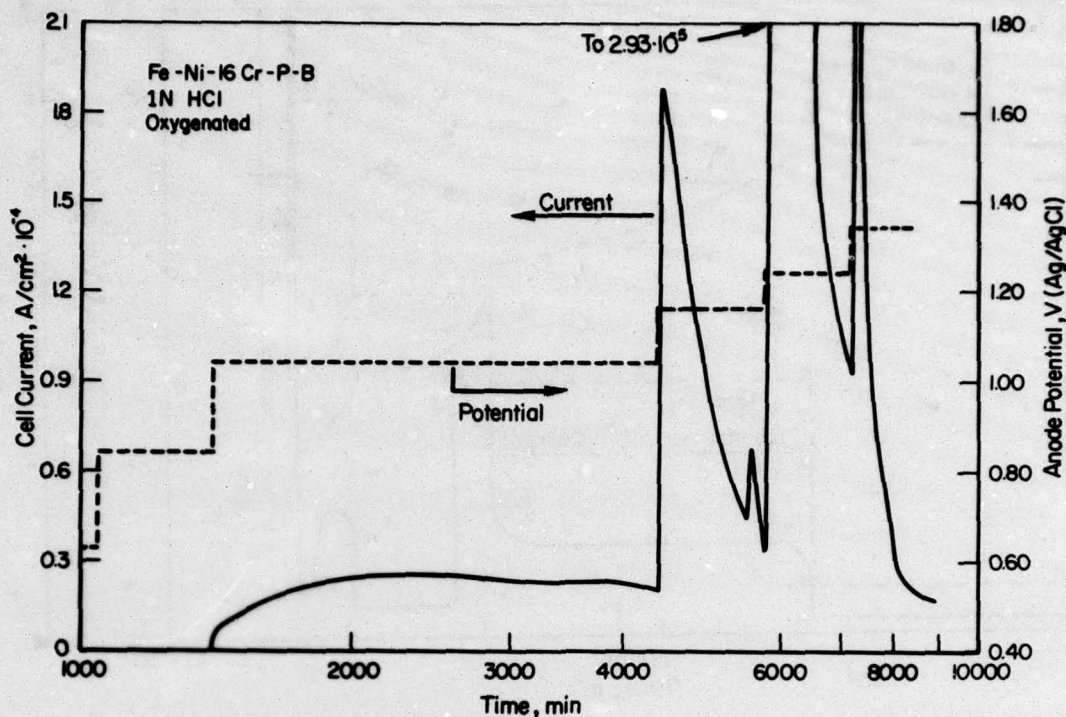


**FIGURE 30. CELL CURRENT AND ANODE POTENTIAL VERSUS TIME FOR THE 16 Cr AMORPHOUS ALLOY EVALUATED IN THE INSTRUMENTED CREVICE CELL IN 1 N HCl, OXYGENATED, AT 22 C**

produce a corrosion rate within the prepared crevice greater than several  $\mu A/cm^2$ . A total time of about 24 hours elapsed at these various potentials, which has proved to be sufficient for crevice corrosion to initiate under less corrosive conditions. It was not until 1.00 V(SCE) was applied that a substantial cell current of about  $20 \mu A/cm^2$  was measured. Maintenance of this potentiostatically applied potential for about 48 hours resulted in a fairly constant cell current, i.e., catastrophic crevice corrosion did not ensue. Increasing the potential to higher values produced, as in previous experiments with 1 M NaCl, sharp transients in cell current followed by rapid decay with time. It is apparent that even a potential of 1.30 V(SCE) did not produce self-sustaining crevice corrosion, and the tendency for passivation was still evident. The experiment was discontinued at this potential because it was suspected that one or more filaments in the crevice chamber had corroded and broken, thereby substantially altering the anode area.

Two experiments were performed that further emphasize the ability of the amorphous alloys to maintain passivity under conditions promoting crevice corrosion. One such experiment is depicted in Figure 31, which provided data on the crevice protection potential. In this trial crevice corrosion of a 16 Cr filament was rapidly initiated in 1 M NaCl by applying 1.40 V(SCE) to the cathode specimen, thus creating a cell current exceeding  $200 \mu A/cm^2$  and a pH below 2. Next, the applied potential was decreased by 100 mV to 1.30 V(SCE), resulting in a similar shift in anode potential from 1.44 to 1.34 V(Ag/AgCl) and a decrease in cell current essentially to zero. Further decreases in potential produced no measurable effects on



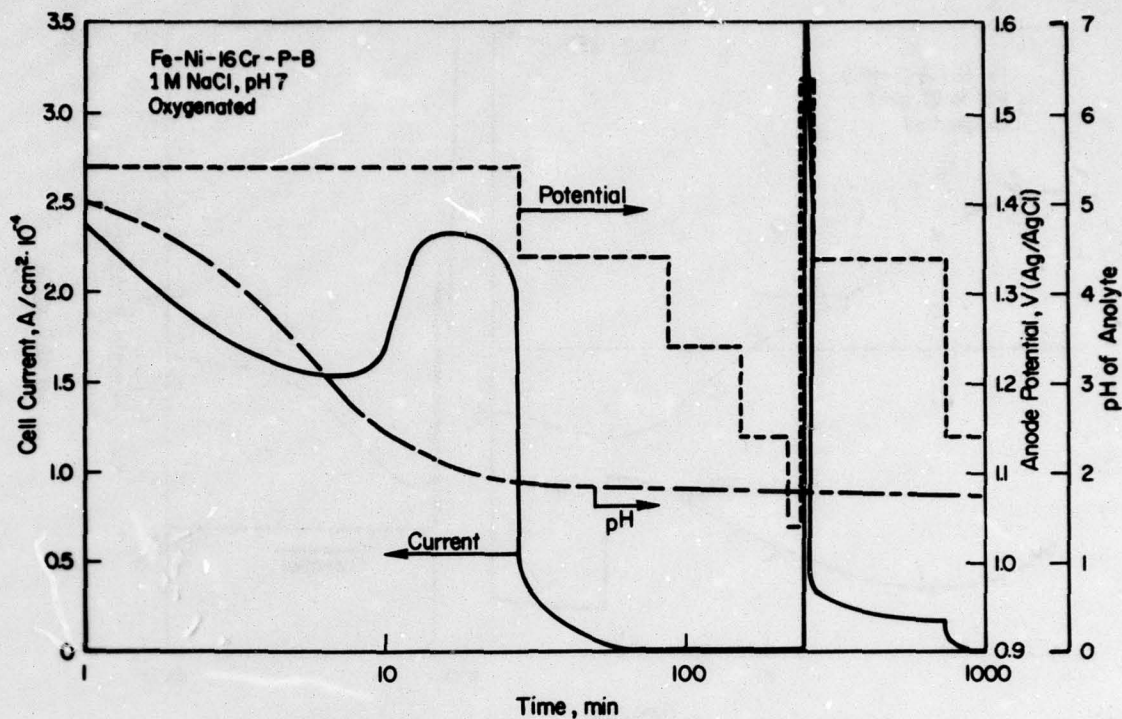


**FIGURE 31. CELL CURRENT, ANODE POTENTIAL, AND ANOLYTE pH VERSUS TIME FOR THE 16 Cr AMORPHOUS ALLOY EVALUATED IN THE INSTRUMENTED CREVICE CELL IN 1 M NaCl, pH 7, OXYGENATED, AT 22 C**

cell current. This cycle could be repeated, as indicated by the onset of crevice corrosion when 1.50 V(SCE) was applied to the cathode and the decrease in current when the potential was returned to less noble values. Similar trends in potential-current behavior were evident for Metglas 2826A, as shown in Figure 32.

These two experiments are significant because they demonstrate that once crevice corrosion is initiated with the 14 Cr and 16 Cr amorphous alloys, passivity is restored if the potential is decreased by only about 100 mV below that required to initiate the attack. Thus, the difference between the crevice initiation potential and the crevice protection potential is only about 100 mV. This is a very narrow span compared to those of crystalline stainless steels, which can be several hundred millivolts. The narrow range between these two potentials emphasizes the ability of amorphous alloys to passivate readily once the very noble potentials required to propagate crevice corrosion are reduced.

Several crevice corrosion experiments were conducted at 85 C to determine whether an elevation in temperature would substantially alter the behavior of the alloys under investigation. No significant differences were noted between corrosion behavior determined at 22 C and 85 C. There may have been subtle effects of increasing the temperature, such as an increase in corrosion rate (cell current) or a decrease in the potential required to initiate attack. However, if they occurred, these effects were not discernable outside of the range of experimental reproducibility. The data show that crevice attack even at 85 C occurred only at potentials above about 1 V(SCE) for the chromium-containing amorphous alloys, in general agreement with experiments performed at room temperature.

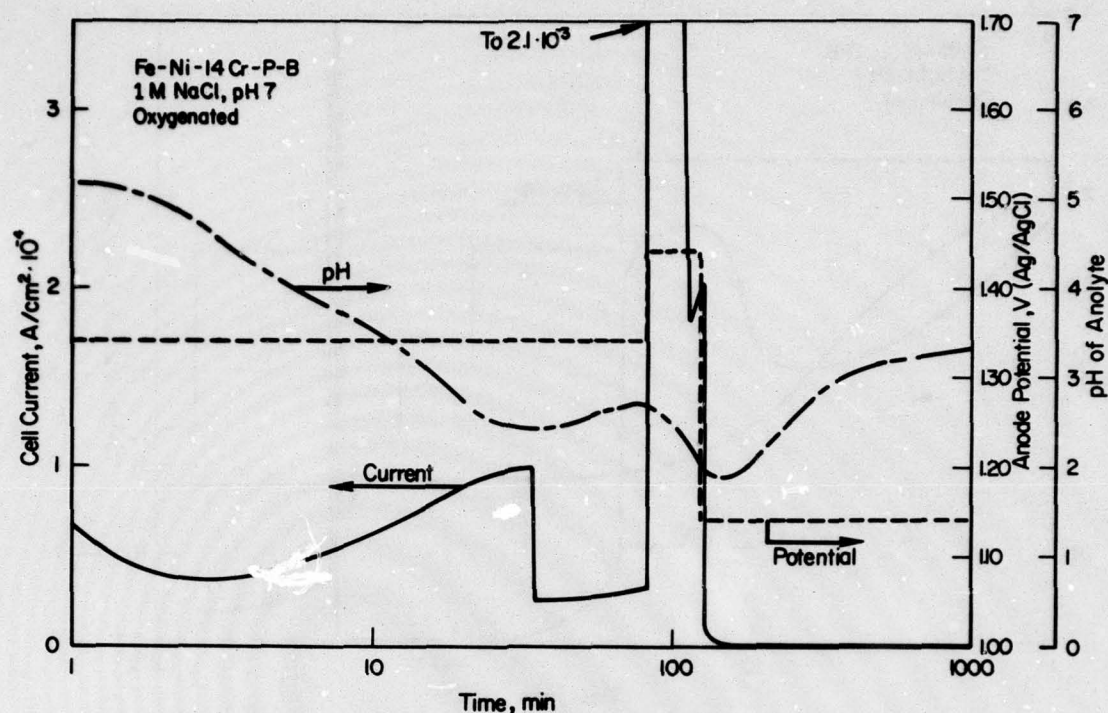


**FIGURE 32. CELL CURRENT, ANODE POTENTIAL, AND ANOLYTE pH VERSUS TIME FOR METGLAS 2826A EVALUATED IN THE INSTRUMENTED CREVICE CELL IN 1 M NaCl, pH 7, OXYGENATED, AT 22 C**

#### **Summary and Interpretation of Phase I Research**

The primary reason for investigating crevice corrosion susceptibility of amorphous alloys was to differentiate between initiation-related and propagation-related corrosion behavior. It was reasoned that crevices would provide ready-made, or artificial sites for initiation of localized attack, sites which do not exist on freely exposed amorphous alloy surfaces because of the very homogeneous nature of the alloy structure. Measurement of susceptibility to crevice corrosion would help to determine whether the corrosion resistance exhibited by these alloys extends to propagation as well as initiation phenomena.

The anodic potentiodynamic polarization curves showed that crevice corrosion should logically be expected to occur: the alloys exhibited enhanced corrosion at reduced electrolyte pH such as would be expected to develop during occluded cell corrosion, thus ensuring some degree of stability of active-passive cells on specimen surfaces. However, the very corrosive conditions that are required to produce corrosion of these alloys at sensible rates indicated that the degree of susceptibility to crevice corrosion would be considerably less than that of many crystalline steels of similar chromium content under similar exposure conditions. Subsequent experiments confirmed these predictions. Specifically, cold rolling of the filaments produced a slight susceptibility to enhanced dissolution, presumably due to the formation of surface microcracks that initiated crevice corrosion. However, the depth of attack was only several  $\mu\text{m}$  when the crevices passivated. (See Appendix A for a quantitative treatment of the rate of crevice attack on cold rolled filaments).



More extensive experimentation, initially with the sandwich-type crevice cell and subsequently with an instrumented cell, verified that susceptibility of the chromium-containing amorphous alloys to crevice corrosion was indeed slight. Although classical crevice attack involving localized anodic dissolution and acidification of the anolyte could be made to occur, quite oxidizing (noble) potentials were required. These potentials were more than 1000 mV more noble for the 16 Cr amorphous alloy than for T304 stainless steel. Very interestingly, the potentials of amorphous crevice specimens did not decrease markedly after the onset of crevice corrosion, but rather they usually remained within several millivolts of the potential applied to the cathode. This behavior can be interpreted as a resistance to the loss of passivity, dissolution occurring instead *through* a passive film that prevailed relatively intact during crevice corrosion. This tendency of these alloys to remain covered by a passive layer is in contrast to the behavior of crystalline stainless steels, which experienced a loss of passivity that increased with time as corrosive conditions within the crevice became established. An indication of such a time-dependent activation is the large cathodic shift in electrode potential exhibited by T304 stainless steel in Figures 25 and 26.

The results of Phase I research indicate that corrosion resistance of amorphous alloys used in this research extends to propagation as well as initiation phenomena. The alloys exhibited an apparent strong tendency to remain covered with a passive film, which other studies have shown to be analogous in structure and composition to the hydrated chromium oxyhydroxide found on conventional chromium-bearing steels.<sup>(5,15)</sup> It is the ability of this film to exist under extremely corrosive conditions that confers excellent corrosion resistance. This ability, in turn, results presumably from the homogeneous nature of the alloys; that is, the absence of structural defects in the alloy matrices contributes to the integrity of the film. It is probable that the chemistry of the alloys also contributes to their excellent passivity. It has been claimed that the presence of phosphorus is necessary for this enhanced passivity, and that it confers corrosion resistance by creating rapid anodic dissolution at unfilmed sites and thereby accelerating reformation of the film; in other words, by promoting passivity.<sup>(16,17)</sup> However, results presented recently by Wang and Merz<sup>(18)</sup> have shown that extremely corrosion resistant amorphous alloys can be prepared without any phosphorus, thereby casting doubt on the concept that phosphorus is essential for corrosion resistance. The question of the role of phosphorus, and other metalloid additions, on conferring passivity should be the subject of future research.

## Phase 2-Sputtering

### Sputtering Selectivity

Once it became clear that sputtering would be a useful technique for depositing amorphous chromium-containing alloys, experiments were performed to determine whether the sputtering process is selective. "Selective" refers to preferential removal, or non-removal, of certain elements in the target during sputtering, such that the nominal composi-

(15) Diegle, R. B., "Corrosion of Amorphous Alloys", Final Report to Corporate Technical Development, Battelle Memorial Institute, December 12, 1978.

(16) Naka, M., Hashimoto, K., and Masumoto, T., Sci. Rep. Res. Inst. Tohoku Univ., A286, 283-289 (1977).

(17) Naka, M., Hashimoto, K., and Masumoto, T., J. Noncryst. Solids, in press.

(18) Wang, R., and Merz, M. A., "Corrosion Resistant Amorphous Stainless Steels Containing Tungsten," presented at the spring meeting of The Electrochemical Society, Boston, May 6-11, 1979.

tion of the deposit differs from that of the target. Such selectivity is not uncommon, since the ease of sputtering elements from a target is a function of atomic weight, morphology of the element in the target, and other sputtering parameters. Selectivity during sputtering is generally undesirable; it either creates a deposit of different and often unpredictable composition from that of the starting composition, or else it necessitates making the target of a different composition from that desired to compensate for the selective sputtering.

Several analyses were made by energy dispersive spectroscopy, EDS (X-ray fluorescence), of alloys before and after they were sputtered. The results are presented in Table 3. Table 3 shows that variations in concentration between target and deposit were generally one atomic percent or less. An exception is the chromium content of the nominal 16 Cr alloy, which was 2.3 atomic percent higher in the deposit. Since this value is close to the desired composition, some doubt is cast on the validity of the 13.0 value for the target. A very important observation is that phosphorus is not depleted in the substrate. Since phosphorus is needed to achieve the amorphous state and to enhance corrosion resistance, it is reassuring to know that it can be sputtered at a concentration that is close to that which exists in the target. No information could be obtained about the initial and final concentrations of boron, since quantification of boron by EDS was not possible. Therefore, its concentration was assumed to be six atomic percent, the value that was introduced during melting and casting.

TABLE 3. RESULTS OF COMPOSITIONAL ANALYSIS OF CAST TARGETS AND SPUTTERED DEPOSITS OF TWO ALLOYS(a)

Nominal Chromium Content, atomic percent	Specimen	Concentration of Given Element, atomic percent					
		Fe	Ni	Cr	V	P	B
2	Target	44.6	30.9	1.6	2.4	14.4	6
2	Deposit	45.4	31.6	1.6	2.3	13.1	6
16	Target	32.1	32.9	13.0	2.0	14.1	6
16	Deposit	31.0	31.6	15.3	2.2	13.9	6

(a) By EDS; absolute accuracy is about  $\pm 0.5\%$ .

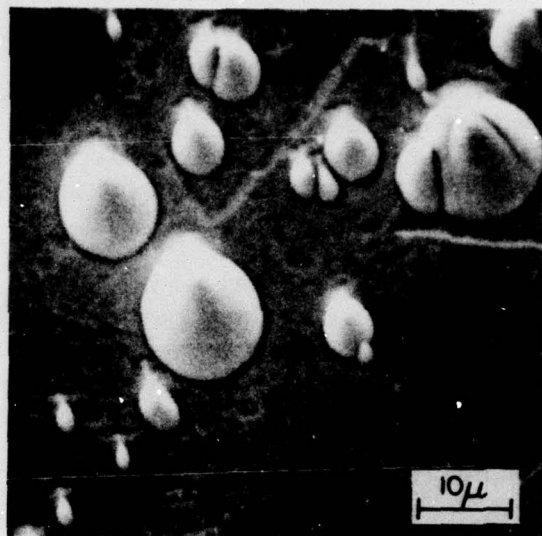
### Surface Characterization

The surface topography of sputtered specimens was characterized by the presence of hillock-shaped mounds. Figure 33 shows SEM photographs of the as-sputtered surfaces of several deposits. Figure 33(a) shows these hillocks, which were present to a greater or lesser degree on all sputtered specimens. Figure 33(b) is a higher magnification view of these features. Although still present, the hillocks were smaller and fewer on the 16 Cr specimen sputtered earlier in the program onto a water cooled substrate, Figure 33(c). It is not known if substrate temperature influenced their formation. Apparently chromium content in the alloy does not strongly affect their formation, for as shown in Figure 33(d), they were also

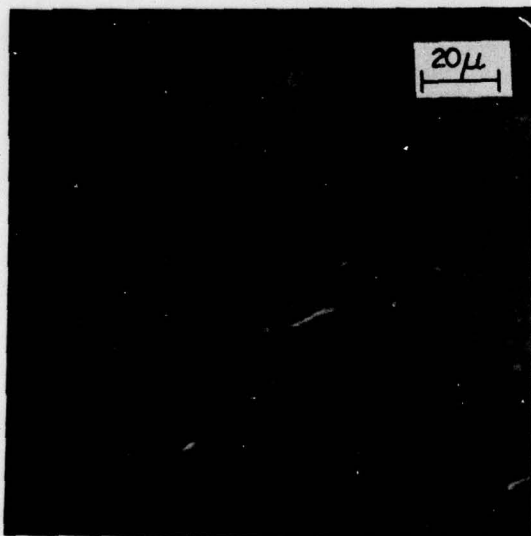




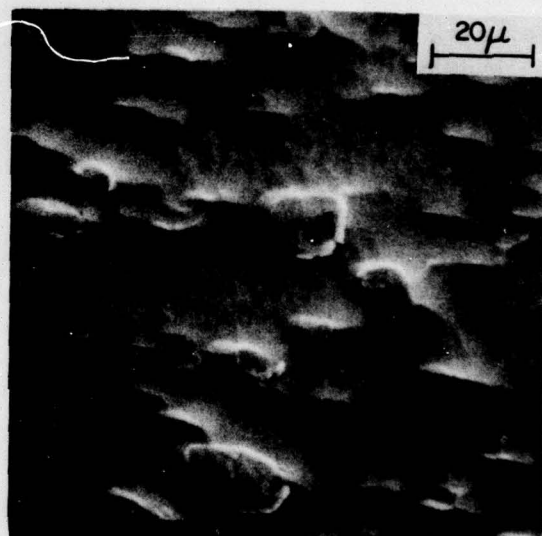
(a)



(b)



(c)



(d)

**FIGURE 33. SEM PHOTOGRAPHS OF SURFACE OF SPUTTERED DEPOSITS. (a) 16 Cr (LN<sub>2</sub> SUBSTRATE); (b) ENLARGED VIEW OF (a); (c) 16 Cr (WATER-COOLED SUBSTRATE); (d) 2 Cr (LN<sub>2</sub> SUBSTRATE)**

present on the deposit containing 2 Cr. (Several of the larger hillocks had been broken off during handling, hence their truncated appearance). For comparison, the surfaces of a 16 Cr filament prepared by melt spinning are shown in Figure 34. Figure 34(a) shows the shiny side, i.e., that which was away from the copper wheel during solidification. Note that mound-shaped features are present on this surface, although they are less cone-shaped than on sputtered specimens. The very rough surface in Figure 34(b) was in contact with the copper wheel during solidification, and it presumably reflects the volume shrinkage that occurred during solidification of the melt.

The source of the hillocks shown in Figure 33 is not clearly understood. They appear on other types of alloys, including crystalline alloys, of considerably different compositions than those that were sputtered for this research. They are thought to result from growth instabilities that occur during deposition of atoms onto a substrate. Their significance to alloy properties is not known; however, it will be shown in a later section that they were not preferred sites for localized corrosion, neither did they significantly compromise the corrosion resistance of the deposits.

### Structural Characterization

Thin foil specimens of several sputtered deposits were examined by transmission electron microscopy (TEM) and selected area electron diffraction (SAED) to characterize the state of amorphousness. Thin foil TEM photographs are shown in Figures 35 and 36. Figure 35 shows a view of a specimen that was examined immediately after preparation. No evidence of crystallinity is apparent. Figure 36 shows the SAED pattern obtained from a similar specimen; the broad diffuse rings document its essentially 100 percent amorphous nature. The features shown in Figure 35 and 36 are typical of those of all sputtered specimens that were examined. (Only 16 Cr specimens were evaluated in this manner, since these specimens were sputtered at two substrate temperatures and they thus provided the opportunity for investigating the effect of temperature on crystallinity.) Regardless of whether the substrate was cooled by water or liquid nitrogen, the deposits were completely amorphous within the limits of resolution of TEM. In this regard they resembled the structure of melt spun filaments, which also showed no resolvable crystallinity in an earlier study.<sup>(2)</sup>

However, evidence of some type of crystalline phase could be detected if the thin foil specimens were stored in acetone for several hours before examination. The bright spots near the center of Figure 37 are very small islands of crystalline material. These islands appeared consistently upon prolonged exposure of the deposits to acetone. It is not known whether they are surface reaction products or regions of crystallized alloy. In either case, they are not considered pertinent to the present investigation because of the unique circumstances required to create them.

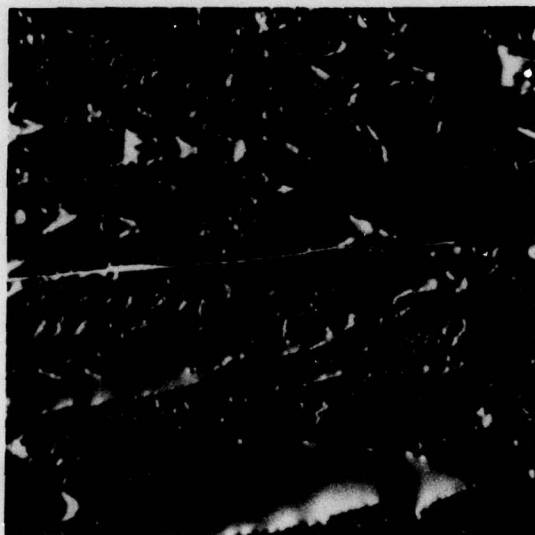
### Crystallization Behavior

A further definition of alloy structure was obtained indirectly by differential scanning calorimetry. This experimental technique was applied not only to the sputtered deposits, but also to melt spun filaments of the same nominal compositions. In this manner, a comparison was made of the crystallization behavior of amorphous alloys produced by sputtering relative to that of alloys produced by a more conventional technique, namely, liquid quenching.





(a)



(b)

**FIGURE 34. SEM PHOTOGRAPHS OF SURFACES OF 16 Cr FILAMENT PREPARED BY MELT SPINNING. (a) SHINY SIDE (IN CONTACT WITH VACUUM DURING MELT SPINNING); (b) DULL SIDE (IN CONTACT WITH COPPER WHEEL DURING MELT SPINNING)**

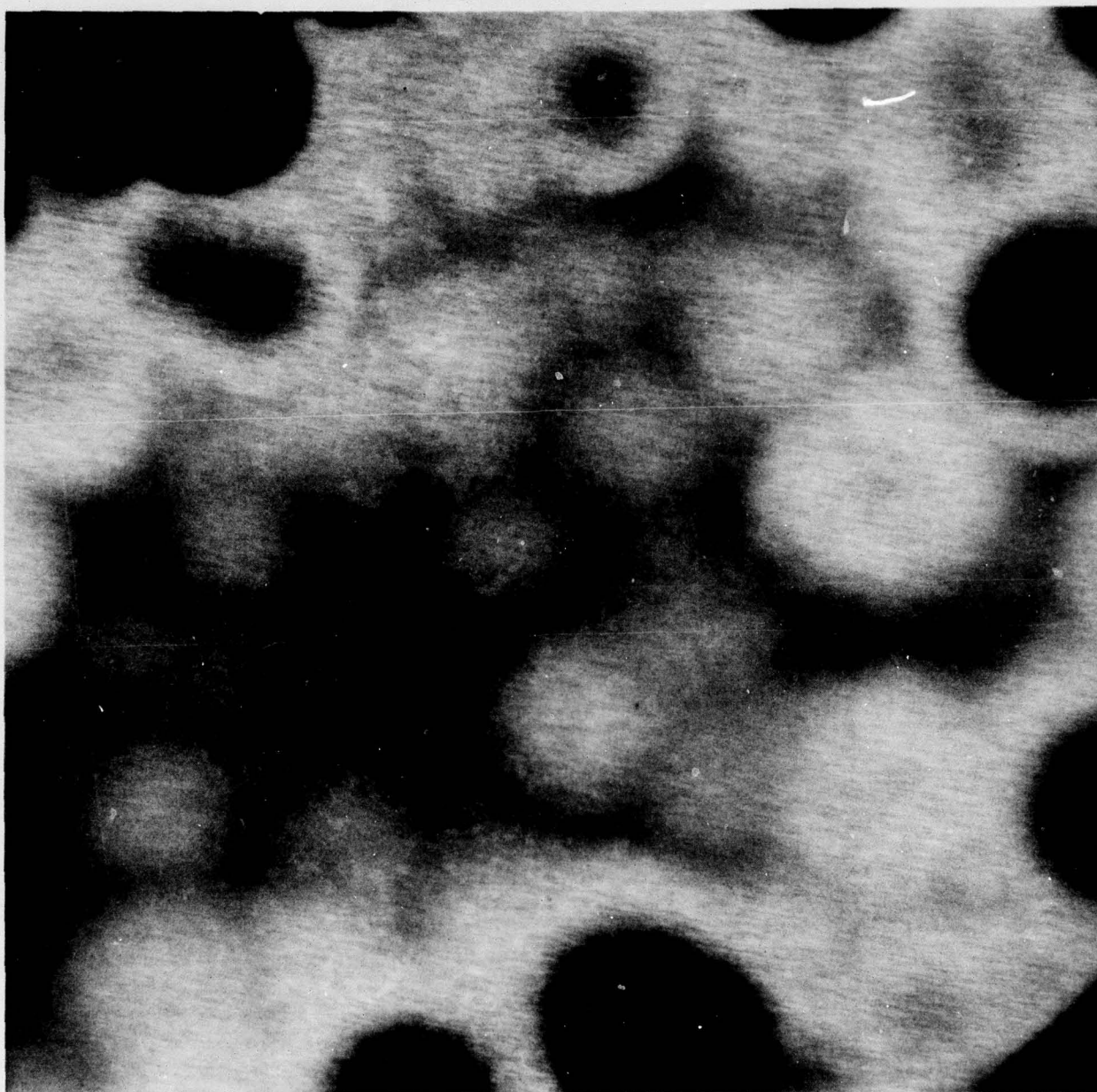


**FIGURE 35. TEM PHOTOGRAPH OF 16 Cr DEPOSIT  
SPUTTERED ONTO A LIQUID  
NITROGEN-COOLED COPPER SUBSTRATE.  
Specimen was examined soon after preparation**



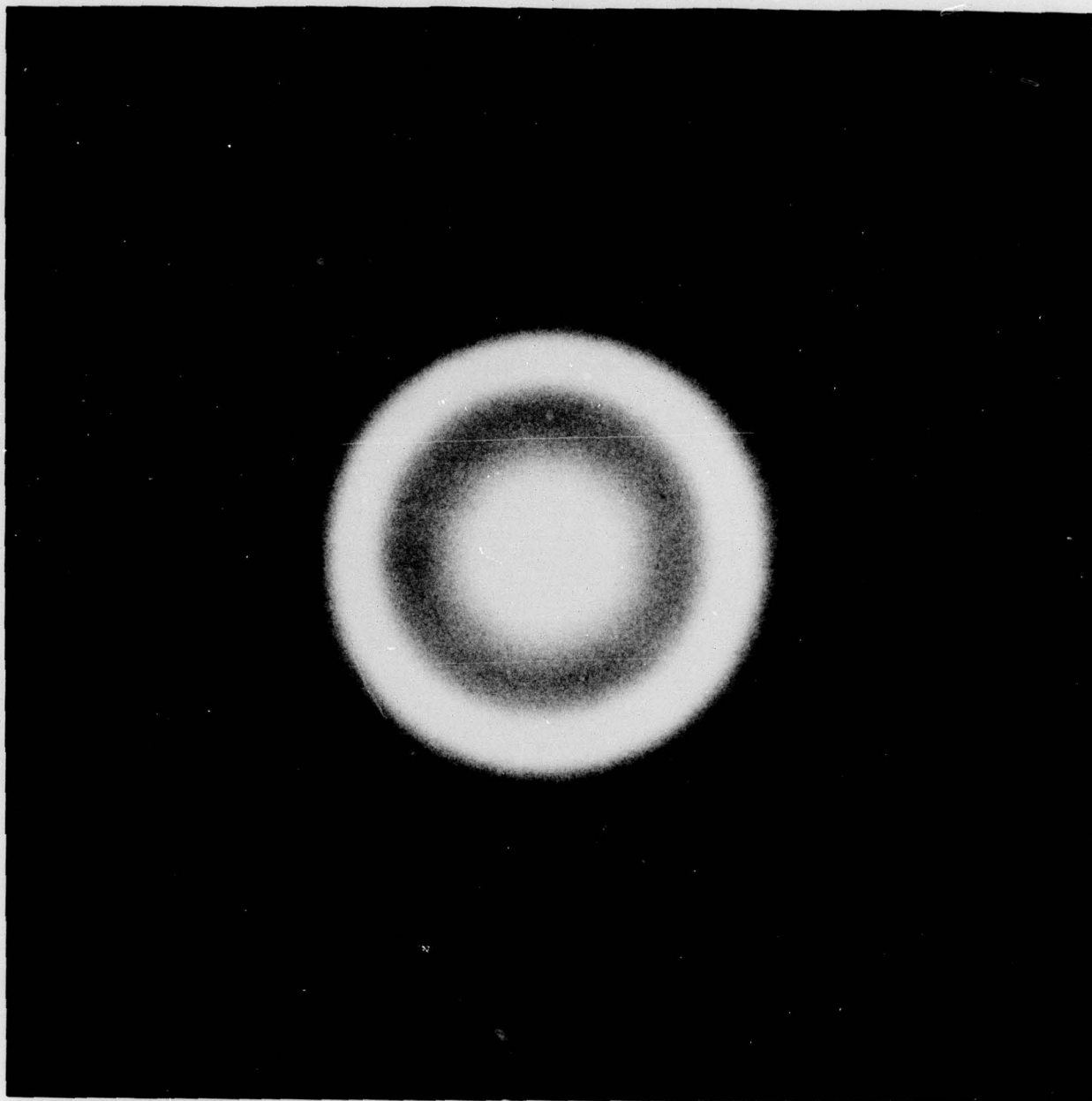


**FIGURE 36. SAED PATTERN OF 16 Cr DEPOSIT SPUTTERED  
ONTO LIQUID NITROGEN-COOLED COPPER  
SUBSTRATE**

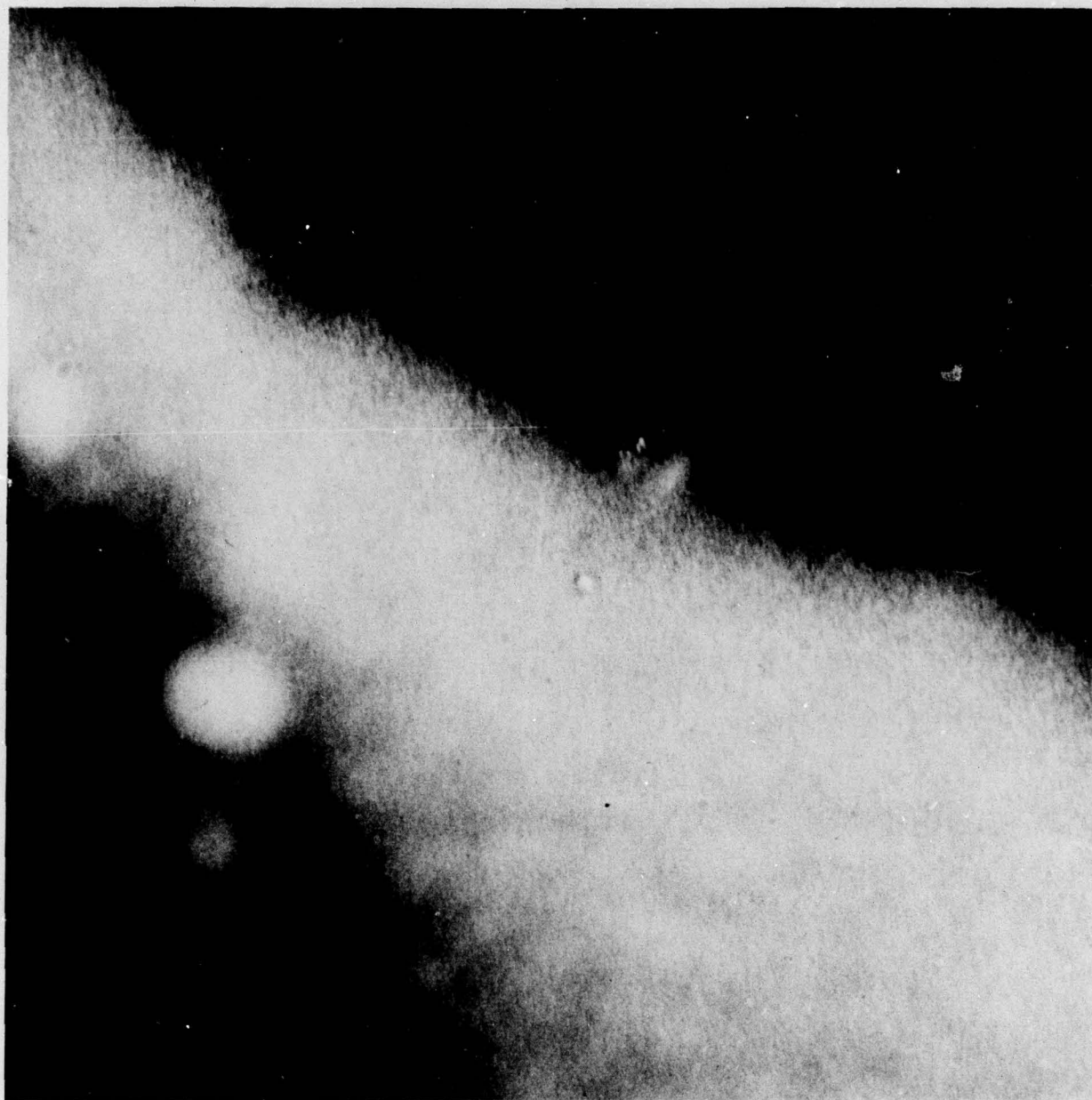


**FIGURE 37. TEM PHOTOGRAPH OF 16 Cr DEPOSIT  
SPUTTERED ONTO A WATER-COOLED COPPER  
SUBSTRATE. Specimen was stored in acetone  
prior to examination**



Typical DSC curves are shown in Figure 38 for sputtered and melt spun samples of a 2 Cr alloy. The curves exhibit rather sharp exothermic peaks indicative of crystallization, and thus they are qualitatively similar to peaks reported by other workers.<sup>(10)</sup> The crystallization temperatures, defined as that temperature at which a curve begins to rise above background, are 428 C and 439 C for the sputtered and melt spun alloys, respectively. The heats of crystallization, defined as the area under the curves above background referred to a molar weight of sample, are 1275 and 1095 cal/g-atom for the sputtered and melt spun specimens, respectively. The results of several DSC measurements are summarized in Table 4. The crystallization temperatures of sputtered versus melt spun alloys differ by 11 C for the 2 Cr alloy, and by only 4 C for the 16 Cr material. The heats of crystallization vary by about 16 percent for the 2 Cr alloys and by about 12 percent for the 16 Cr sample. There are no obvious trends in  $T_{\text{cryst}}$  and  $\Delta Q_{\text{cryst}}$  relative to the method of specimen preparation, i.e., sputtering or melt spinning. Furthermore, the effect of substrate temperature on these parameters for the 16 Cr material does not appear to be significant.

It must be concluded that the crystallization behavior of the sputtered 2 Cr and 16 Cr deposits was similar to that of melt spun alloys of similar compositions. The similarities of the specimens are striking when the very different nature of the two preparation techniques is considered.

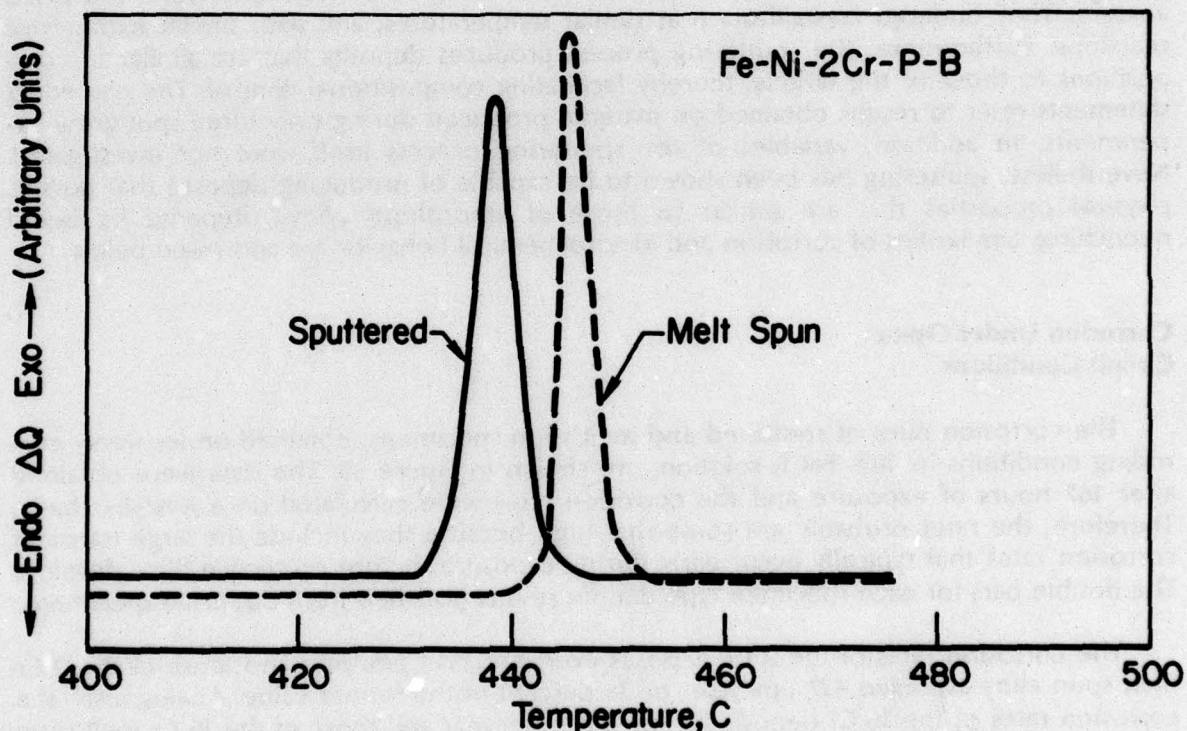


FIGURE 38. DSC CURVES FOR 2 Cr ALLOY PRODUCED EITHER BY MELT SPINNING OR BY SPUTTERING. SCAN RATE WAS 20 C/MIN

**TABLE 4. TEMPERATURES AND HEATS OF CRYSTALLIZATION OF SPUTTERED AND MELT-SPUN AMORPHOUS ALLOYS(a)**

Chromium Content, at. %	Preparation Technique	Substrate Temperature, C	T <sub>cryst.</sub> , C	ΔQ <sub>cryst.</sub> , cal/g-atom
2	Sputtering	-196	428	1275
2	Melt spinning	~ 15	439	1095, 1115
16	Sputtering	-196	460	1070, 1110
16	Sputtering	~ 15	464	1230
16	Melt spinning	~ 15	461	1095, 1115

(a) By DSC.

To summarize the results of the preceding property studies, the deposits prepared by sputtering were similar in structure and behavior to those prepared by melt spinning. The sputtered deposits are completely amorphous according to conventional TEM and SAED analysis. They undergo crystallization at similar temperatures, and with similar exothermic reactions. Furthermore, the sputtering process produces deposits that are similar in compositions to those of the targets, thereby facilitating compositional control. The preceding statements refer to results obtained on material produced during only three sputtering experiments. In addition, variables of the sputtering process itself were not investigated. Nevertheless, sputtering has been shown to be capable of producing deposits that possess physical properties that are similar to those of amorphous alloys prepared by liquid quenching. Similarities of corrosion and electrochemical behavior are addressed below.

#### **Corrosion Under Open Circuit Conditions**

The corrosion rates of sputtered and melt spun specimens, obtained under freely corroding conditions in 10% FeCl<sub>3</sub> solution, are shown in Figure 39. The data were obtained after 167 hours of exposure and the corrosion rates were calculated on a μm/year basis. Therefore, the rates probably are somewhat high because they include the large transient corrosion rates that typically occur early during exposure, before protective films develop. The double bars for each specimen type denote results obtained from duplicate specimens.

The corrosion rates of the 2 Cr deposits averaged 1114 μm/year and those of the 2 Cr melt spun alloy averaged 427 μm/year, or 38 percent of the former value. Analogously, the corrosion rates of the 16 Cr deposit averaged 8.1 μm/year and those of the 16 Cr melt spun alloy, 3.5 μm/year, or 43 percent of the former value. Three features are particularly noteworthy regarding these data, as follows:

- (1) The effect of increasing the chromium concentration in the sputtered deposits was to greatly reduce the corrosion rates, in parallel with the behavior of melt spun specimens.



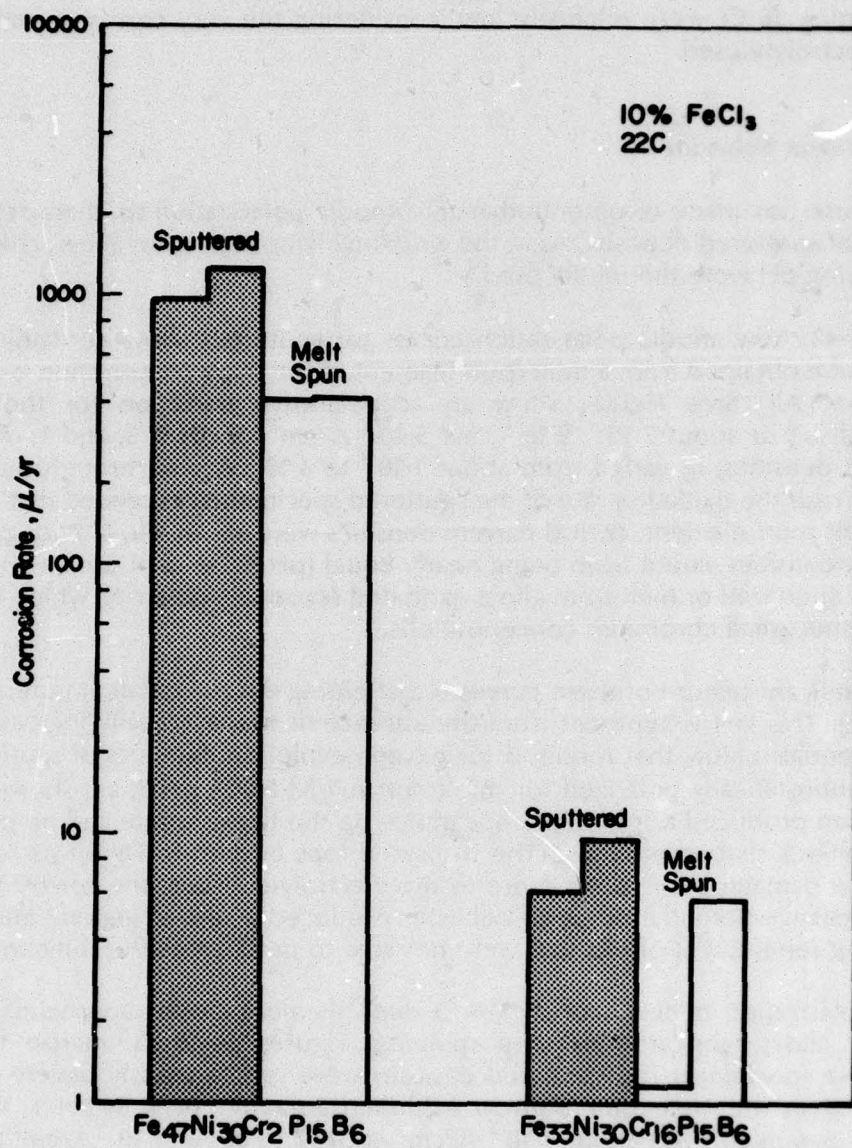


**FIGURE 39. CORROSION RATES, OBTAINED BY MEASUREMENT OF WEIGHT LOSS AFTER 167 HOURS OF EXPOSURE IN 10 PERCENT Fe Cl<sub>3</sub> SOLUTION, FOR SPUTTERED AND MELT SPUN SPECIMENS**

- (2) The corrosion rates of the deposits were about 2 to 3 times greater than those of the melt spun specimens.
- (3) The corrosion rates of both the melt spun specimens and the sputtered deposits containing 16 Cr were relatively low, considering the very corrosive nature of the electrolyte used.

### Anodic Polarization Behavior

Extensive use was made of potentiodynamic anodic polarization to characterize corrosion behavior of sputtered deposits. As in the work involving melt spun alloys, chloride electrolytes of varying pH were the media used.

Figures 40-42 show anodic polarization curves for sputtered alloys containing 2 Cr. In each case, a curve obtained from a melt spun filament of the same composition is also shown for comparison. All three Figures show an active-passive transition for the sputtered specimens, with  $i_c$ 's of about  $2 \cdot 10^{-4}$ ,  $9 \cdot 10^{-4}$ , and  $5 \cdot 10^{-3}$  A/cm<sup>2</sup> for pH 7, 3, and 1, respectively. Passive current densities,  $i_p$ , varied from about  $1 \cdot 10^{-4}$  to  $4 \cdot 10^{-4}$  A/cm<sup>2</sup> through this same pH range. In each case the oxidation rate of the sputtered specimen(s) exceeded that of the corresponding melt spun filament, critical current densities were about 4 to 8 times greater, and passive current densities varied from being nearly equal (pH 3) up to about 30 times greater (pH 1). Neither sputtered or melt spun alloys exhibited secondary passivity, which is probably due to their rather small chromium concentrations.

A very significant feature of these curves is that pitting did not occur at potentials below about 1 V(SCE). This fact is apparent from the absence of monotonically increasing anodic current at potentials below that required for oxygen evolution. Surfaces of sputtered alloys that were potentiostatically polarized for one hour in 1 M NaCl, pH 3, are shown in Figure 43. The corrosion produced a scalloped appearance on the flat substrate and no preferential attack of the hillock-shaped mounds. (The truncated tops evident in Figure 43(b) were the result of surface damage prior to exposure to the electrolyte.) Thus, the corrosion that occurred in the passive potential range of behavior produced a sort of general attack, a surface roughening reminiscent of pits that were not able to propagate after initiating.

Anodic polarization behavior of the 16 Cr deposits more closely approximated that of corresponding alloys fabricated by melt spinning. Figures 44-46 summarize the anodic kinetics of these specimens. The sputtered deposits were spontaneously passive at all three pH values, whereas the melt spun filament exhibited an active peak at pH 1. The passive current densities ranged from about  $1 \cdot 10^{-4}$  A/cm<sup>2</sup> at pH 7 to about  $3 \cdot 10^{-5}$  A/cm<sup>2</sup> at pH 1. At pH 7,  $i_p$  of the sputtered deposit was about 5 times greater than  $i_p$  of the melt spun alloy; however, at pH 3 and 1 the  $i_p$ 's of these two materials were nearly equal. Transpassive dissolution of chromium as Cr<sup>+6</sup> was evident at all pH values for the melt spun alloys, whereas it occurred only at pH 1 for sputtered specimens.

Although returning the electrode potential by reverse scanning created some degree of positive hysteresis of current, in each case the current reached a value of 0 A/cm<sup>2</sup> at a potential that was anodic to the original corrosion potential. This behavior indicates the absence of severe pitting. Such absence was verified by SEM observation of specimen surfaces that had not been polarized above about 1 V(SCE). Polarization well into the oxygen evolution region of potential did produce pitting, two examples of which are shown in Figure 47. The maximum pit size was greater on the specimen sputtered onto a water-cooled substrate, and pit



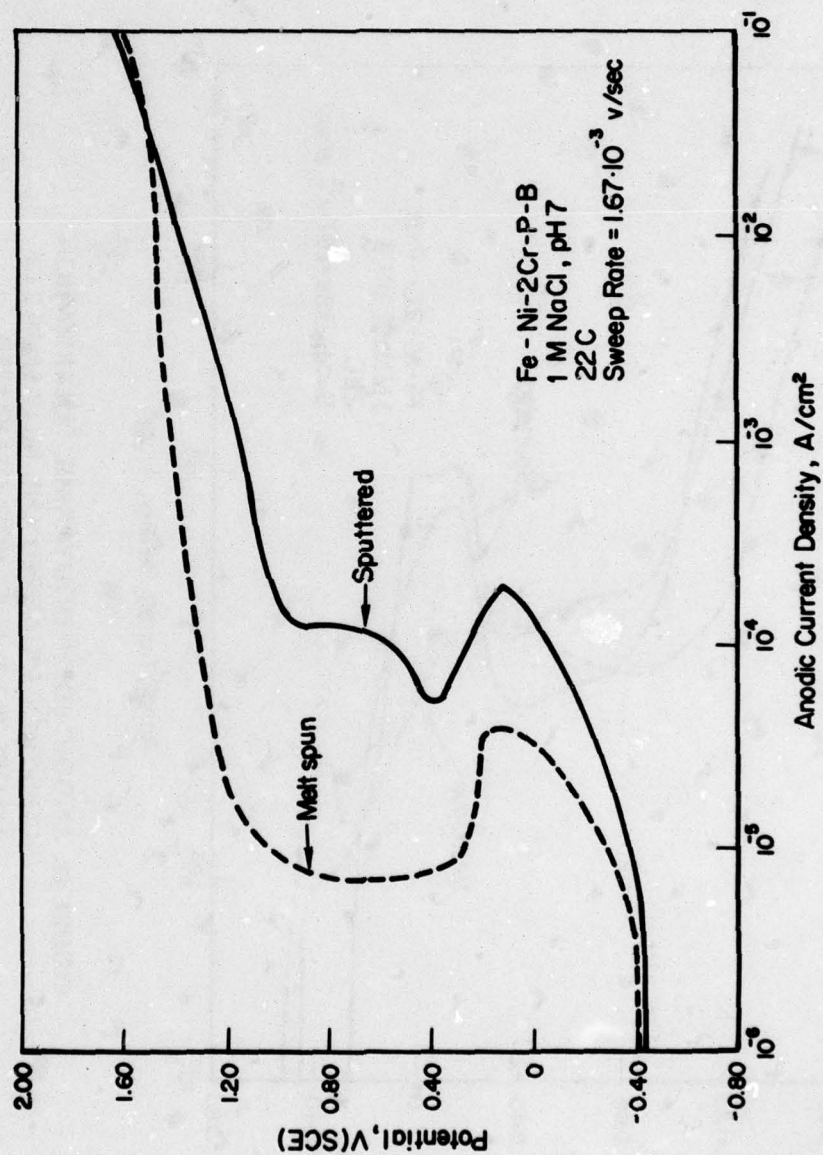


FIGURE 40. ANODIC POTENTIODYNAMIC POLARIZATION CURVES OF SPUTTERED AND MELT SPUN 2 Cr ALLOYS IN 1 M NaCl, pH 7, DEAERATED

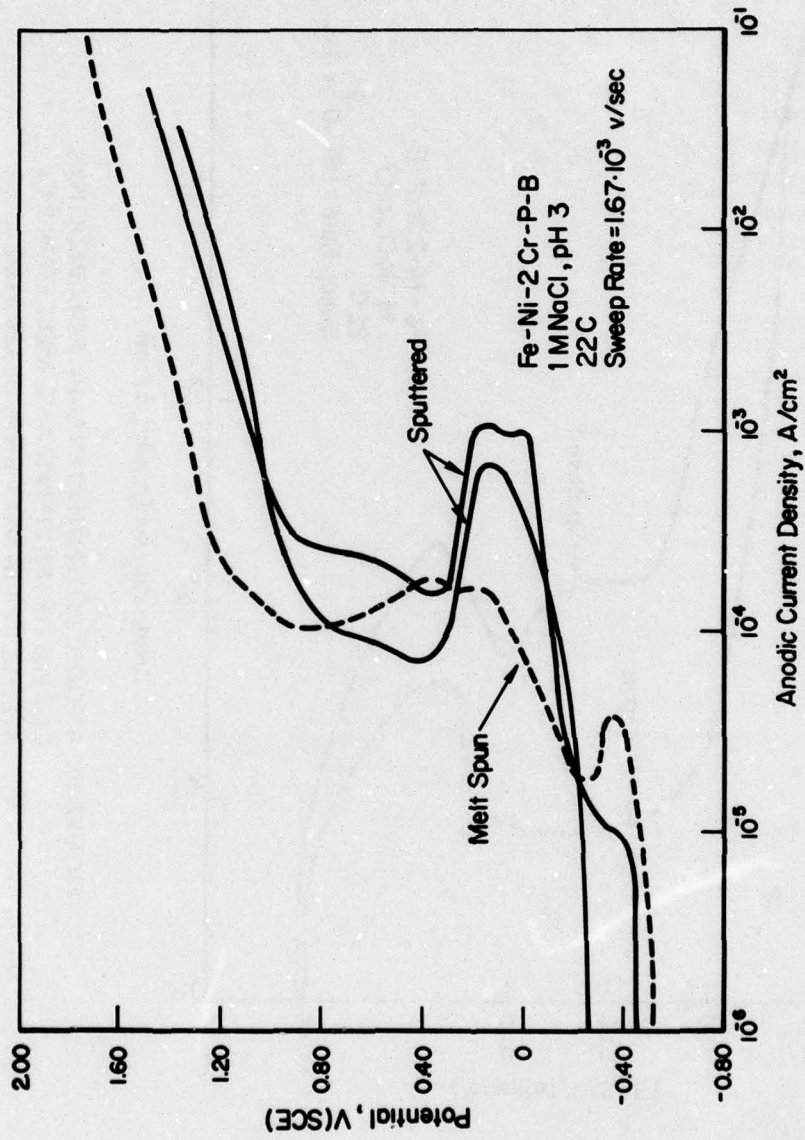


FIGURE 41. ANODIC POTENTIODYNAMIC POLARIZATION CURVES OF SPUTTERED AND MELT SPUN 2 Cr ALLOYS IN 1 M NaCl, pH 3, DEAERATED



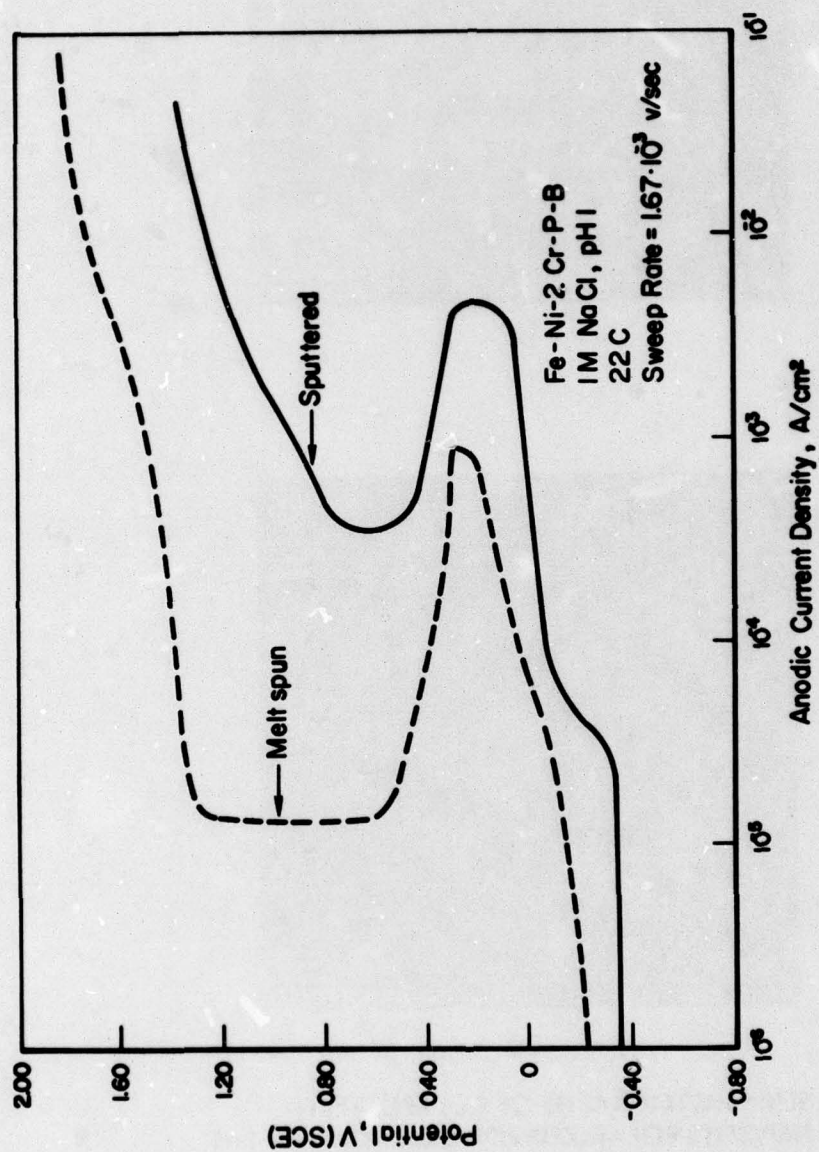
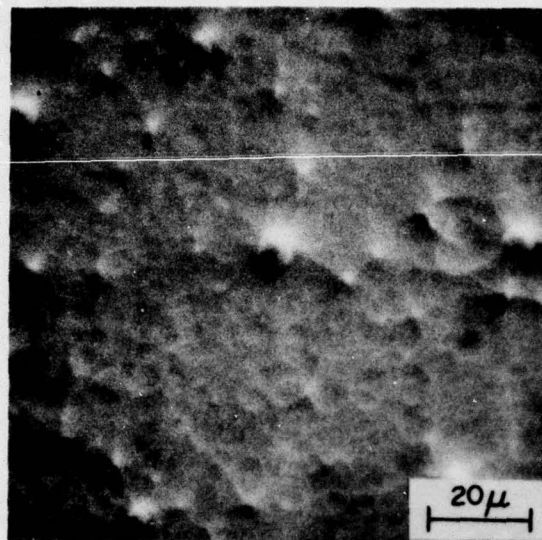


FIGURE 42. ANODIC POTENTIODYNAMIC POLARIZATION CURVES OF SPUTTERED AND MELT SPUN 2 Cr ALLOYS IN 1 M NaCl, pH 1, DEAERATED



(a)



(b)

**FIGURE 43. SEM PHOTOGRAPHS OF 2 Cr SPUTTERED DEPOSITS POLARIZED FOR ONE HOUR IN 1 M NaCl, pH 3, AT THE FOLLOWING POTENTIALS: (a) 0.60 V(SCE); (b) 1.10 V(SCE)**



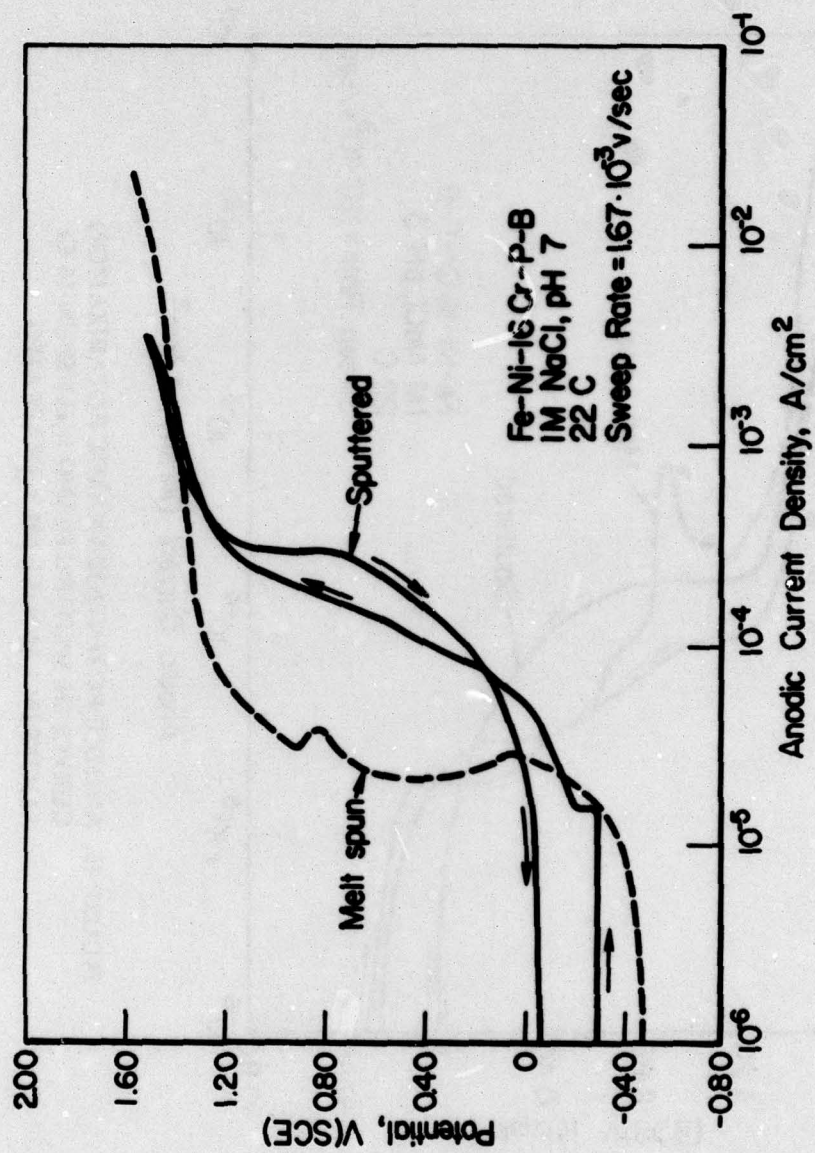


FIGURE 44. ANODIC POTENTIODYNAMIC POLARIZATION CURVES OF SPUTTERED AND MELT SPUN 16 Cr ALLOYS IN 1 M NaCl, pH 7, DEAERATED

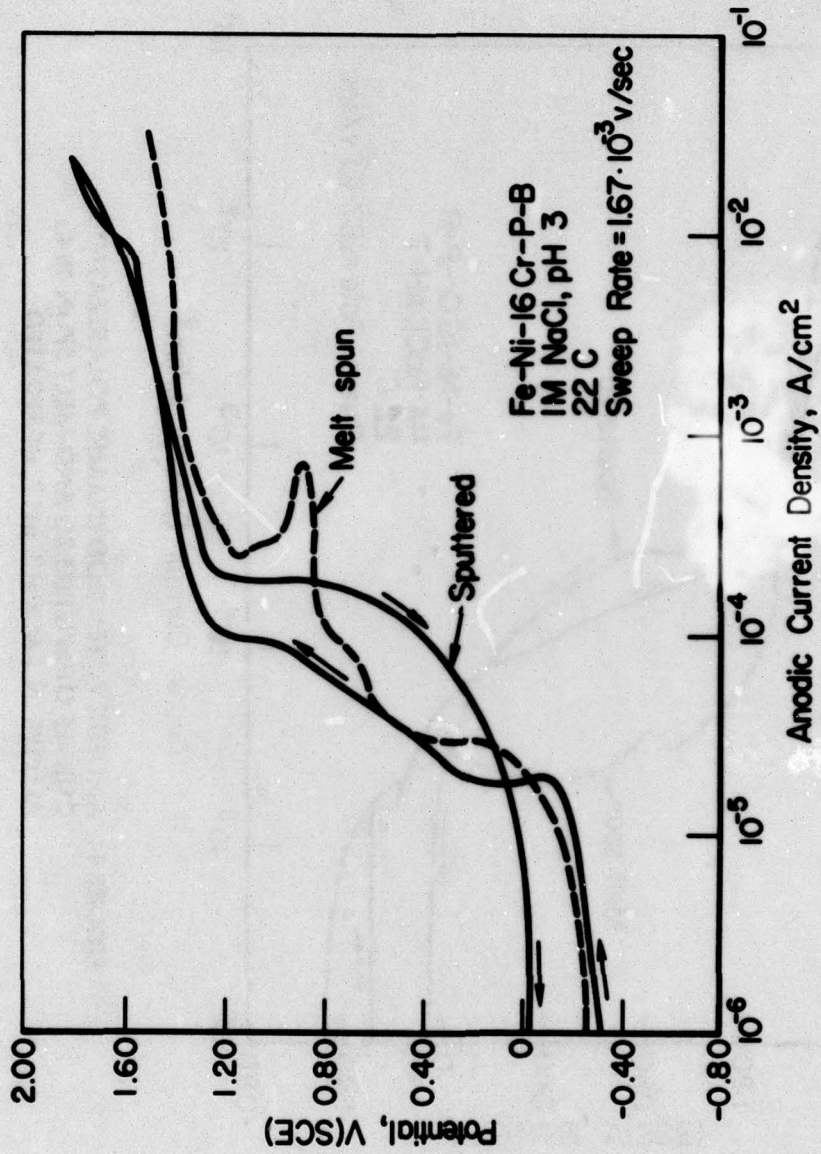


FIGURE 45. ANODIC POTENTIODYNAMIC POLARIZATION CURVES OF SPUTTERED AND MELT SPUN 16 Cr ALLOYS IN 1 M NaCl, pH 3, DEAERATED



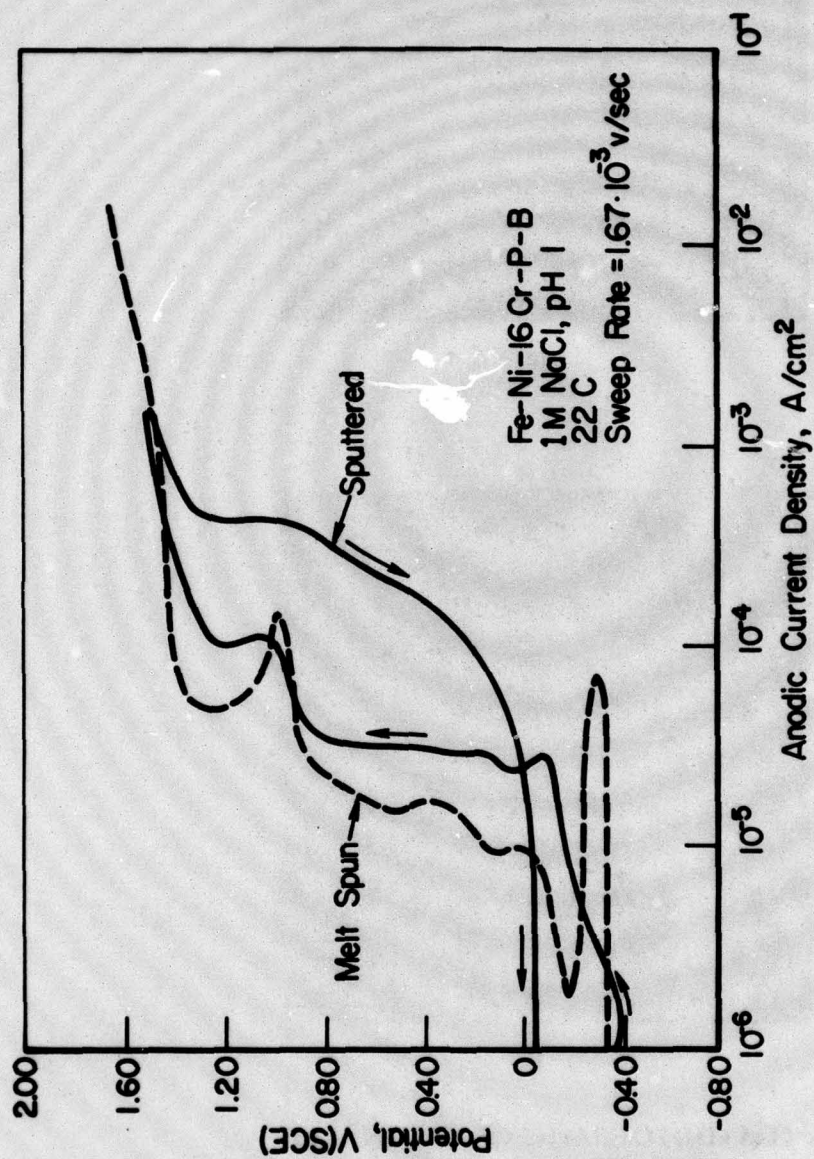
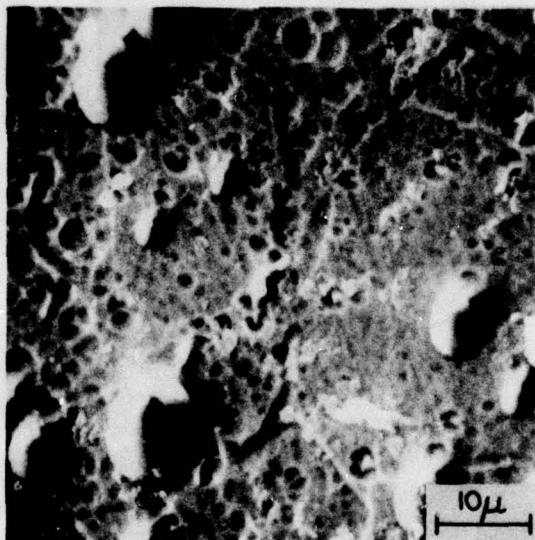


FIGURE 46. ANODIC POTENTIODYNAMIC POLARIZATION CURVES OF SPUTTERED AND MELT SPUN 16 Cr ALLOYS IN 1 M NaCl, pH 1, DEAERATED



(a)



(b)

**FIGURE 47. SEM PHOTOGRAPHS OF PITS ON 16 Cr SPUTTERED DEPOSITS POLARIZED IN 1 M NaCl, pH 3, TO 1.8 V(SCE). (a) SPUTTERED ONTO WATER-COOLED SUBSTRATE; (b) SPUTTERED ONTO LN<sub>2</sub>-COOLED SUBSTRATE**



density (number per unit area) was much greater on the specimen sputtered onto a substrate cooled to liquid nitrogen temperature. Because the number of sputtered deposits that could be prepared during this research was limited, it was not possible to investigate the effect of substrate temperature in detail. Although the photographs in Figure 47 seem to suggest that a colder substrate may favor shallower pit formation, this question needs further attention. It also should be noted that no significant differences were observed in polarization behavior for deposits prepared at the two temperatures. As shown in Figure 48, both types of deposits were spontaneously passive, with  $i_p$  of the water-cooled deposits being somewhat greater than  $i_p$  of the liquid nitrogen-cooled material. However, all four curves converge in the transpassive region, where pitting occurs, thereby indicating that the pitting rates (although not necessarily the pitting morphologies) are equivalent.

### Summary

Sputtering can produce amorphous chromium-containing alloys that essentially are completely amorphous in structure. The physical properties of the sputtered alloys, such as degree of crystallinity, temperature of crystallization, and heat of crystallization closely resemble those of amorphous alloys of the same composition but prepared by liquid quenching, in this case melt spinning. The sputtered deposits exhibit topographic features that indicate a degree of instability of deposition during the sputtering process; however, subsequent research demonstrated that these features are not preferred sites for corrosion, including pitting.

Furthermore, the corrosion and electrochemical behavior of the sputtered deposits resembles, but is not identical to, that of melt spun alloys of the same composition. Specifically, the open circuit corrosion rates and the oxidation rates during anodic polarization of the sputtered deposits exceeded those of melt spun specimens, sometimes by about an order of magnitude. However, the sputtered deposits retained the same excellent resistance to pitting corrosion as their melt spun counterparts, with pitting occurring to a large degree only at potentials above about 1 V(SCE) in acidified chloride solutions. Thus, sputtering is a viable alternate technique for depositing amorphous Fe-Ni-Cr-P-B alloys while retaining their very good resistance to pitting corrosion.

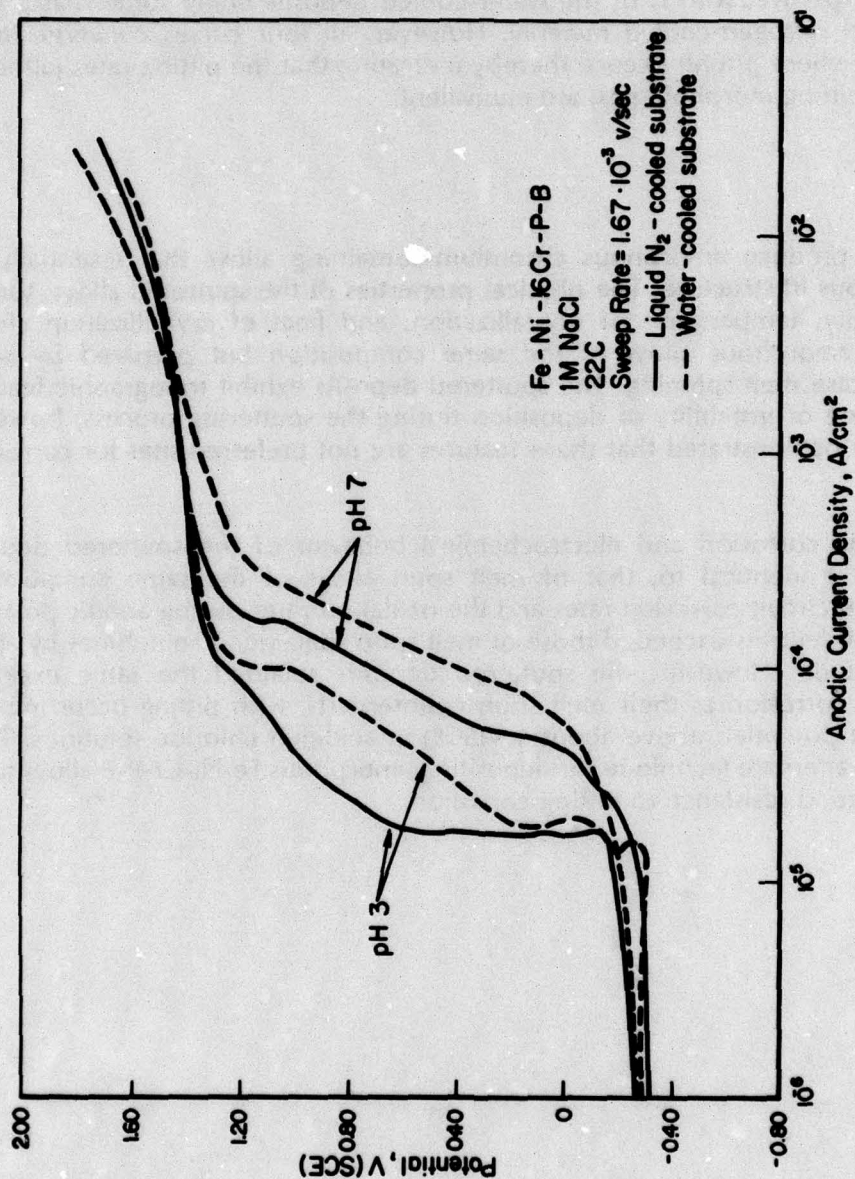


FIGURE 48. ANODIC POTENTIODYNAMIC POLARIZATION CURVES OF 16 Cr DEPOSITS SPUTTERED ONTO EITHER WATER-COOLED OR LIQUID NITROGEN-COOLED COPPER SUBSTRATES. ELECTROLYTE WAS 1 M NaCl, pH 7 and 3, DEAERATED.



## CONCLUSIONS

The conclusions from Phase 1 research are as follows:

- (1) The amorphous chromium-containing alloys evaluated during this research program satisfy two primary requirements for susceptibility to crevice corrosion and to O.C.C. in general: they exhibit active-passive transitions in certain corrodents, and their corrosion rates increase with decreasing pH.
- (2) The alloys undergo crevice corrosion in prepared crevices, but only at very noble applied potentials exceeding about 1 V(SCE).
- (3) Although acidification of anolyte pH occurs during crevice corrosion, activation of the potential of the anode is slight. This behavior indicates that a fairly protective film may be present even during crevice attack.
- (4) Crevice corrosion resistance, as evaluated in crevice test cells, of amorphous alloys containing from 2 to 16 atomic percent Cr greatly exceeds that of T304 stainless steel.
- (4) Cold rolling of amorphous alloys reduces the initiation potential for crevice corrosion to values near the free corrosion potential. This phenomenon is ascribed to the formation of surface micro-cracks, after Devine<sup>(6)</sup>. During growth the crevices widen, passivate, and cease to propagate.
- (6) Increasing the chromium content in the alloys decreases  $i_c$  considerably and  $i_p$  to a lesser degree, and increases the resistance to crevice corrosion.

These amorphous chromium-containing alloys exhibit considerable resistance to corrosion under conditions favoring easy initiation, namely, in prepared crevices. It must be concluded that their corrosion resistance is not simply the result of difficulty in initiating localized dissolution, but that it results in large part from the ability of the alloys to *maintain* passivity under extremely aggressive conditions.

Phase 2 research leads to the following conclusions concerning sputtering:

- (1) Sputtering can be used to deposit chromium-containing alloys that display amorphous structures quite similar to those of alloys prepared by melt spinning.
- (2) The corrosion resistance of sputtered specimens is somewhat less than that of melt spun specimens of similar compositions, regarding open circuit corrosion rates and dissolution during anodic polarization.
- (3) The resistance to pitting of sputtered alloys is essentially the same as that of melt spun alloys of similar composition. Pitting corrosion occurs rapidly in acidified chloride electrolytes only at potentials above about 1 V(SCE).

Sputtering is an alternate technique to that of liquid quenching for preparing amorphous Fe-Ni-Cr-P-B alloys with good corrosion resistance.

**APPENDIX A**

**CALCULATION OF RATE OF CREVICE CORROSION  
ON COLD ROLLED FILAMENT SURFACES**



## APPENDIX A

CALCULATION OF RATE OF CREVICE CORROSION  
ON COLD ROLLED FILAMENT SURFACES

The corrosion rate within crevices in cold rolled filaments can be estimated as follows. Let  $d$  equal the diameter to which a typical pit grew during the time period of active growth; this period was the interval between about  $-0.6$  V and the end of the 60-minute hold time (from Figure 17), or 1.2 hour. From Figure 16(b) a typical pit radius,  $r$ , is seen to be about  $5 \cdot 10^{-4}$  cm. The corrosion current,  $i$ , required to form pits of this size over the growth period of about 1.2 hour can be approximated as<sup>(1-A)</sup>.

$$i = \frac{r\rho F}{tE} \quad (A-1)$$

in which  $\rho$  is the alloy density ( $\sim 8.5$  g/cm<sup>3</sup>),  $F$  is the Faraday (96,500 coulombs/equivalent),  $t$  is the growth time (1.2 hour or 4320 seconds), and  $E$  is the equivalent weight of the alloy (24.8 g/equivalent). To approximate  $E$ , the effective molecular weight of the alloy first was calculated by adding the atomic weights of the various elements present but weighted by their respective atomic fractions; this value is 49.7 g. If dissolution is presumed to occur as  $M = M^{++} + 2e$ , where  $M$  is predominantly Fe and Ni, then  $E = 24.8$  g/equivalent. Use of the preceding values in the equation above results in  $i = 3.8 \cdot 10^{-3}$  A/cm<sup>2</sup>. If the potential within the crevice is assumed to have been more active than that applied potentiostatically because of IR drop effects, then the maximum corrosion current that could have existed was  $i_c$ . Reference to Figures 12 and 13 shows that  $i_c$  was, respectively  $9 \cdot 10^{-5}$  A/cm<sup>2</sup> and  $4 \cdot 10^{-5}$  A/cm<sup>2</sup> in 1 M NaCl, pH 1, and 1N HCl. These solutions should simulate reasonably well the chloride and pH conditions within crevices and pits. It is apparent that the average current density within the crevices was about 40 times greater than the maximum observed in a simulated crevice electrolyte.

Although the calculated average corrosion current of  $3.8 \cdot 10^{-3}$  A/cm<sup>2</sup> is an approximation, it is still considerably greater than the values of  $i_c$  quoted above. This discrepancy is somewhat surprising in view of the fact that the solutions used to generate the polarization curves were quite aggressive. It is conceivable that the chloride concentrations within the crevices actually exceeded one molar, and that this high chloride concentration increased the corrosion rate to the observed average value of  $3.8 \cdot 10^{-3}$  A/cm<sup>2</sup>. Alternatively, the degree of oxygen depletion within the crevices may have substantially increased the dissolution rate relative to that measured during potentiodynamic polarization in bulk electrolyte.

(1-A) Galvele, J. R., Lumsden, J. B., and Staehle, R. W., "Effect of Molybdenum on the Pitting Potential of High Purity 18% Cr Ferritic Stainless Steels", J. Electrochem. Soc., 125 (8), 1204 (1978).

**APPENDIX B**

**LISTING OF ALL TECHNICAL  
REPORTS, PUBLICATIONS, AND  
PRESENTATIONS RESULTING FROM  
THIS CONTRACT**



**APPENDIX B****LISTING OF ALL TECHNICAL  
REPORTS, PUBLICATIONS, AND  
PRESENTATIONS RESULTING FROM  
THIS CONTRACT****Technical Report**

Diegle, R. B., Lineman, D. M., and Boyd, W. K., "Investigating Localized Corrosion and Sputtering Feasibility of Amorphous Chromium-Containing Alloys", Interim Technical Report No. ONR-00014-77-C-04-0488 to Office of Naval Research, April, 1978.

**Publications**

- (1) Diegle, R. B., "Localized Corrosion of Amorphous Fe-Ni-Cr-P-B Alloys", Corrosion, 35(6), 250 (1979).
- (2) Diegle, R. B., "Crevice Corrosion of Amorphous Fe-Ni-Cr-P-B Alloys", in preparation.
- (3) Diegle, R. B., and Merz, M.D., "Corrosion Behavior of Amorphous Fe-Ni-Cr-P-B Alloys Prepared by Sputtering", in preparation.

**Presentations**

- (1) Diegle, R. B., "Simulated Crevice Corrosion of Amorphous Fe-Ni-Cr-P-B Alloys", presented at NACE's Corrosion/78, Houston, March, 1978.
- (2) Diegle, R. B. "Corrosion of Metallic Glasses", presented at TMS-AIME symposium, St. Louis, October, 1978.
- (3) Dahlgren, S. D., presentation of selected research results at the Third International Conference on Rapidly Quenched Metals, Sussex, July, 1978.
- (4) Diegle, R. B., and Merz, M. D., "Localized Corrosion Behavior of Amorphous Chromium-Containing Alloys", presented at NACE's Corrosion/79, Atlanta, March, 1979.
- (5) Diegle, R. B., and Merz, M. D., "Corrosion and Structural Characterization of Amorphous Fe-Ni-Cr-P-B Alloys", presented at the spring meeting of The Electrochemical Society, Boston, May, 1979.
- (6) Diegle, R. B., "Corrosion of Amorphous Alloys", to be presented at the NACE (Canadian Region) Ottawa Conference, Ottawa, October, 1979.
- (7) Diegle, R. B., "Localized Corrosion Behavior of Amorphous Chromium-Containing Alloys", to be presented at the Fall Meeting of The Electrochemical Society, Los Angeles, October, 1979.
- (8) Diegle, R. B., "Localized Corrosion Research in Metallic Glasses", to be presented at the Annual Meeting of the Materials Research Society, Boston, 1979.